TECNOLOGIA SETÚBAL
ESCOLA SUPERIOR
POLITÉCNICO SETÚBAL

ANTÓNIO CARLOS RODRIGUES LOPES GARCÊS

NUMERIC STUDY OF 3D PRINTING PARAMETERS INFLUENCE ON GEOMETRIC TOLERANCES

Relatório de Dissertação do Mestrado em Engenharia de Produção

ORIENTADOR

Professor Doutor Ricardo António Lamberto Duarte Cláudio

Professor Doutor Paulo Jorge Pires Moita

Dezembro de 2023

PRR Plano de Recuperação e Resiliência
REPÚBLICA PORTUGUESA
Financiado pela União Europeia NextGenerationEU

ANTÓNIO CARLOS
RODRIGUES
LOPES GARCÊS

NUMERIC STUDY OF 3D PRINTING PARAMETERS INFLUENCE ON GEOMETRIC TOLERANCES

Júri

Presidente: Professor Doutor Pedro Filipe do Carmo Cunha

Arguente: Professor Doutor Bruno Alexandre Rodrigues Simões Soares

Vogal: Professor Doutor Ricardo António Lamberto Duarte Cláudio

Dezembro de 2023

Agradecimentos

Em primeiro lugar gostaria de expressar os meus agradecimentos, ao Professor Ricardo Cláudio e ao Professor Paulo Moita, pelo apoio constante e conhecimentos transmitidos.

À Escola Superior de Tecnologia de Setúbal do Instituto Politécnico de Setúbal por ter disponibilizado tudo o que era necessário para o desenvolvimento deste trabalho.

Ao Eng. Bruno Borges da S4Metro e ao Nuno Pedro pela cooperação e contribuição na aquisição de resultados.

Aos Professores Cesar Fernandez e à Professora Paula Pereira por terem auxiliado com a parte estatística deste trabalho.

Um agradecimento especial à minha namorada Cristina Pereira pelo seu apoio e pela motivação ímpar.

Aos meus amigos dentro e fora do IPS pela amizade, incentivo e preocupação durante esta jornada.

Por último, gostaria de agradecer à minha família pela paciência e preocupação durante alguns momentos menos bons e constante incentivação para realizar este trabalho e nunca desistir.

À memória do meu querido avô António Rodrigues.

Abstract

Numerous issues affect the final quality of printed parts in additive manufacturing, especially in Fused Filament Fabrication (FFF). The printed parts may experience deformation due to residual stresses caused by thermal gradients during the heating and cooling phases. Research in this field usually focuses on assessing dimensional accuracy, which includes factors like tolerances and measurements compared to the intended design. However, research on geometric accuracy, or the integrity of the printed part´s shape and features with the original design, has been limited. The main objective of the present study is to find how parameters of the 3D printing process influence the geometric tolerances on printed parts.

Generally, physical experiments are performed, but in this study, numerical simulations were executed based on thermomechanical analysis in specialised software. Taguchi method and analyses of variance (ANOVA) were used in experimental design and analysis to evaluate the effects of process parameters on the output of the system, namely flatness, cylindricity, concentricity, parallelism, and perpendicularity.

From the numeric analysis carried out, the results concluded that chamber temperature, extrusion temperature, layer height, and print speed have a very impactful influence on responses. The other parameters discussed have low significance.

Keywords: FFF; Taguchi method; ANOVA; Process Parameters; FFF; Geometric Tolerances.

Resumo

A qualidade final de peças produzidas por manufatura aditiva é influenciada por vários fatores, especialmente no processo por Fabrico de Filamento Fundido (FFF). As peças impressas podem sofrer deformação devido a tensões residuais causadas por gradientes térmicos durante as fases de aquecimento e arrefecimento. Normalmente, os trabalhos científicos sobre este assunto focam-se mais na precisão dimensional, que incluem tolerâncias e medidas comparadas com a geometria pretendida. Contudo, relativamente à precisão geométrica, ou a integridade de partes e formas de uma peça impressa relativamente à forma pretendida, os estudos encontrados são muito limitados. O objetivo principal deste trabalho é determinar como os parâmetros de impressão 3D influenciam as tolerâncias geométricas de peças impressas.

Normalmente são realizados ensaios experimentais para determinar a influência de parâmetros, contudo, neste estudo, foram executadas simulações numéricas do comportamento termomecânico usado um software especializado. O Método de Taguchi e a análise de variâncias (ANOVA) foram usados para planeamento de experiências numéricas e para analisar os efeitos de parâmetros de impressão nos resultados do sistema, nomeadamente tolerâncias de planeza, cilindricidade, concentricidade, paralelismo e perpendicularidade.

Da análise numérica efetuada, concluiu-se que a temperatura da câmara, temperatura de extrusão, altura de camada e velocidade de impressão têm uma influência muito significativa nas respostas. Outros parâmetros discutidos apresentaram pouca significância.

Palavras-chave: FFF; Método de Taguchi; ANOVA; Parâmetros de Impressão; FFF; Tolerâncias Geométricas.

Table of Contents

List of Figures

List of Tables

List of Acronyms

3D	Tridimensional
ABS	Acrylonitrile Butadiene Styrene
ANOVA	Analysis of Variance
CAD	Computer-Aided Design
CCD	Central Composite Design
CFF	Continuous Filament Fabrication
DoE	Design of Experiments
FDM	Fused Deposition Modeling
FFF	Fused Filament Fabrication
GPS	Geometrical Product Specifications
OA	Orthogonal Array
PC	Polycarbonate
PEEK	Polyether Ether Ketone
PETG	Polyethylene Terephthalate Glycol
PLA	Polylactic Acid
SLS	Selective Laser Sintering
SAG	Specific Angle Geometry
STL	Standard Triangle Language
STEP	Surface Tesselation Engine Parameter

List of Symbols

ºC	Degree Celsius
GPa	Gigapascal
MPa	Megapascal
mm	Millimetre
%	Percentage
s	seconds

Chapter 1

Introduction

1.1. Introduction and motivation

From 2021 to 2022, the student was actively involved in the “Accurate 3D” project, a comprehensive program aiming at improving accuracy in 3D printing, and later, in the end of 2022 and 2023 in ProAero3D of Aero.Next, Portugal's agenda aims to bring these improvements to the production of tools and jigs for aerospace. These projects had several goals, one of which was to improve the geometric accuracy of printed parts made of polymeric materials using FFF and numerical simulations.

In today´s industry, integrating tools to improve production processes is critical. Traditional manufacturing processes can involve lengthy duration, resulting in increased costs and bottlenecks in the production chain. In contrast, 3D printing technology has advanced dramatically. However, intrinsic limits in 3D printing remain, notably in terms of warping, shrinking, and achieving inferior mechanical qualities.

Despite tremendous advances, the field of 3D printing remains with many unresolved problems, particularly in minimising warping tendencies and improving mechanical robustness. These limitations, albeit considerable, have driven vigorous research efforts to enhance the technology’s capabilities, pushing the boundaries and unlocking its full potential in making high-complexity components with exceptional accuracy and dependability.

The choice of using numerical analysis resulted from considerable limitations in previous experimental research, specifically the lack of reproducibility, which hampered a thorough knowledge of the influence of printing parameters. Because of the enormous computational time required for each geometry and the large number of experiments involved, numerical analysis became a must. As a result, a methodology similar to traditional experimental procedures was required, requiring the application of experimental design methods and advanced statistical analysis. This computational approach enabled a controlled and systematic exploration of various parameter interactions, compensating for the limitations of direct experimental investigations and allowing a more comprehensive understanding of the intricate effects of printing parameters on geometric characteristics.

1.2. Objetives

The primary objective of this thesis is to undertake comprehensive numerical research to examine and analyse the effect of various 3D printing process parameters on the geometric tolerances of printed parts. Furthermore, using the Design of Experiments gives an in-depth knowledge of the complicated interactions between various process parameters and geometric accuracy. Following that, the data generated from the simulations will be examined using statistical methods to detect significant effects. By giving insights and empirical data towards optimising 3D printing, precision and accuracy in creating geometrically exact parts will be achieved by synthesising findings from different approaches.

1.3. Structure

This present study is composed of six chapters. In the first chapter, the research begins by defining the primary motives of the investigation and specifying the exact aims and goals that will be pursued through the study.

In the second chapter, a thorough assessment of the 3D printing landscape will be made. It begins with outlining the fundamental aspects of 3D printing and then explores the wide range of materials used. Following that, it delves into the inner intricacies of printing parameters, revealing their roles and effects on the printing process. Furthermore, this chapter dives into the several aspects that have a substantial impact on printing accuracy. It also provides a detailed explanation of the Design of Experiments (DoE), which covers several approaches and a theoretical exploration of ANOVA. Finally, it delves into the crucial features of geometric and dimensional tolerance in 3D printing.

The third chapter lays the framework for the experiments. It carefully describes the process of defining parameters and their corresponding levels. It also validates the use of the DoE approach and gives insights into preliminary numerical simulation—closing with the presentation of digital measurements.

The fourth chapter unveils the data collected through the experiments. It also includes a complete description of the statistical analyses performed, providing quantitative comprehension of the data achieved.

The fifth chapter undertakes a comprehensive analysis and discussion of the results obtained. It goes into the result's intricacies, allowing for a complete grasp and interpretation of their significance.

Finally, the sixth chapter summarises the study´s findings, giving concise and comprehensive conclusions based on the research. Furthermore, it suggests potential future work in the dynamic field.

Chapter 2

Literature Review

2.1. 3D printing

Additive manufacturing, commonly referred to as 3D printing, is a manufacturing technique that produces solid objects directly from a computer-aided design (CAD) model. Unlike traditional manufacturing processes that remove material, the AM process involves layer after layer of material addition. This process has several benefits, including the ability to produce parts with complicated geometries quickly and the capacity to remove waste [1]. According to the American Society for Testing and Materials ISO/(ASTM)52900-15, there are seven families of additive manufacturing (Figure 1) [2]:

1. **Vat photopolymerisation** – "*Liquid photopolymer in a vat is selectively cured by light-activated polymerization*" (Description quoted from the Wohlers Report 2014)
2. **Material jetting** – "*Droplets of build material are selectively deposited*" (Description quoted from the Wohlers Report 2014)
3. **Binder jetting** – "*A liquid bonding agent is selectively deposited to join powder materials*" (Description quoted from the Wohlers Report 2014)
4. **Material extrusion** – *"Material is selectively dispensed through a nozzle or orifice"* (Description quoted from the Wohlers Report 2014)
5. **Powder bed fusion** – "*Thermal energy selectively fuses regions of a powder bed*" (Description quoted from the Wohlers Report 2014)
6. **Sheet lamination** – "*Materials sheets are bonded to form an object*" (Description quoted from the Wohlers Report 2014)
7. **Directed energy deposition** – "*Focused thermal energy is used to fuse materials by melting as the material is deposited*" (Description quoted from the Wohlers Report 2014)

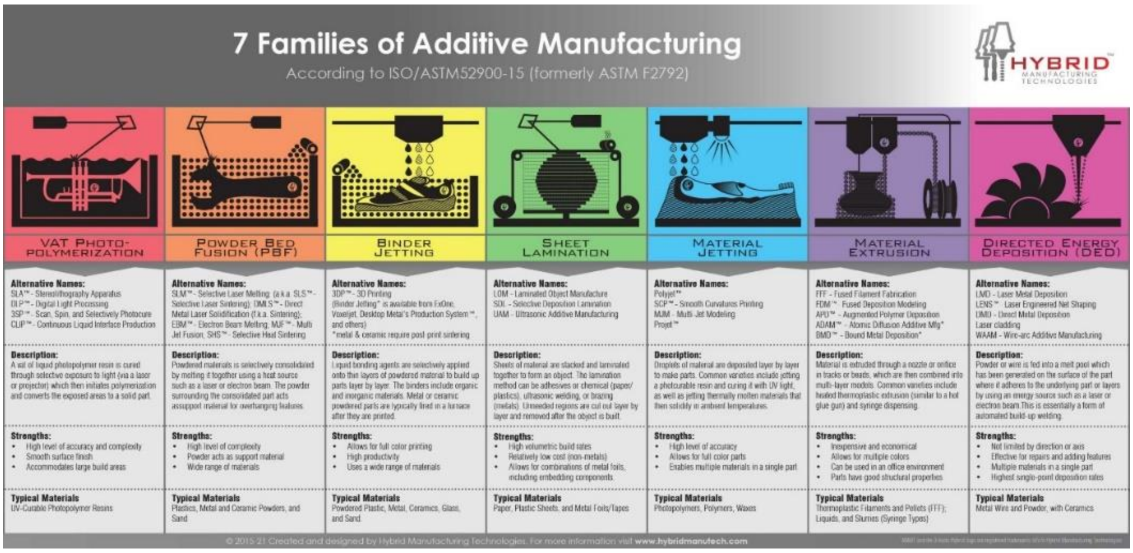

Figure 1 - Seven families of additive manufacturing [2]

The type of material used in each procedure and the manufacturing method differ. By layering materials in successive layers, complex solid parts can be produced without the need for conventional or intermediate tooling. Compared with traditional manufacturing, it enables the development of unique solid parts for functional prototypes and finished goods in a shorter amount of time [3]. The manufacture of functional prototypes, designing and testing, custom parts, and small-scale manufacturing processes have all benefited from the usage of additive manufacturing (AM). Although rapid prototyping was the original purpose of additive manufacturing when it first appeared in the 1980s, later advancements have made the processes into a production-ready technology known as rapid manufacturing. Today, applications concentrate on products from different industries, demonstrating that their industrial relevance has expanded substantially [4]. By continuously building layers in the z-direction, additive manufacturing builds metals, polymers, composites, etc., as well as parts by sculpting each layer in the construction plane. It also develops the third dimension. The cycle time for product design has been accelerated by the ability to manufacture parts directly. In small-scale manufacturing, more traditional manufacturing technologies have taken the role of producing unique components and end-user products [5].

2.1.1. FFF in detail

The process flow can be broken into three key stages: design and development, preparation, and manufacturing. At each stage, specialised software plays a pivotal role in bringing the concept to life.

Specialised software, such as Dassault Systèmes CATIA and SolidWorks, enables the designer to analyse the element digitally during the design and development stage. The standard triangle language (STL) file is imported, manufacturing details are specified, and 3D objects are sliced into groups of 2D planes using pre-process software during preparation. In the STL file, the triangles are represented by a set of coordinates (X, Y, Z) for each of the three vertexes, as well as a normal vector (x, y, z) indicating which face of the triangle forms the interior of the part. The final stage, known as the manufacturing phase, is affected by several factors, including the selected additive manufacturing technology, the strength properties of the chosen material, and the desired level of surface finish. After printing the part, the user can perform finishing procedures, such as removing unnecessary material (Figure 2) [6].

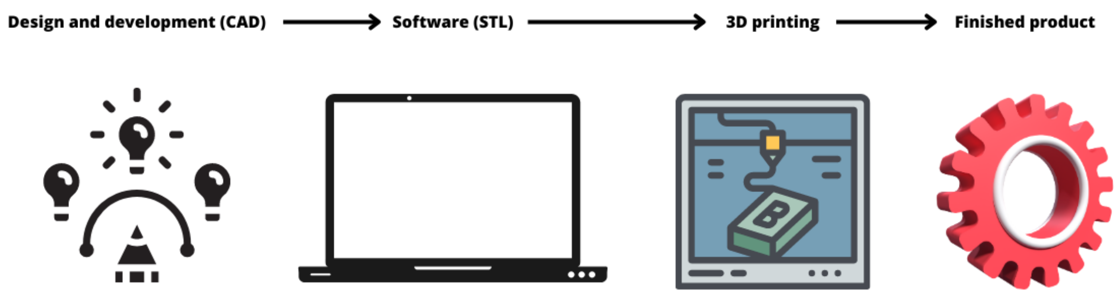

Figure 2 - Process flow of additive manufacturing

Fused filament fabrication (FFF) is one of the most popular additive manufacturing technologies. It is still used as a necessity for support structures because of the length of the building process, the low resolution, and the limited precision. The Bowden or direct extruder method is used to push the filament into the heater block (in the case of thermoplastics) at the beginning of the FFF process. The heatsink, which generates the necessary temperature for molten filament, is contained in the nozzle thermal block. The layer is then formed by extruding the molten filament through a nozzle and onto the build plate (Figure 3). There are two methods to add layers: fixed platforms and movable platforms. G-code files, which contain information on the heated bed, nozzle temperatures, toolpath, infill strategy, extruder speed, nozzle movement coordinates, and other crucial characteristics, are used to upload the printing sequence to the printer [7].

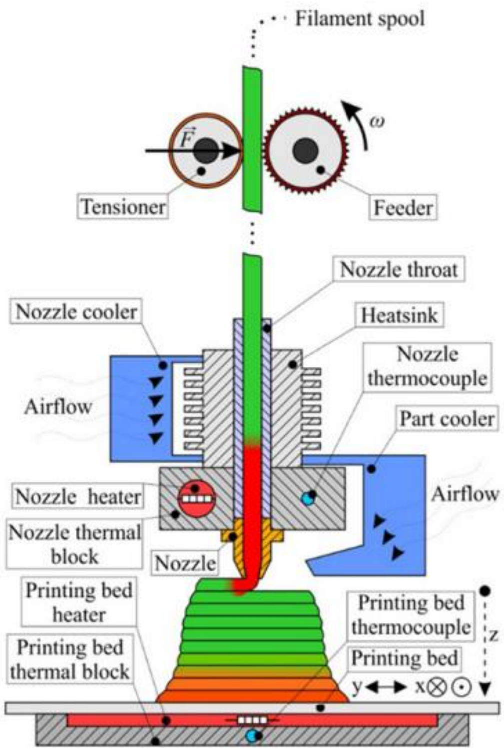

Figure 3 – FFF process schematic (extracted from [8]*)*

2.2. Materials/filaments

FFF heavily relies on polymers as fundamental materials, allowing for a diverse variety of applications. In Table 1, some common polymers used in FFF and their properties are displayed. Composites are frequently used to improve structural properties by mixing polymers with carbon, metal, glass, and other fibres. However, establishing consistent composite output across all FFF 3D printers might be difficult. Although 3D printing for food and biological pastes is theoretically viable, this practice is mainly confined to experimental research reasons. Another essential material type in FFF printers is "support" material, which is required for printing parts with complicated shapes or orientations, such as components with considerable overhangs. User-friendly support materials are carefully prepared.

Table 1 - Properties of some common polymers used in FFF (extracted from [9]*)*

Polymer	Melting temperature (° C)	Tensile strength (MPa)	Young's modulus (GPa)	Extrusion temperature (° C)	Printing speed (mm/s)
ABS	177 - 320	11 – 65	1 – 2.65	215 – 275	25 – 40
PLA	120 – 205	30 – 65	2.3 – 2.9	160 – 230	25 – 110
PEEK	343	100	3.56 – 4.00	340 – 440	5 – 30

PETG	230 – 260	29 – 56	0.42 – 0.88	220 – 250	15 – 45
PC	250 – 343	58.6 - 72	1.79 – 3.24	200 – 280	25
PA	216 – 300	35 – 186	0.45 – 3.50	250 – 250	40
HDPE	120 – 220	24.5 – 27.5	0.88 – 1.10	200 – 260	25 – 250
PP	150 - 160	17 - 21	0.79 – 0.88	165 - 250	8 - 60

Although there are many materials used in FFF, some stand out as the most used. These materials have grown in popularity due to their distinct properties and practical use in a wide range of sectors. Most of them are used based on the project's unique requirements and the capabilities of the 3D printer in use.

As such, the following materials are highlighted:

2.2.1. ABS

Acrylonitrile Butadiene Styrene (ABS) is a popular and versatile thermoplastic that may be used as a feedstock filament in FFF applications. The appealing properties of this material come from its favourable mechanical qualities, capacity to endure fluctuating temperatures, cost-effectiveness, moderate flexibility, and melting temperature range compatible with FFF methods. ABS is a popular material for producing a variety of parts that require resistance to cyclical loads and temperature changes. Despite its various benefits, ABS has several restrictions that limit its application in some situations. ABS tends to exhibit contraction and warping, which can impact print accuracy and dimensional stability. Furthermore, adherence to the printing platform might be an issue, resulting in separation during the printing process [9].

2.2.2. PLA

Polylactic Acid (PLA) is a biodegradable and environmentally friendly polymer that is commonly used in extrusion-based 3D printing. It is derived from renewable resources such as corn starch or sugarcane and can be composted under the right conditions. PLA is also used in a variety of other applications, including packaging films and biomedical devices, due to its biocompatibility and slow degradation rate. PLA is the most widely used raw material in FFF due to several advantages. PLA is easy to use and is compatible with a wide range of FFF printers. PLA has a low melting point and can be extruded at low temperatures, which makes it easy to work with and less likely to cause clogs or other printing issues. Additionally, PLA is available in a wide range of colours and finishes, which allows users to create visually appealing prints. However, PLA shows some disadvantages, like low toughness, high brittleness, low melt strength, poor heat bending temperature, poor thermal stability, narrow processing window, and nonconductivity. Additionally, the mechanical strength of PLA is lower than that of other polymers, such as ABS and PC. PLA components may also experience volume changes and stress during 3D printing, which can affect their dimensional stability. Today, there are several ways to address these limitations. PLA composites can be prepared with suitable additives to improve their properties. For example, adding fillers such as carbon fibres or glass fibres can increase the strength and stiffness of PLA components. Other additives, such as plasticisers, impact modifiers, and processing aids, can improve the toughness, flexibility and processability of PLA. Additionally, these new PLA composites have been developed for use in various industries, including biomedical, tissue engineering, and automotive, which may have specific requirements for material properties [10].

2.2.3. PEEK

Polyether Ether Ketone (PEEK) is a semi-crystalline thermoplastic that is highly valued in the manufacturing industry for its superior mechanical properties. It has grown in prominence in the field of additive manufacturing in recent years. It is now available as a filament for all FFF, and it is rapidly becoming available as a powder for the selective laser sintering (SLS) process. PEKK is widely used in the aerospace, medical, and automotive sectors because of its exceptional resistance to heat and wear, and it may even be used as a potential alternative for some metals because of its excellent strength-to-weight ratio. PEEK requires precise management of the crystallisation process in 3D printing since it affects the material’s density. These demands keep extrusion, build plate, and chamber temperatures consistently high while eliminating temperature swings. To effectively 3D print with PEEK, a printer with a 400ºC extruder, a chamber that can be heated to 120ºC, and a build plate that can reach 230ºC is necessary. This guarantees appropriate component release at the end of the printing process and aids in warping prevention. Furthermore, PEEK changes density during printing and compresses as it cools.

Despite its demanding nature, PEEK has attractive mechanical and chemical qualities for a variety of applications. It has great chemical resistance, is sterilisable, and has excellent dielectric characteristics. Due to its high strength-to-weight ratio, PEEK is frequently used as a metal alternative. Furthermore, its flame resistance makes it an appealing 3D material for industries with high fire and smoke regulations, such as aerospace. PEEK outperforms ULTEM in terms of mechanical strength when compared to other high-performance thermoplastics [11].

2.2.4. PETG

Polyethylene Terephthalate Glycol (PETG) is a popular thermoplastic used in additive manufacturing. PETG is a popular choice for filaments and FFF because of its flexibility, combining the user-friendliness of PLA with the toughness of ABS. This amorphous plastic has the potential for total recyclability and shares the same chemical makeup as its well-known abbreviation, PET. To obtain a thorough grasp of this material, the upcoming guide will outline its distinguishing qualities, critical factors for effective 3D printing, principal used, and significant manufacturers.

PETG has an extrusion temperature range of 220ºC to 260ºC when it comes to printing conditions. It is strongly advised to use a heated printing bed with a temperature range of 75ºC to 90ºC. A reasonable printing speed is between 40 and 60mm/s. PETG is not recommended for use as a support material because it adheres too firmly to itself, making post-print removal difficult. While PETG is typically easy to print with, it does offer a somewhat higher level of complexity than PLA yet maintains admirable qualities. There are, however, certain disadvantages to consider. Notably, avoiding warping is critical, and a heating plate is required. Furthermore, as compared to PLA, PETG is more prone to scratches. Finally, keep in mind that PETG absorbs moisture quickly and should be stored in a cold, dry location. Furthermore, because of its high viscosity, it is prone to print head blockages [12].

2.2.5. PC

Polycarbonate (PC) is renowned for its high impact resistance and optical clarity. This thermoplastic finds a balance between lightweight design and toughness, making it ideal for a wide range of professional applications. While it is more difficult to 3D print than PLA or PETG because of the higher extrusion and bed temperatures required, it is an exciting alternative for creating complicated components with outstanding thermal, mechanical, and optical properties. PCs are mainly utilised on FFF machines and are primarily available in filament form. Nonetheless, it’s worth mentioning that certain PC resins are photopolymerization-compatible.

Working with polycarbonate necessitates an extrusion temperature range of 260ºC to 290ºC, with certain varieties requiring temperatures as high as 320ºC. Furthermore, a heated build plate set to a minimum of 110ºC is required. Given its propensity for warping, providing strong adherence to the plate is critical. Due to the probability of temperature fluctuations, deformations, and cracks, it is recommended to use a closed chamber to avoid these problems [13].

2.3. Printing parameters

In FFF, countless parameters can affect the properties of the final product. Therefore, in the following chapters, we will consider those that can be more influential towards the improvement of geometrical accuracy, which are chamber temperature, infill density, layer height, extrusion temperature, print Speed, and infill strategy. [14], [15], [1], [16], [5], [17]–[20]. Bed temperature was considered equal.

Figure 4 demonstrates how the different printing parameters lead to the quality of the part.

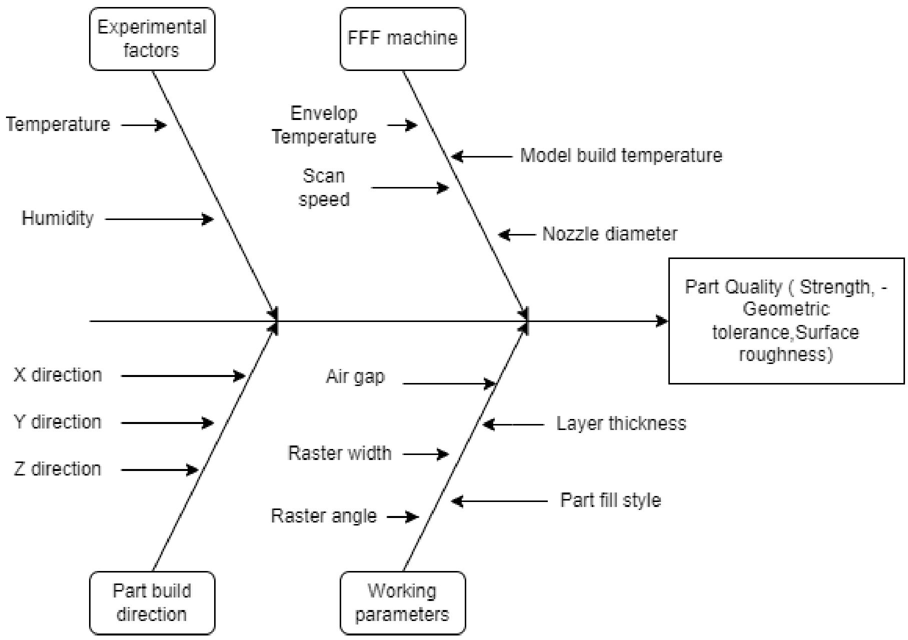

Figure 4 - Ishikawa diagram of the printing parameters (extracted from [21])

2.3.1. Chamber Temperature

Chamber temperature, also known as build chamber temperature or ambient temperature, is the temperature of the closed build chamber in which the 3D printing takes place. The build chamber’s temperature plays an essential part in the FFF process since it influences the printing quality, adhesion, and warping of the printed pieces. Maintaining the correct chamber temperature is critical to producing high-quality FFF prints. Several studies were found on the influence of chamber temperature printing parameters on varied materials. Sikder et al. (2022) [22] explored the effects of various 3D printing parameters on the mechanical properties of PEEK. His study concluded that a higher chamber temperature aided in the development of PEEK parts with superior mechanical characteristics. The chamber temperature had a considerable impact on the crystallinity of the component. Notably, although it produced components with high mechanical properties, the temperature was insufficient to produce entirely crystalline parts. However, it aided in the production of homogeneously crystalline 3D-printed PEEK parts with enhanced mechanical properties. Samy et al. 2021 [15] investigated the behavior of polypropylene under various fused deposition modeling (FDM) conditions. The conclusions drawn from his research indicated that increasing the ambient temperature from 25 to 75 ° C improves the bonding between the nearby filaments and maintains a uniform cooling condition, reducing the resultant thermal residual strains. However, increased crystallisation of the polymer molecules may result in increased warpage of the printed samples. Thumsorn et al. 2023 [23] used five different commercially available and laboratory-made PLA filaments in their study. The crystalline structure and dynamic mechanical qualities of 3D printed items increased when the chamber temperature was increased, particularly in PLA composites. However, the additives in the PLA composite induced an anisotropic characteristic that resulted in the delamination of the interlayer bonding in the transverse-orientation products. Kuo et al. 2019 [24] investigated warpage on ABS prototypes using a low-cost FFF machine. They found that the chamber temperature in which the ABS physical model was created substantially impacted the extent to which it warped. A variety of temperatures, including 35 ºC, 37ºC, 40ºC, 43ºC, and 45ºC, were tested to establish the best. Due to the low temperature, a high degree of warpage was observed when the chamber temperature was set at 35°C. In contrast, poor dimensional precision was observed when the temperature was set at 45°C due to an increase in the solidification time. As a result, a chamber temperature of 40ºC was determined to be the most suitable.

2.3.2. Infill density

This parameter determines the density and strength of the printed part. When printing, it refers to the percentage of internal space that is filled with material. A higher infill percentage indicates that more material is used, which results in a denser part, but also in a longer print time and more material usage. Lower infill percentages produce lighter and less sturdy parts, but they also require less time and material to print. The infill percentage can be modified in the slicing program. Some studies have shown to be more interested in the tensile testing of 3D printed specimens regarding the infill density. Porter et al. 2019 [25] studied the influence of infill properties of structural beams manufactured using an FFF 3D printer. They found that the optimal infill density that maximised the relation between the flexural rigidity of beams and weight was determined to be between 10% and 20%. Dave et al. 2021 [26] did an experimental study to explore various process parameters in open-source 3D printers, including infill density, on tensile properties. Tests were made using 60%, 80%, and 100% infill density on PLA specimens. They concluded that the tensile strength also increases with an increase in infill density—specimens with 100% exhibit maximum strength. Specimens with 80% showed some ductile behaviour due to minor air gaps. Finally, specimens with 60% showed brittle fractures.

2.3.3. Layer height

Layer leight, also known as layer thickness, is the measurement between extruded layers. The layer height determines the resolution and the level of detail of the model. The parameter is adjusted in the slicing program and significantly impacts the final part. In general, increasing layer height will decrease the resolution and quality of the print but result in a faster print. On the other hand, a small layer height results in smother surfaces and higher details, but it takes longer as more layers need to be printed. It also requires a well-calibrated and precise 3D printer. The optimum layer height should be a balance between quality and print speed, both for large and small print. Watanabe et al. 2016 [27] studied the effects of process parameters on part warpage. In his study, increasing the layer height from 0.1mm to 0.3mm decreased the warpage. A lower layer height is also a thinner fabricated part, which means it cools more quickly and, as such, leads to a higher warpage. Zharylkassyn et al. 2021 [16] made a comprehensive review of publications that investigated the effect of process parameters on dimensional accuracy. In his conclusions, he found that the literature suggests layer height levels should be between 0.1 and 0.2mm to achieve optimal dimensional accuracy. Still, the optimal layer height might differ from material to material. Furthermore, the dimensions of the pieces, such as length, width, and thickness, have an impact on printing accuracy.

2.3.4. Extrusion temperature

The extrusion process consists of heating the materials, such as ABS, above the melting temperature for semicrystalline polymers or above the glass transition temperature for amorphous polymers to enhance flow and deposition and then force the semiliquid through a nozzle when pressure is applied and form a continuous profile. When the filament exits the nozzle, it cools, and the viscosity of the polymer increases dramatically, retaining its shape [28]. Printing the material with its specific extrusion temperature is the best way to ensure its quality. Each material has its extrusion temperature. Alafaghani et al. 2017 [29] investigated the independent effect of each parameter on the mechanical properties and dimensional accuracy. The conclusions state that a lower extrusion temperature and layer height improve dimensional accuracy, but a higher extrusion temperature and layer height are needed to improve mechanical properties. Zharylkassyn et al. 2021 [16] mentioned before, stating that most research showed that raising the extrusion temperature reduces dimensional accuracy, showing a linear connection between extrusion temperature and dimensional deviation. Despite this, there is a specific temperature over which the rise in dimensional deviations became insignificant. The material type determines the limitation temperature. The influence of extrusion temperature was discovered to be explored mainly by utilising PLA material. This might be owing to PLA shrinking less than ABS. According to data, the ideal extrusion temperature range for PLA parts should be between 180ºC and 220ºC. Furthermore, with PLA material, the width and thickness of printed specimens tend to have positive deviations.

2.3.5. Print speed

Algarni et al. 2021 [30] state that print speed is the speed of the nozzle on the build platform during extrusion and deposition. It calculates the entire printing time. The printing technology and the material used determine it. It typically varies between 15 and 90 mm/s. Print speed has the most significant effect on the material distribution and forming dimension of any FFF process parameter. In Algarni's study about the effects of process parameters on the mechanical behaviour of printed parts, he reveals that different print speeds have a significant impact on the distribution and forming dimension of the material. Higher print speeds in smaller parts cause material deformations due to fresh layers being put on top of layers that have not yet fully solidified. As a result, the new layer's weight deforms the prior layer. Print speed has a more significant impact on deposition width than it does on deposition height. Researchers like Samy et al. [15] and

Agarwal et al. [70] discovered that faster print speeds reduce tensile strength significantly. Furthermore, higher print speed alters how the filament melts, resulting in poor layer-to-layer adhesion and poorer strength.

2.3.6. Infill strategy

The inner structure of a printed part is usually called infill. The infill strategy is the 2D layers that provide internal support for the part. Infill strategys recreate some of the mechanical qualities and give stability while remaining light. The strength-to-weight ratio is the most essential criterion that influences the selection of an infill strategy. Using less material reduces print time and leads to lighter parts. Depending on the design of the infill strategy, some prints can lead to higher print times. If a pattern is more complex, the nozzle speed is reduced, resulting in longer print times [31]. There are several infill strategys available, each with its function and mechanical attributes such as stiffness and strength (Figure 5):

Rectilinear – It generates a rectilinear grid by printing one layer in one direction, then the following layer rotated by 90 degrees, and so on. This saves filament and prevents material accumulation at crossings. It´s one of the quickest infills to print.

Grid – It´s printed in both directions (rotated by 90º) in each layer, as opposed to rectilinear. As a result, material is collected at the points where the paths intersect. Although grid infill is more solid (and has higher layer adhesion) than rectilinear infill, it can occasionally produce print failure owing to the nozzle passing over the crossings where material accumulates.

Honeycomb – This infill generates a hexagonal grid. Its primary benefit is its mechanical resistance and ideal pathways without crossovers. The primary drawbacks are increased material consumption (about 25% more) compared to other infills and print time that can be up to twice as long as previously discussed alternatives.

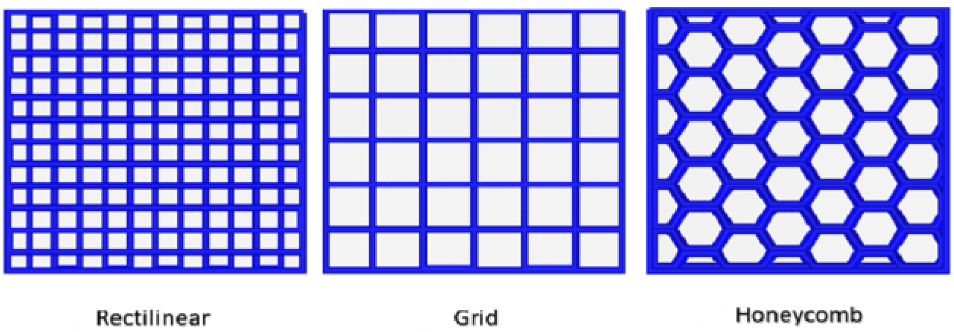

Figure 5 - Rectilinear, grid and honeycomb pattern (extracted from [32])

2.4. Factors that affect accuracy

2.4.1. Shrinkage

In the FFF modelling process, understanding shrinkage is crucial, as shrinkage is one of the significant challenges associated with 3D printing. The hot extrusion process starts with the deposition of polymer beads or filaments through a nozzle, typically at a temperature close to the melting point [15]. As the newly deposited material is in contact with the layers previously formed, it begins to lose heat through conduction. The heat is transferred from the hot material to the cooler layers. This heat transfer process causes the successive lines of material to cool down and eventually solidify on top of the previously formed layers.

During these cooling and solidification phases, a thermal gradient is established within the part. The outer layers of the recently deposited material are exposed to the cooler ambient temperature, while the inner layers are in contact with the still-hot material. This temperature gradient gives rise to a nonuniform heat distribution within the part. Due to the temperature gradient and inconsistent heat distribution, internal stresses occur within the layers of the printed part. These stresses are caused by the material’s differential cooling and contraction in various locations. Those in contact with colder surroundings cool faster and contract more, whereas those in contact with hotter material beneath cool and contract less. Internal stresses and strains are created as a result of this unequal contraction within the printed part.

Alsoufi et al. [33] investigated a method for resolving shrinkage issues. They explained how shrinkage can be managed by the use of a particular infill structure to enhance the dimensional accuracy of hole/slot features in the parts produced.

2.4.2. Warpage

Most 3D printers work with thermoplastic materials that will be exposed to high temperatures due to the extrusion process. Warpage is a geometric flaw caused by the cooling process after the extrusion when the material cools down to the highest thermal gradient in the air. After the extrusion, the material accumulates residual stresses caused by the cooling process. These residual stresses cause shrinkage, which is prevented by the building platform until the part is extracted from the platform. The warpage happens with the release of stresses and is followed by the shrinkage of layers, which eventually causes a bending distortion warpage.

Samy et al. [15] concluded that increasing the print speed from 30 mm/s to 60 mm/s decreases the cool time and reduces the crystallinity of the polymer, resulting in low crystallisation; therefore, newly deposited layers in fast printing can reduce thermal stresses and distortion of the part.

Hong et al. [34] conducted a study to minimise warping deformation of open-source FFF 3D prints, focusing on the different process parameters, such as the print speed and the nozzle temperature with PLA. It was concluded that a minimum error of warping can be reached if the nozzle temperature is at 220ºC, and the print speed is 20 mm/s.

2.4.3. Stairstepping

Stairstepping is a visual artefact created during the 3D printing process. It's named after the surface roughness of the final printed part, which resembles a staircase. It appears on the surface of a 3D-printed part as a succession of visible and distinct flat lines or steps. Following the curves of the object, these lines typically give a rough, textured look, especially on sloping or curved surfaces. The layer-to-layer additive aspect of 3D printing mainly causes stairstepping. When printing a 3D printed part, the printer must approximate curves and contours using a sequence of flat layers. As a result, the surface is not entirely smooth but instead looks like a series of flat, linked segments or steps. However, several other factors could contribute to the occurrence of stairstepping.

Hong et al. [35] conducted a study on the stairstepping effect in rapid prototyping. He is concerned that this effect on the surface of the printed part is directly correlated with part shrinkage. The layer height can also contribute to the effect, as thicker layers may result in more noticeable steps.

Umaras et al. [36] mention the STL format conversion as a design/software-related inaccuracy that leads to stairstepping. As the accuracy depends on an error propagation mechanism, the resulting error is an effect of the accumulation of individual errors. When the CAD geometry is converted to STL format from a triangulated mesh, errors in the layering process can be caused. (Figure 6). Geometric inaccuracy can be caused by the fundamental construction process, in which each layer's contour adds to a stairstep effect on the part's surface.

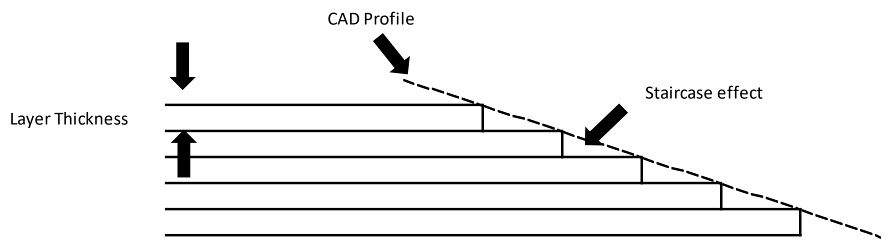

Figure 6 - Staircase layering effect

2.4.4. Thermal behaviour

The thermal behaviour of the printing process is critical in 3D printing because it includes the controlled application and management of heat during material deposition and solidification. Different 3D printing processes use different thermal concepts. FFF printers, for example, rely on heating and extruding thermoplastic filaments layer-by-layer, whereas SLA printers use UV lasers to cure the liquid resin selectively. A thorough understanding of these processes is required to optimise print settings and select appropriate materials. Ramos et al. 2022 [37] did an essential study on heat transfer in FFF to obtain accurate stress prediction and high-quality printing. Their findings demonstrated that infill density had a substantial impact on steady-state temperature and heating rates. Still, extrusion parameters and air void sizes did not appear to influence heat transmission in the printed samples. Furthermore, heat transmission in the printed samples did not appear to be affected by the kind of infill strategy (e.g., rectilinear vs gyroid). Specific heat and thermal expansion parameters heavily control temperature distribution and heat dispersion in 3D printing. In another relevant study, Samy et al. 2021 [15] investigated the behaviour of semi-crystalline polymers under various FFF circumstances. Their findings demonstrated a link between layer height, nozzle speed, and part distortion. Notably, as newly deposited material was repeatedly warmed before cooling, increased nozzle speed resulted in high cooling rates. Reducing the temperature difference between the ambient and melt temperatures was discovered to enable more homogenous heat transmission, thus increasing layer bonding. The experimental findings showed that items printed at higher ambient temperatures had improved mechanical characteristics. Print speed and temperature must be balanced to provide robust and dimensionally exact prints. Furthermore, good temperature management is a vital part of 3D printing, with a significant impact on the end product´s quality and performance. Several factors must be addressed to guarantee good heat management in 3D printers. Empirical heat transfer modelling in 3D-printed polymer rods, for example, provides information on material thermal conductivity. Hriţuc et al. 2022 [37] investigated the influence of numerous factors on the heat conductivity of polymer materials used in 3D printing, therefore helping 3D-printed product optimisation (Figure 7).

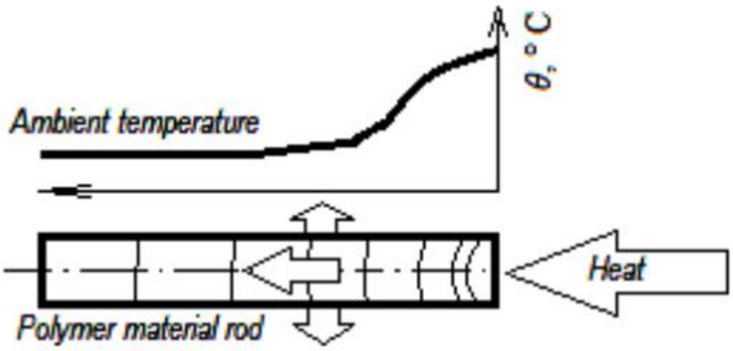

Figure 7 - Schematic representation of how heat transfer through the cylindrical rod of polymeric material is assumed to occur (extracted from [37])

2.4.5. Analysis of each parameter influence

The table below gives a complete summary of several research papers focusing on the significant aspects and parameters of 3D printing processes, with a focus on material-related issues. These studies, undertaken by several authors, investigate a number of parameters spanning a wide range of materials used in 3D printing.

Table 2 - 1) Chamber temperature, 2) Infill density, 3) Layer height, 4) Extrusion temperature, 5) Print speed, 6) Infill strategy

Factor	Material	Parameters studied	Author	Article
Shrinkage	ABS	1, 4, 5	Dilberoglu et al.	[33]
Shrinkage	ABS	1	Choi et al.	[38]
Shrinkage	ABS	3	Sood et al.	[39]
Shrinkage	PolyPhenylene Sulfide	4, 5	Fitzharris et al.	[40]
Shrinkage, Stairstepping	Photo-Polymer	3	Hong et al.	[35]
Stair stepping	Ceramic-based composites, metal matrix, fiber-reinforced and polymer composites	3	Solomon et al.	[41]
Stair stepping	Various materials	-	Guo et al.	[42]

Stair stepping	ABS	3	Haidiezul et al.	[43]
Thermal Behavior	PLA	3, 4, 5	Zhou et al.	[44]
Thermal Behavior	PolyPropylene	1,	Spoerk et al.	[45]
Thermal Behavior	ASTM D638 polymer composite		El Moumen et al.	[46]
Thermal Behavior	Ultem 9085		Padovano et al.	[47]
Thermal Behavior	PLA	6	Pernet et al.	[31]
Warpage	Semi-Crystalline Polimer	1, 5	Samy et al.	[15]
Warpage	Nylon PA12	2, 3, 4	Alzyod et al.	[7]
Warpage	PLA+	4, 5	Alsoufi et al.	[34]
Warpage	ABS	1	Wang et al.	[48]
Warpage	PolyPropylene	3, 4, 5	Spoerk et al.	[49]
Warpage	ABS	3	Armillotta et al.	[50]
Warpage	PolyPropylene	3	Samy et al.	[51]
Warpage	PolyPropylene	3, 4, 5	Watanabe et al.	[27]
Warpage	PolyPhenylene Sulfide	4, 5	Fitzharris et al.	[40]

2.5. Design of Experiments – DoE and statistical procedures

The use of experimental design, also known as Design of Experiments (DoE), is extensively employed in various scientific and industrial domains. It serves as a statistical approach to aid in the creation and enhancement of products and processes. DoE encompasses a range of statistical tools that are systematically utilised to classify and measure the cause-and-effect relationships between variables and outcomes within the investigated process or phenomenon. The ultimate goal of employing experimental design is often to identify the optimal settings and conditions that lead to process optimisation.

2.5.1. Key concepts of DoE

There are essential principles connected to organising and doing experiments to examine the impact of various conditions on a response variable or outcome (Figure 8). Here is a brief explanation of each term:

Parameters: Controllable inputs. Variables that have the potential to influence the response variables in an experiment

Levels: A minimum of two levels are required for each parameter, each representing a specific value or setting.

Output: The outcome of the analysis is also referred to as the response variable, as it represents the effect of the study.

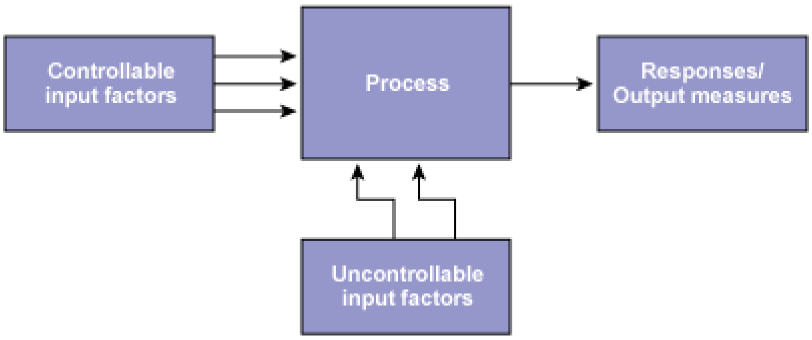

Figure 8 - Process parameters and Responses (extracted from [52]*)*

2.5.2. Guidelines for designing an experiment

A well-structured and effective experiment is an essential stage in scientific research. Following this method guarantees a unified and disciplined research endeavour, allowing for the correct interpretation of findings. Here are the following guidelines [53]:

1. **Recognition of and statement of the problem (pre-experimental)** – A precise problem description is essential for better understanding the phenomenon under investigation and finding an appropriate solution. It is critical to keep the main objectives in mind during the experimental phase.
2. **Selection of the response variable (pre-experimental)** – Selecting the appropriate response variable is critical for getting relevant information about the examined process. The response variable is often the average or standard deviation of the measured characteristic. Multiple answers may be considered, and the procedures for measuring and calibrating them should be outlined ahead

of time. The measuring system's capabilities are critical for detecting parameter effects accurately. Replication or averaging of repeated readings may be used in circumstances with low gauge capabilities. Addressing these concerns before experimenting is crucial to its success, and tailored experiments are sometimes used to improve measuring system performance.

3. **Choice of parameters, levels, and ranges (pre-experimental)** – Parameters might be classified as possible design parameters or nuisance parameters. The variables of interest are design parameters, held-constant parameters, which are regulated but not of interest, and allowed-to-vary parameters, which are nonhomogeneous variables. Nuisance parameters, which can be controlled, uncontrollable, or noise parameters, can have significant impacts yet are not the primary focus of the investigation. Selecting design parameters, identifying their ranges and levels, and controlling how they will be controlled and monitored are all part of pre-experimental planning. Process understanding is essential during this stage. When doing parameter screening or process characterisation, it is better to keep the number of parameter levels low and the region of interest broad at first, narrowing as more information is gathered.
4. **Choice of experimental design** – Involves choosing the sample size, selecting an appropriate run sequence, and considering any blocking or randomisation constraints. It is critical to examine the unique experimental design while choosing an experimental design. Some parameter levels are predicted to result in various responses in engineering experiments, and the primary focus is on identifying these significant parameters and determining the amount of the response change. On the other hand, in certain circumstances, the critical concern is to ensure consistency across different parameter levels
5. **Experimenting** – During the experimental phase, extensive monitoring is required to guarantee that the planned method is followed. Trial runs or pilot runs are recommended before the actual experiment; these runs give helpful information and a chance to practice the overall experimental approach. This is also a time to reconsider decisions made earlier in the planning process if necessary.
6. **Statistical analysis of the data** – Statistical methods guarantee objective data analysis outcomes and conclusions. When trials are adequately conceived and carried out, statistical analysis is usually simple. Hypothesis testing, confidence

interval estimates, and empirical modelling are valuable tools for analysing experimental data. Statistical approaches do not show causal effects, but they guide the reliability and validity of the data, allowing for a level of confidence in conclusions. Statistical tools, when combined with engineering expertise and common sense, may offer objectivity to the decision-making process, resulting in reasonable findings.

7. **Conclusions and recommendations** – The experimental process is iterative, encompassing the formulation of hypotheses, the execution of experiments, and the drawing of practical findings. Graphical approaches aid in the presentation of results to others. Confirmation testing and follow-up runs support the results. Well-planned experiments result in good outcomes, whereas ill-planned experiments result in wasted resources and unsatisfactory results.

2.5.3. Fisher's principles of DoE

An English statistician named Sir Ronald Fisher was the father of modern-day experimental design. His book, "The Design of Experiments," includes the knowledge to thoroughly investigate the causal effects of treatments on a response variable of interest. Today, Fisher's principles of DOE are a vital part of any experiment. They help ensure that the study is carried out in a way that is both effective and feasible [54]. The three principles for designing practical experiments are the following:

Randomisation: Process of assigning experimental units to various treatment groups or experimental conditions at random. This aids in the elimination of biases and assures that any observed effects are not the result of systematic variations across groups.

Replication: Replication of an experiment under the same or comparable conditions. Researchers can examine the variety of outcomes and derive more solid conclusions by performing several repeats. Replication also enables the estimate of experimental error and enhances the generalizability of results.

Blocking: This is the classification of experimental units into homogenous subsets or blocks based on known or suspected causes of variability. The influence of these sources can be decreased by blocking, making it more straightforward to detect the effects of the methods under study.

2.5.4. Quantitative vs qualitative approaches

In designing experiments, there are generally two primary approaches [55]:

Quantitative – It is frequently coupled with a more conventional scientific approach of collecting data in an organised, objective manner so that conclusions may be generalised to other people. Quantitative organised designs are based on probabilities or likelihood – they use ‘p’ values, power analysis, and other scientific approaches to assure the rigour and repeatability of the results to different populations. Experimental, quasi–experimental, descriptive, or correlational designs are examples of quantitative designs.

Qualitative – Like the quantitative approach, it takes a systematic approach. When the topic is about life experiences or meaning, the qualitative approach is often favoured. The qualitative approach investigates the complexities, depth, and richness of a specific situation from the perspective of the informants – the person or people who provide the information. The concept that reality is dependent on perceptions and may be different for each individual, frequently changing over time, is at the heart of the qualitative approach. Phenomenological, ethnographic, and grounded theory are some examples of qualitative designs.

2.5.5. Taguchi

The Taguchi method is a technique for design optimisation that offers a systematic and efficient approach widely used in product design and process optimisation. One of the key advantages of using the Taguchi technique is its ability to simplify the experimental plan and study the interaction between different parameters, leading to fewer experiments, reduced time, and lower costs. Taguchi’s method suggests an experiment plan using an orthogonal array; each provides a different combination of parameters and their levels for each experiment. By exploring the entire parameter space with minimal necessary experiments, the method enables researchers to gain insights into the system's behaviour while minimising resource equipment. After conducting the experiments, the primary effect analysis is performed based on the average output value at each parameter level. By leveraging the Taguchi method and its principal effect analysis, researchers can efficiently optimise designs, identify essential parameters, and gain insight into the systems’ behaviour while minimising the cost and time associated with experimentation [56].

2.5.5.1. Signal-to-noise ratio

A measure of robustness is used in Taguchi designs to discover control elements that minimise variability in a product or process by reducing the influence of uncontrolled sources (noise parameters). Design and process parameters that may be regulated are referred to as control parameters. Noise variables cannot be controlled during product manufacture or usage but may be managed during testing. In a Taguhi-designed experiment, the noise parameters must be changed to create variability and then use the findings to determine optimal control parameter settings that make the process or product robust or resistant to noise parameter fluctuation. Higher signal-to-noise ratio values indicate control parameter settings that minimise the impacts of noise components.

Taguchi experiments frequently employ a two-step optimisation approach:

Step 1: Determine the control elements that decrease variability using the signal-to-noise ratio.

Step 2: Identify control parameters that increase the mean closer to the target while having little or no influence on the signal-to-noise ratio. The signal-to-noise ratio quantifies how the response fluctuates about the nominal or goal value under various noise situations [57].

Table 3 - Signal-to-Noise ratios of common interest for optimization of static problems (extracted from [57]*)*

Signal-to-noise ratio	The goal of the experiment	Data characteristics	Signal-to-noise ratio formulas
Larger is better	Maximize the response	Positive	$\frac{S}{N} = -10 * \log\left(\sum\left(\frac{1}{Y^2}\right)/n\right)$
Nominal is best	Target the response and base the signal-to-noise ratio on standard deviations only	Positive, zero, or negative	$\frac{S}{N} = -10 * \log\left(\sigma^2\right)$
Smaller is better	Minimize the response	Non-negative with a target value of zero	$\frac{S}{N} = -10 * \log\left(\sum\left(Y^2\right)/n\right)$

2.5.6. Response Surface Design

2.5.6.1. Central Composite Design

Central Composite Design (CCD) is a method used in DoE. Its primary purpose is to evaluate the effect of variables and their interaction on a response variable. The design features a centre point and axial points, with each parameter adjusted by a different amount (Figure 9). This method makes it easier to estimate components with entirely quadratic effects. However, when dealing with expensive simulations, CCD can be inefficient.

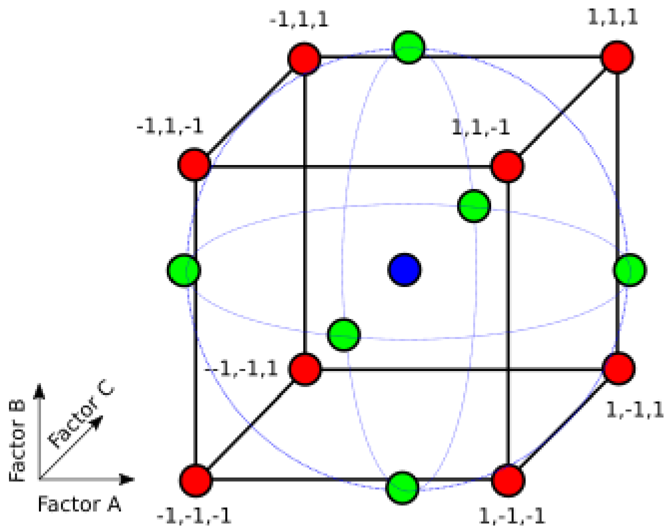

Figure 9 – Central Composite Design (extracted from [58]*)*

2.5.6.2. Box-Behnken

The Box-Behnken design (Figure 10) is a statistical method for optimising analytical procedures by investigating the influence of many parameters at three levels. This approach allows for the examination of the effects of various parameters on the response of interest. Its benefits include its efficiency in reducing the number of trials required, its ability to effectively represent quadratic responses, and its versatility to handle various response variables. There are various advantages to using the Box-Behnken design to optimise analytical procedures. For starters, it dramatically minimises the number of experiments necessary, saving time and resources. Second, the design enables correct modelling of quadratic responses, resulting in a more thorough knowledge of variable interaction. Finally, because it can handle numerous response variables, it is a versatile and effective tool in experimental design and optimisation.

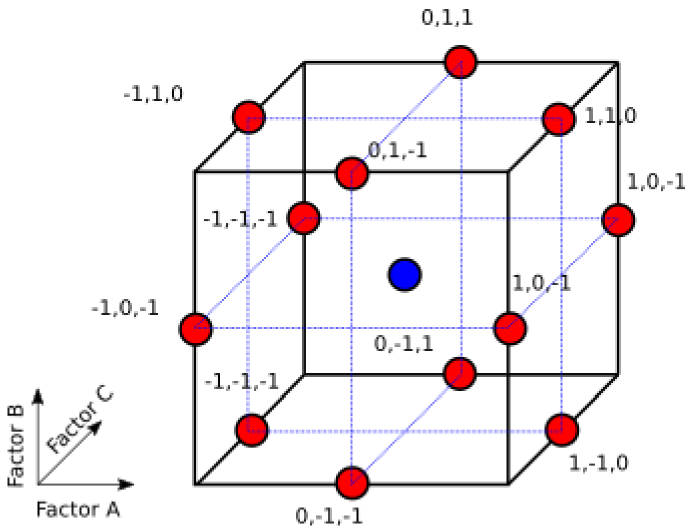

Figure 10 - Box-Behnken (extracted from [58]*)*

2.5.7. Fractional factorial and full factorial design

A fractional factorial design uses fewer experimental runs than a complete factorial design to estimate main effects and specific interaction effects. Only a portion of the potential possibilities of parameter levels are included in the experiment when using a fractional factorial design. When there are many elements on levels in an experiment, or there are few resources available, this method may be more effective and practical. Design generators, which are high-order interactions that split their test runs for a complete factorial into fractions with acceptable attributes, provide the foundation for choosing the subset of factor-level combinations. In experiments, fractional factorial design has various advantages. One of the primary benefits is that they allow researchers to estimate main effects and chosen interaction effects with fewer experimental runs than complete factorial designs. This intelligent use of resources results in time savings, cost savings, and the conservation of essential materials. Another key benefit is that statistical features of fractional factorial designs are known ahead of time. This allows researchers to make educated judgments concerning the design and analysis of the experiment, resulting in robust and dependable results. The capacity to forecast statistical qualities increased overall confidence in the results of the investigation. Furthermore, fractional factorial designs are highly adaptable, as they may be extracted to various experimental situations and pope uses. The use of this design aids in knowledge-based decision-making.

Full factorial design, also known as complete factorial design (Figure 11), is an experimental design that includes all potential parameter-level combinations. They provide various advantages in experiments, beginning with increased full factorial designs that can achieve improved efficiency by encompassing all main effects and interactions, needing fewer experimental runs than alternative designs. Furthermore, full factorial designs allow for a more thorough analysis of all potential combinations of parameter levels, making them helpful in examining complicated connections between parameters. This comprehensiveness improves comprehension of the system under investigation. Another benefit is the more extensive inductive foundation that complete factorial designs give. By considering all parameter combinations, the results gained can be more generalised, allowing for broader conclusions that can be applied to a larger population in a system. However, when working with a high number of variables or levels or when resources are limited, complete factorial designs may not always be the most practical or efficient solution. In such circumstances, fractional factorial design, which allows for selective reduction or parameter combinations, may be more appropriate since it can deliver significant information while conserving resources [59].

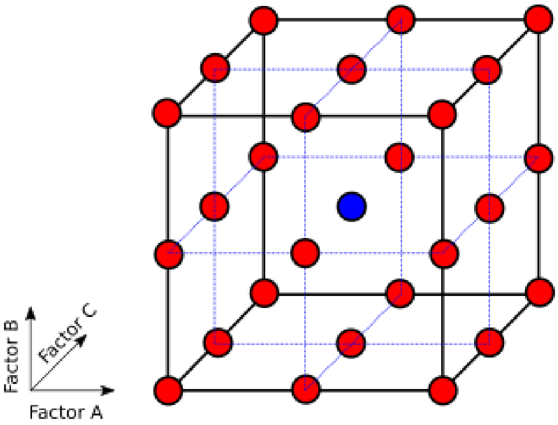

Figure 11 - Full factorial (extracted from [58]*)*

2.5.8. Analysis-of-Variance

Analysis of Variance (ANOVA) is a statistical procedure used to assess for differences between two or more groups, according to [60]. It is a mean difference test. However, the reference to variations is sometimes ignored. ANOVA calculates the common variance for all samples. Whether they come from populations with the same means (null hypothesis) or populations with different means (alternative hypothesis). In ANOVA, the F-test statistic is determined by the ratio of these two estimated variances.

In design experimental research, ANOVA is widely used to compare the means of two or more groups. It is frequently used to determine if observed variations in sample averages are attributable to random variability or are statistically significant. ANOVA compares the null hypothesis that all population means are the same to the alternative that at least two are not. ANOVA tests all mean differences at once, rather than one pair at a time, as a t-test does. This is beneficial because running numerous t-tests raises the incidence of type 1 error – the chance of a ‘false positive’ when one wrongly believes the samples are from populations with different means – but using ANOVA to test all mean differences at once does not.

An ANOVA summary table (Table 4) contains the p-value and the effect size. The p-value is the likelihood of receiving a test statistic as severe as the one observed if the null hypothesis is true. If the p-value is less than the significance level (typically 0.05), the null hypothesis is rejected, and a statistically significant difference between the groups is determined. The effect size is a measure of how much of the variance in the dependent variable is explained by the independent variable(s).

Table 4 - ANOVA summary table

Source of Variation	Sum of Squares	Degrees of Freedom	Mean Squares (MS)	F
Within	$SSW = \sum_{j=1}^{k}\sum_{j=1}^{l}(X - \overline{X}_J)^2$	$df_w = k - 1$	$MSW = \frac{SSW}{df_w}$	$F = \frac{MSB}{MSW}$
Between	$SSB = \sum_{j=1}^{k}(\overline{X}_J - \overline{X})^2$	$df_b = n - k$	$MSB = \frac{SSB}{df_b}$	
Total	$SST = \sum_{j=1}^{n}(\overline{X}_J - \overline{X})^2$	$df_t = n - 1$		

ANOVA presupposes that the observed data are from regularly distributed populations with equal variances. When evidence contradicts one of these assumptions, researchers' findings may be deceptive. ANOVA is classified into three types: one-way ANOVA, two-way ANOVA, and repeated measures ANOVA. When there is just one independent variable, one-way ANOVA is employed, whereas two-way ANOVA is used when there are two independent variables. When the same subjects are assessed many times under various settings, repeated measures ANOVA is employed.

2.6. Geometric and dimensional tolerances

Geometric and dimensional tolerances are not merely theoretical concepts but indispensable tools for achieving accuracy and reliability in this innovative manufacturing process. By mastering these concepts, it’s possible to create 3D-printed objects with precision, consistency, and quality that meet or exceed the most stringent requirements of today’s rapidly evolving industries.

The design and production of products have been entirely transformed by additive manufacturing. It enables precise and effective creation of intricate geometries and customised components. It is critical to follow standardised dimensions and tolerances for 3D-printed parts to integrate seamlessly into existing assemblies or meet specific specifications. DIN EN ISO 286-1 is used in engineering. International tolerances for linear dimensions and fits are specified in DIN EN ISO 286-1, which is a member of the ISO 286 series. The interoperability and dependability of printed parts can be improved by using this standard in 3D printing, which is frequently used in conventional manufacturing processes. Consistent dimensional accuracy is one of the main benefits of using DIN EN ISO 286-1 in 3D printing. Due to variables like material properties, the printing process, and environmental parameters, 3D printers frequently produce parts with variations. Engineers and designers can reduce these variations and achieve the desired accuracy by following the specified tolerances.

Additionally, DIN ISO 286-1 makes it possible to create parts that perfectly fit together. Tight tolerances may be essential to ensuring efficient component interactions in complex assemblies. By using the ISO 286-1 series’ standardised fits, connecting parts are guaranteed to align correctly, lowering the possibility of functional problems and improving the final product’s overall dependability. The compatibility with traditional manufacturing techniques is another significant advantage of using this standard for 3D printing. Traditional machining techniques are still used in many industries, and seamless integration and replacement are made possible by having 3D-printed components that adhere to the exact tolerances of machine parts. Engineers can optimise the design and production processes by combining the benefits of both manufacturing techniques thanks to this compatibility.

Implementing DIN EN ISO 286-1 in 3D printing presents some difficulties, however. The selection of materials is one of the critical factors. Not all materials may be suitable for meeting the required tolerances because different materials with unique properties are used in different 3D printing technologies. Engineers must carefully choose materials that can be produced with the necessary accuracy without sacrificing the finished part’s mechanical qualities. Moreover, dimensional accuracy can be impacted by the printing process. Factors like layer adhesion, warping, and thermal stresses can cause variations from the intended dimensions. To minimise these effects and guarantee compliance with the standard calibration, meticulous control of the printing parameters is crucial.

2.6.1. Geometrical product specifications (GPS): Part 1 - Dimensional tolerances

Dimensional tolerances are destined to limit dimensional errors in part manufacturing. Here are some terms and definitions (Table 5) according to ISO 286-1[61]:

Table 5 - Terms and definitions

Terms	Definitions
Element	"geometrical shape defined by a linear or angular dimension which is a size"
Shaft	"external feature of the size of a workpiece, including external features of size which are not cylindrical"
Hole	"internal feature of the size of a workpiece, including internal features of size which are not cylindrical"
Tolerance	"a tolerance is the difference between the upper limit of size and the lower limit of size."
IT	"Standard tolerance grades designated by the letters IT, followed by the grade number, e.g., IT7."

According to Lieneke et al. 2016 [4], the values of tolerance for each IT class associated with additive manufacturing, considering FFF, are indicated in Table 6. This table allows us to acquire the value of tolerance and the position of the tolerance zone until 400mm of dimension.

Table 6 - IT classes and positions of the tolerance zone according to the fit system of DIN EN ISO 286-1 (extracted from [4]*)*

Dimension [mm]	IT class			Position of tolerance zone		
	x	y	z	x	y	z
3	IT14	IT14	IT14	j	k	r
6	IT13	IT14	IT14	j	j	k
10	IT13	IT13	IT13	j	j	>zc
18	IT13	IT13	IT12	j	j	zc
30	IT12	IT12	IT13	J	j	y
50	IT12	IT12	IT12	m	j	z
80	IT12	IT12	IT12	n	j	r
120	IT10	IT11	IT10	u	f	t
180	IT10	IT11	IT11	u	f	u
250	IT10	IT11	IT11	v	d	v
315	IT09	IT11	IT11	v	e	t
400	-	-	IT11	-	-	r

Lieneke et al. 2016 [4]. The investigation aimed to analyse the dimensional accuracy of additive manufacturing processes, specifically FDM, and deduce dimensional tolerance values. Lieneke used DIN EN ISO 286-1 to classify the dimensional tolerances of FDM parts, using the minimum and maximum values of the measured local dimensions in the x, y, and z alignments. According to the classification, the FDM process reaches IT classes between IT09 and IT14 under the specified boundary conditions. By the upper and lower deviation for the external dimension, the position of the tolerance zone was also sorted into the DIN EN ISO 286-1 fit system (Table 7).

Table 7 - Overview of IT classes for various manufacturing processes (extracted from [4])

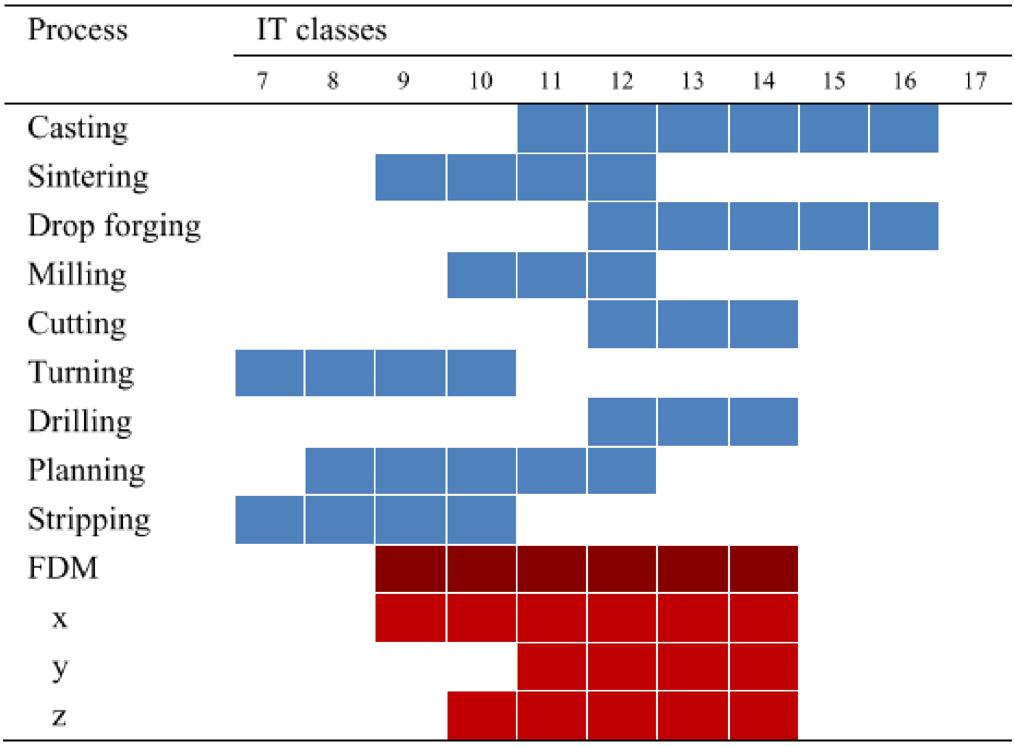

2.6.2. Geometrical product specifications (GPS): Part 2 – Geometrical tolerance

Achieving precision often involves an in-depth understanding of geometric tolerances, a set of specifications that regulate the form, orientation, and position of features and parts. These tolerances are fundamental in various engineering and manufacturing processes, as in FFF, and they play a crucial role in ensuring that components meet the design specifications [62]. This introduction sets the stage for focusing on five essential geometric tolerances:

Flatness - This is a tolerance that controls the variation in the Flatness of a surface or feature. It guarantees that the extracted (actual) surface is contained between two parallel planes within a specified tolerance zone. The distance between the planes is equal to or less than the value of the specified tolerance. The planes' orientation should be set so that the most significant distance between them is as little as possible (Figure 12).

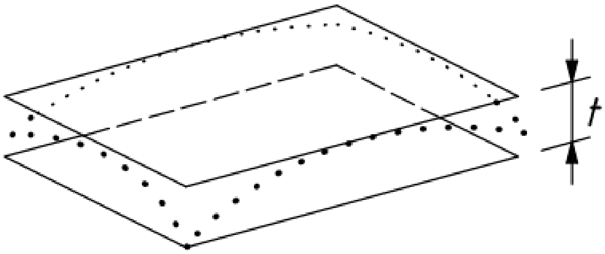

Figure 12 - Flatness tolerance (extracted from [62]*)*

Like dimensional tolerances, there are also geometric tolerances. There are three general classes of geometric tolerances (designated with H, K and L) according to the norm ISO 2768. Geometric tolerances are appropriate to all geometric characteristics of elements except Cylindricity, line contour and surface, angularity, and concentricity.

In Table 8, the general tolerances are presented for straightness and flatness. For flatness, the length is the longest side of the rectangle.

Table 8 - General tolerances for straightness and flatness according to ISO 2768

STRAIGHTNESS AND FLATNESS

Ranges in nominal lengths in mm	Tolerance class		
	H	K	L
up to 10	0.02	0.05	0.1
over 10 up to 30	0.05	0.1	0.2
over 30 up to 100	0.1	0.2	0.4
over 100 up to 300	0.2	0.4	0.8
over 300 up to 1000	0.3	0.6	1.2
over 1000 up to 3000	0.4	0.8	1.6

Parallelism - This is the tolerance that controls the alignment of two defined features or datum planes in a parallel manner. It ensures that a surface, line, or axis remains parallel to a specified datum plane or axis within a tolerance zone (Figure 13).

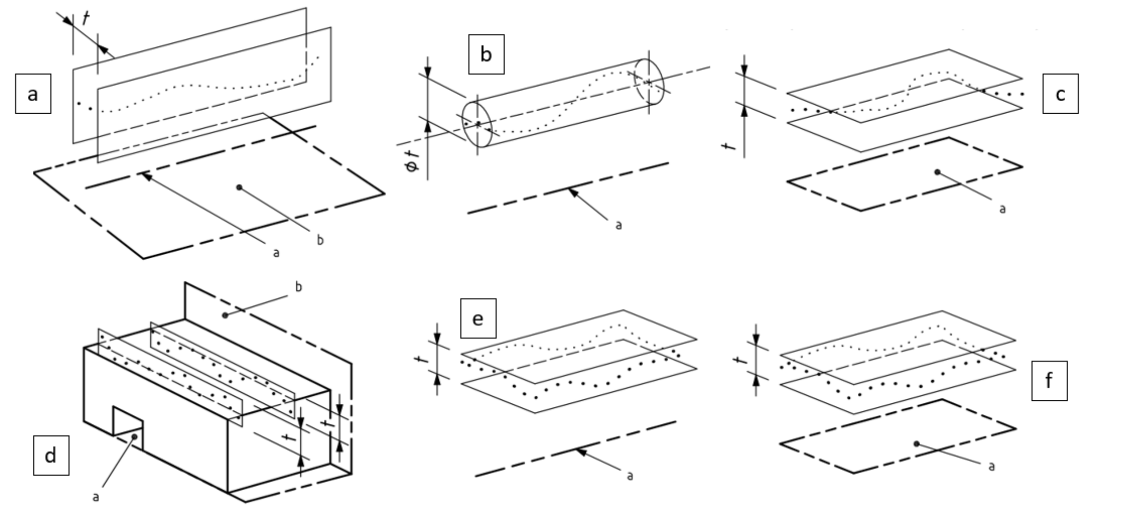

Figure 13 – a) - Parallelism tolerance of a line related to a datum system; b) - Parallelism tolerance of a line related to a datum line; c) – Parallelism tolerance of a line related to a datum line; d) – Parallelism tolerance of a surface related to a datum plane; e) – Parallelism tolerance of a surface related to a datum line; f) – Parallelism tolerance of a surface related to a datum plane (extracted from [62]*)*

The general tolerance for parallelism is equal to the more significant value of dimensional tolerance or the tolerance of straightness/flatness. The most significant value of both elements should be considered the referential.

Perpendicularity - Determines the connection between two reference features or datum planes. It ensures that a surface, line, or axis maintains a 90-degree orientation concerning a datum plane or axis within a specified tolerance range (Figure 14).

a)

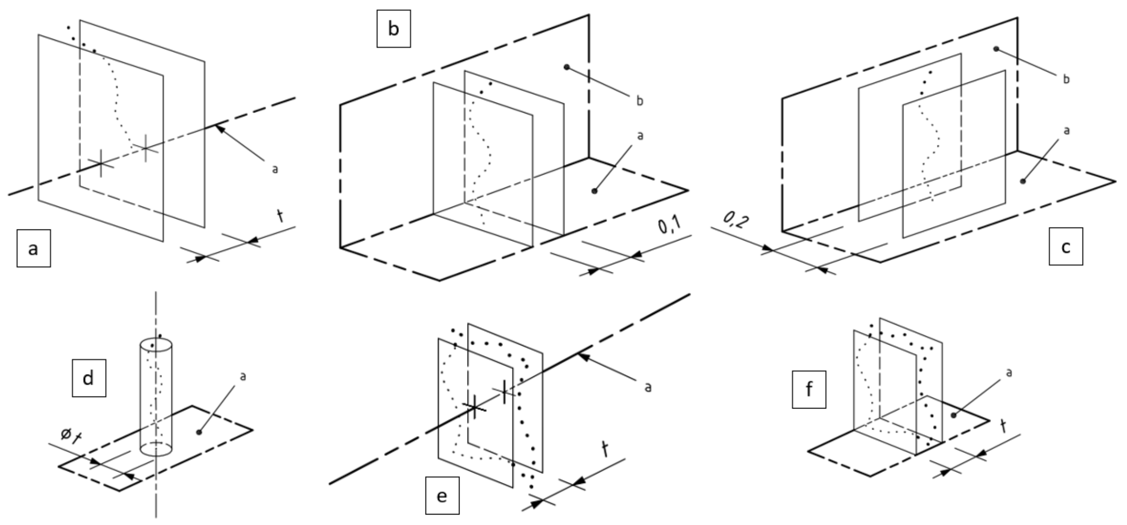

Figure 14 – a) - Perpendicularity tolerance of a line related to a datum line; b) and c) - Perpendicularity tolerance of a line related to a datum system; d) – Perpendicularity tolerance of a line related to a datum plane; e) – Perpendicularity tolerance of a surface related to a datum line; f) – Perpendicularity tolerance of a surface related to a datum plane (extracted from [62]*)*

The general tolerances for perpendicularity are presented in Table 9. The longest of both sides is considered referential, being the determined value of the tolerance for the nominal length of the shorter side.

Table 9 - General tolerances for perpendicularity according to ISO 2768

PERPENDICULARITY

Ranges in nominal lengths in mm	Tolerance class		
	H	K	L
up to 100	0.2	0.4	0.6
over 100 up to 300	0.3	0.6	1
over 300 up to 1000	0.4	0.8	1.5
over 1000 up to 3000	0.5	0.8	2

Cylindricity - The cylindricity of a single tolerance feature is considered accurate when it is restricted between two coaxial cylinders and the difference in radii is equal to or less than the stipulated tolerance value. The axes of these cylinders and their radii must be set so that the difference in radii between the two coaxial cylinders is as tiny as possible (Figure 15).

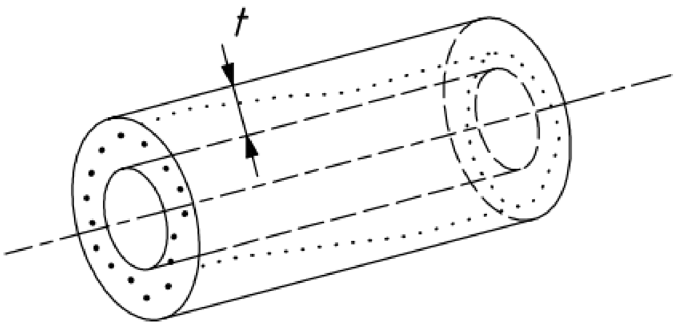

Figure 15 – Cylindricity (extracted from [62] *)*

Is not specified the general tolerances for cylindricity. However, there is run out general tolerances, as shown in Table 10.

Table 10 - General tolerances for cylindricity according to ISO 2768

RUN-OUT

Tolerance class		
H	K	L
0.1	0.2	0.5

Concentricity and Coaxiality - Concentricity is the tolerance that controls how two or more features, such as cylinders, spheres, or circles, align. It ensures that the extracted (actual) centre of the inner feature is within a given tolerance zone of the centre of the outer feature. A circle or cylinder with a specified diameter or difference in radii defines the tolerance zone. Coaxiality is the tolerance that controls the coaxial orientation of two features or datum planes. It assures that a cylinder's extracted (actual) median line is inside a cylindrical zone of as defined diameter and that the cylinder's axis corresponds with the datum axis or straight line within the provided tolerance zone (Figure 16).

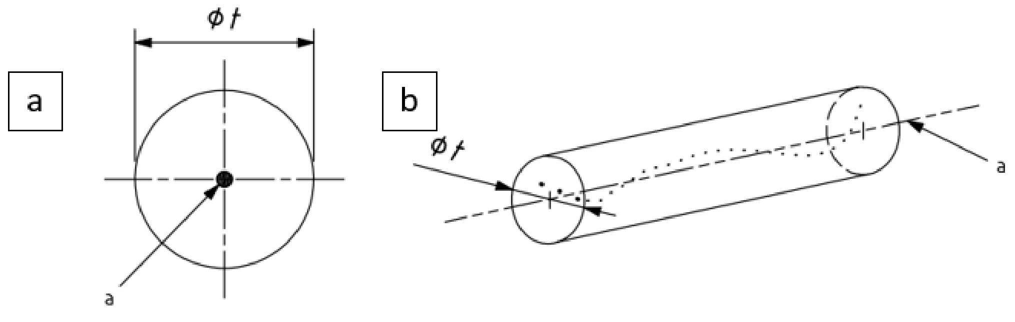

Figure 16 - a) Concentricity tolerance of a point; b) - Coaxiality tolerance of an axis (extracted from [62]*)*

Chapter 3

Materials and methods

3.1. Introduction

The initial research paper, “A study on the effect of layer thickness and infill density on Geometric Tolerance in Fused Deposition Modelling” [20] paved the way for later studies. Mateus Serra’s thesis was crucial in furthering this subject because of his earlier knowledge of DIGIMAT AM and numerical simulation, which emphasised the complexity involved in FFF [63]. Serra’s research resulted in the finding of the publication “Taguchi-based process optimisation for dimensional and tolerance control in fused deposition modelling” [5], which used the Taguchi method and design of experiments. Thanks to the insights gathered from the previous studies, this extensive investigation dug into many aspects impacting their 3D printing process.

ABS was the chosen material due to its extensive use across the industry. ABS is more prone to warping during printing than other materials, but its versatility in various applications makes it an excellent material to investigate.

The preliminary stage was crucial since it required experimental confirmation of given parameters and settings. This was an essential stage to decrease inconsistencies and inefficiencies in the process. In this stage, Digimat AM was introduced, as well as the part geometry, enhancing the phase by providing advanced insights into material behaviour. Subsequently, 27 different printing profiles were generated according to the Taguchi method. These profiles were then numerically simulated using DIGIMAT. Nuno Pedro, a bachelor's student of mechanical engineering from IPS who was doing an internship at Solutions for Metrology company, gathered the 27 warped geometries and digitally measured them with metrology software. This software matched the warped geometries with the leading CAD geometry and calculated deviations based on the required parameters. These deviations are the data that will be analysed further to determine the influence of specific parameters. A flowchart is presented for better interpretation (Figure 17):

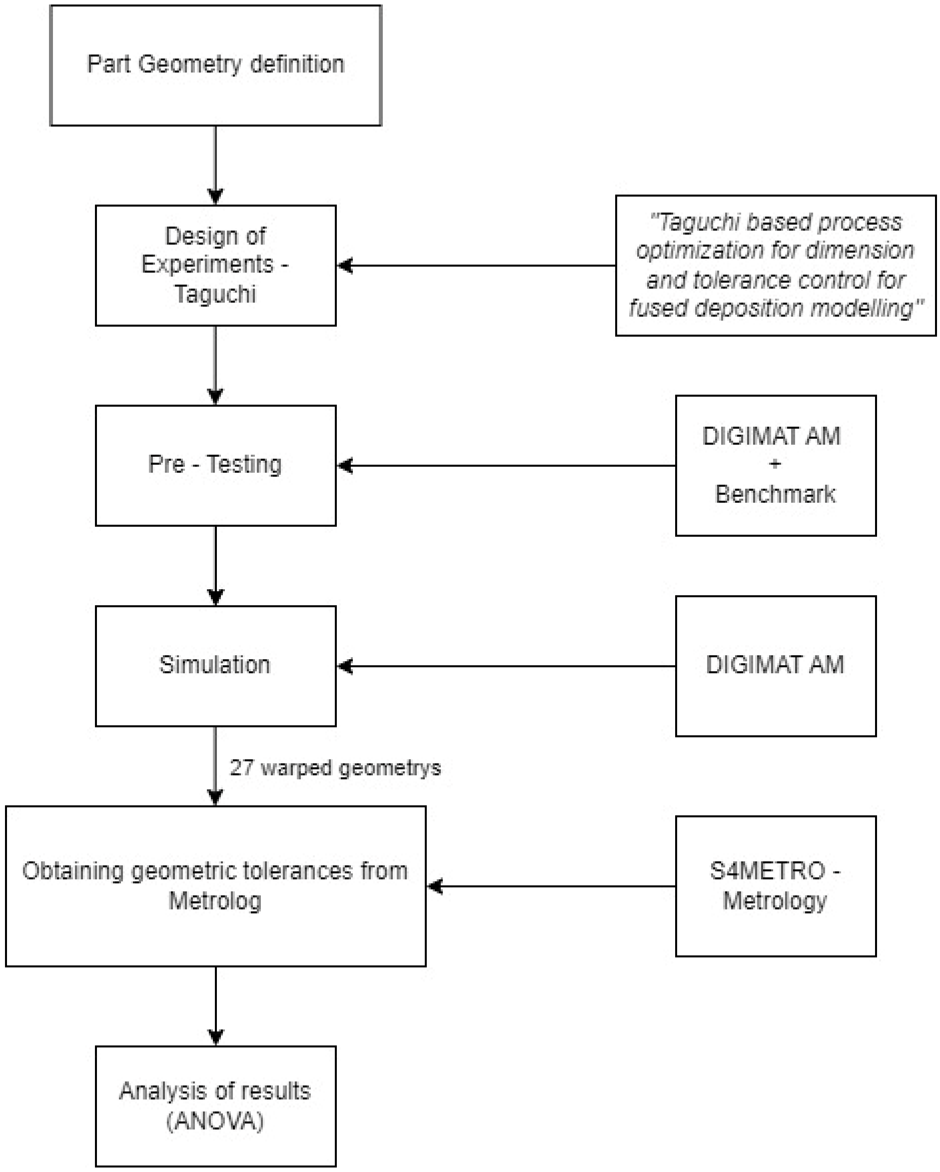

Figure 17 – Flowchart of the investigation

3.2. Design of Experiments

3.2.1. Parameters and levels

The levels chosen for each parameter result from a mix of design requirements, material properties, and production constraints. Here's a summary for selecting each group:

A: Chamber temperature (ºC)

Level 1 (23ºC): The level is considered room temperature. This situation might cause uneven cooling of the ABS material, resulting in warping or poor adhesion between layers. This could manifest as minor warping in the printed part's geometry.

Level 2 (80ºC): At 80ºC, the ABS filament is expected to have a more stable environment that adheres and cools down. This can lead to enhanced interlayer adhesion and a lower risk of warping. The greater temperature helps to keep the print environment constant. This leads to improved geometrical accuracy and smoother surface finish, as there's less probability of warping.

Level 3 (120ºC): A temperature of 120ºC in the chamber gives an even more regulated atmosphere. This considerably reduces the possibility of warping, and the ABS material is expected to cool consistently and achieve highly accurate geometrical properties.

B: Infill density (%)

Level 1 (20%): A low infill density may result in poorer structural integrity, potentially affecting geometrical accuracy, and it's worth investigating how this impacts the overall geometrical properties of the printed part.

Level 2 (60%): A mid-range infill density that may indicate a trade-off between strength and material usage, contributing to better structural stability and, thus, improved geometrical accuracy.

Level 3 (100%): A complete infill gives the most remarkable structural stability and material density, enhancing overall dimensional stability and geometrical accuracy.

C: Layer height (mm)

Level 1 (0.05mm): Small layer height that provides excellent detail and precision is crucial for achieving intricate geometrical details and smooth surfaces.

Level 2 (0.15mm): This middle layer height balances detail with print speed, resulting in good geometrical accuracy.

Level 3 (0.25mm): This rough layer height may result in significantly diminished detail but maintains high overall geometrical accuracy. It can be chosen once speed is prioritised over other parameters.

D: Extrusion temperature (ºC)

Level 1 (230ºC): Lower Extrusion Temperatures may result in somewhat less exact material deposition, which may impair geometric accuracy. This level was chosen to understand better how lower temperatures affect geometric accuracy.

Level 2 (250ºC): The filament flows effectively at this temperature, ensuring precise deposition and high dimensional stability in most applications. This is a typical ABS temperature and should provide reliable geometrical results.

Level 3 (270ºC): Higher Extrusion Temperatures allow better control over filament flow, which is expected to result in higher geometric accuracy, specifically in complicated geometries or more sophisticated features.

E: Print speed (mm/s)

Level 1 (30mm/s): Slower print speed allows more precise motions, improving geometrical accuracy and surface smoothness. This level is appropriate for applications requiring fine details or great accuracy.

Level 2 (60mm/s): A balanced speed preserves high accuracy while boosting efficiency. It's appropriate for most tasks that need a decent balance between speed and precision.

Level 3 (90mm/s): This is not the better option, but it can still produce adequate geometrical precision. It is more appropriate for situations where speed is crucial, although geometric accuracy may be affected.

F: Infill strategy

Level 1 (Rectilinear): The rectilinear infill strategy is made of straight lines that form a grid-like structure. This predictability can produce more uniform and regulated geometries within the printed part's interior. A rectilinear pattern's straight lines offer uniform support to the top levels. This can aid in preserving geometric accuracy, particularly for features that rely on support structures. The rectilinear infill can help parts with stacked or layered components. The linear pattern helps to preserve exact geometric alignments by complementing the layer-by-layer construction.

Level 2 (Grid): Grid infill produces a network of intersecting lines, balancing structural support with material conservation. This can improve the printed part's overall geometric accuracy. Grid infill may take less time to print than the full honeycomb, providing excellent geometrical accuracy. This can be useful for sections with complicated geometry that do not require maximal infill density. The crisscrossing pattern of grid infill can offer sturdy support for overhanging features, improving geometrical accuracy for such parts.

Level 3 (Honeycomb): The honeycomb design uniformly distributes material, improving the part's overall stability and geometrical accuracy. This is especially useful for more extensive or more complicated geometries. Honeycomb infill is very effective for parts with complex interior geometries or fine details. It offers strong support for such features.

Table 11 - Parameters and levels

Parameters	**Level 1**	**Level 2**	**Level 3**
A: Chamber temperature (°C)	23	80	120
B: Infill density (%)	20	60	100
C: Layer height (mm)	0.05	0.15	0.25
D: Extrusion temperature (°C)	230	250	270
E: Print speed (mm/s)	30	60	90
F: Infill strategy	Rectilinear	Grid	Honeycomb

3.2.2. Taguchi method

In experimental design, the Taguchi method plays a vital role. Using the Minitab software, we can quickly create a Taguchi design, and the software carefully makes the matrix design based on several parameters and levels. Taguchi's method uses an orthogonal array (OA) to identify the control level combination for each experiment. An L27 OA is used to evaluate the impacts of six parameters, each with three levels of control, by Taguchi's method design. The L27 OA comprises twenty-seven rows, each indicating a different experiment with different control levels for the individual parameters.

Table 12 - L27 orthogonal array, level control for each experiment

Parameters from Table 2						
Exp.	**A**	**B**	**C**	**D**	**E**	**F**
TGC01	1	1	1	1	1	1
TGC02	1	1	1	1	2	2
TGC03	1	1	1	1	3	3
TGC04	1	2	2	2	1	1
TGC05	1	2	2	2	2	2
TGC06	1	2	2	2	3	3
TGC07	1	3	3	3	1	1
TGC08	1	3	3	3	2	2
TGC09	1	3	3	3	3	3

TGC10	2	1	2	3	1	2
TGC11	2	1	2	3	2	3
TGC12	2	1	2	3	3	1
TGC13	2	2	3	1	1	2
TGC14	2	2	3	1	2	3
TGC15	2	2	3	1	3	1
TGC16	2	3	1	2	1	2
TGC17	2	3	1	2	2	3
TGC18	2	3	1	2	3	1
TGC19	3	1	3	2	1	3
TGC20	3	1	3	2	2	1
TGC21	3	1	3	2	3	2
TGC22	3	2	1	3	1	3
TGC23	3	2	1	3	2	1
TGC24	3	2	1	3	3	2
TGC25	3	3	2	1	1	3
TGC26	3	3	2	1	2	1
TGC27	3	3	2	1	3	2

3.3. Preliminary phase

3.3.1. Numerical simulation

A mathematical model represents or abstractly interprets real-world occurrences so that they may be analysed and calculated [64]. It systematically describes the underlying physical reality, allowing us to acquire insights and make mathematical predictions. Using computers to calculate and approximate the solutions of these mathematical models is known as numerical simulation. It enables replicating complicated systems' behaviour, making it an effective tool for comprehending and forecasting real-world occurrences. Using numerical simulation, we may explore numerous possibilities and watch how the system changes over time, giving crucial knowledge that would be difficult or impossible to gather using analytical methods alone by bridging the theoretical knowledge and practical applications gap by integrating mathematical modelling and numerical simulation [64]. This multidisciplinary method applies mathematics, computer science, and engineering principles to solve real-world issues and make educated judgments in various topics ranging from physics and engineering to economics and environmental studies.

3.3.2. Finite element method

The Finite Element Method (FEM) is a numerical approach used to solve complicated problems controlled by partial differential equations (PDEs) in engineering, physics, and other scientific areas. It offers a fast method for estimating solutions to these equations over complicated geometries and domains. FEM works by dividing the original issue domain into smaller, simpler subdomains known as finite elements. Each element is defined by a set of equations that explain its behaviour, and these equations combine to form a mesh that spans the whole domain. The core of FEM is the interpolation of the unknown solution within each element using basis functions such as polynomials, which allows us to describe the issue as an algebraic equation system. FEM will enable engineers and scientists to acquire approximate solutions to a wide range of issues, including structural analysis, heat transport, fluid dynamics, electromagnetics, and more, by discretising the domain and solving algebraic equations. It is beneficial for problems with irregular geometries or complicated boundary conditions, for which analytical solutions are frequently infeasible. FEM's capacity to adaptively modify the mesh is one of its key characteristics, resulting in improved accuracy in essential locations and lower computing costs in less critical places. This adaptive refinement is advantageous when addressing problems with steep slopes or singularities. Furthermore, it has become a foundational component of computer-aided engineering (CAE) software, allowing engineers to model and optimise real-world systems before prototypes, lowering costs and increasing efficiency. Despite its benefits, FEM is not without its drawbacks. The correctness of the answer is mainly dependent on the element type, mesh density, and issue formulation. Engineers must carefully choose appropriate elements and adjust the mesh to acquire trustworthy results. Furthermore, large-scale FEM model solution requires substantial computer resources and can be time-consuming, necessitating the use of powerful computing platforms and parallel processing techniques.

3.3.3. e-Xstream Digimat-AM software

e-Xstream Engineering provides Digimat Software, a multi-scale material modelling technology that speeds the development of composite materials and structures. Digimat performs extensive microscopic materials examinations and generates micromechanical models of multi-scale coupling of micro and macroscopic features. By combining processing simulation and structural finite element analysis, it is possible to create more predictive models that consider how processing circumstances affect the end product's performance.

Digimat AM is a robust process simulation tool concluded into Digimat software. It enables simulations for various additive manufacturing (AM) methods, including FFF, FDM, SLS, and continuous filament fabrication (CFF), for unfilled and reinforced materials. Before beginning the printing process, engineers can correctly anticipate component warpage, residual stresses, and process-induced microstructure. The software capabilities can be used to optimise printing settings to increase productivity and achieve optimal end component performance. Digimat-AM's simulations considerably lower the requirement for time-consuming trial and error cycles, streamlining the procedure. Digimat-AM enables engineers to make educated decisions for high-precision printing by bridging the gap between the printing method, material attributes, and component performance [65].

3.3.3.1. General workflow

These four steps can be used in a general approach to tackle the multiscale thermomechanical simulation problem of additive manufacturing of polymers and composites. However, the program allows for various application-oriented workflows [66]. The four steps are the following:

Definition – Select the desired printing process and a specific printer and describe the manufacturing component. The piece is defined by its geometry and material.

Manufacturing – Describe how the component is manufactured. Several inputs must be inserted, such as positioning, the toolpath (FFF and FDM), the warpage compensation strategy, the manufacturing steps order, and process parameters depending on process type.

Simulation – Finite element analysis simulation. Voxel meshing of the geometry is proposed, and solution methods can be chosen as material model parameters are adjusted. Submit and monitor.

Results – Provides post-simulation results, such as field visualisation of displacement and stresses, analysis of warpage indicator, visualisation of a warped shape and cut models, history plot, custom reference planes, and export of simulation result (warped geometry, residual stresses, etc.) [66].

3.3.3.2. Specific workflows

Engineers can do complete analysis and optimisation of the AM process using a variety of configurable workflows thanks to the software's advanced capabilities [66]. The software provides the following usual workflows:

Workflow 1: predict warpage and residual stresses for FFF

This workflow (Figure 18) incorporates critical elements such as process parameters and material choices to give relevant insights. By modelling these interactions, engineers can test whether a component can be physically printed with controlled warpage and residual stresses. This guarantees that the additive manufacturing process can be optimised to manufacture parts of the desired quality and performance.

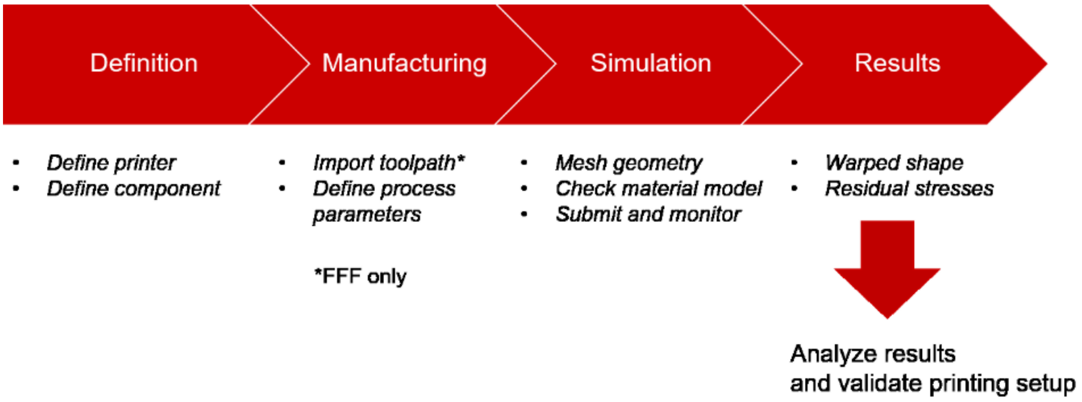

Figure 18 – Workflow to predict warpage and residual stresses for FFF (extracted from [66]*)*

Workflow 2: optimise process parameters

The iterative workflow (Figure 19) entails many runs over the production step parameters to fine-tune the additive manufacturing process. This involves changing process parameters (such as temperature, printing speed, and layer height) and toolpaths (for FFF or other AM processes). Each run includes a fresh simulation that considers the modifications made to the process parameters. The simulation results are then compared to the initial configuration baseline findings.

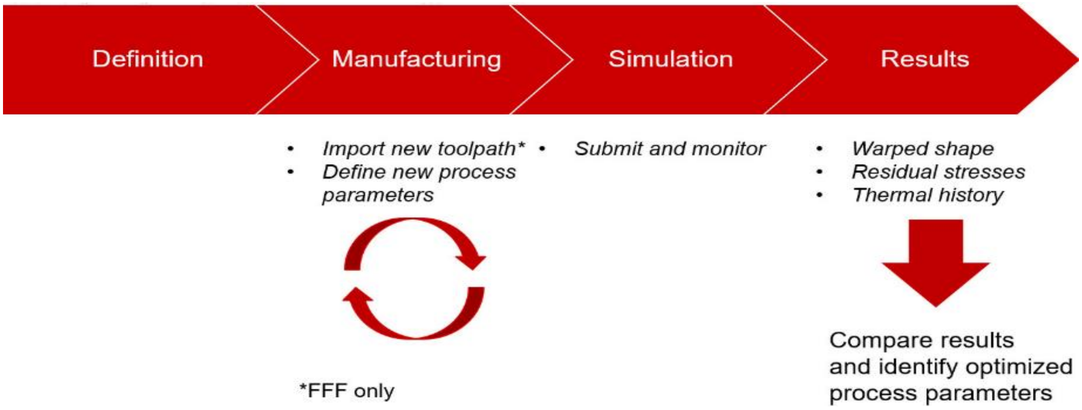

Figure 19 – Workflow to optimise process parameters (extracted from [66]*)*

To perform a numerical simulation in DIGIMAT software, there are seven essential tasks to follow:

Define printing parameters - Printing parameters, such as chamber temperature, infill density, layer height, extrusion temperature, print speed, and infill strategy, are crucial parameters that directly affect the outcome of the AM process. These parameters significantly impact material behaviour, adhesion, structural integrity, and the overall quality of the printed object.

Load the design (.stl file) - The .stl file is a digital representation of the object that is intended to be created. Loading the design is the first step in any AM process simulation, as it provides the geometry on which all subsequent analyses will be based.

Load the toolpath (G-code file) - The g-code file contains precise instructions for the 3D printer, guiding its movements and actions to create the object layer-by-layer. By including the toolpath, the simulation accurately mimics the actual printing process.

Define material properties - Material properties refer to thermal conductivity, specific heat capacity, and Young's modulus. These properties significantly impact how a material reacts to the thermal and mechanical stresses during the AM process. It is essential to represent these properties to obtain realistic simulation results accurately.

Voxelizing the geometry - Voxelization converts a continuous digital model into discrete units called voxels. This mirrors the layer—by—layer deposition process. The discrete representation enables accurate simulation of material behaviour and thermal distribution during printing.

Solving the FEA - FEA is used to predict and analyse the printed object's structural, thermal, and mechanical behaviour. It allows for assessing stress distribution, thermal gradients, and potential distortions, providing valuable insights into the object's performance under different conditions.

Processing the result - post-simulation processing is essential for interpreting the data generated by the FEA. This step involves analysing parameters. It helps validate the simulation, identify potential issues, and optimise printing parameters for improved results.

3.3.4. Part geometry

The artefact used in this work was based on the study of Pombinha et al. (2018) [20]. The part was developed with the inspiration of a benchmark used for the performance characterisation of metal machining tools, commonly known as the circle-diamond-square. The simplicity of circle-diamond-square parts influences the part's design displayed in Figure 20. It has several features that make measuring straightness and angularity easier. It has features for evaluating surface flatness on the xy, zx, and zy planes. The extruded cylindrical tube measures tolerances for circularity, concentricity, and cylindricity. Notably, at half its thickness, the through hole transitions from a circular to a square form, allowing assessment of interior measurement of straightness and flatness. cylindricity, perpendicularity, concentricity, flatness, and parallelism are the geometric tolerances that will be tested on this benchmark part (Figure 21).

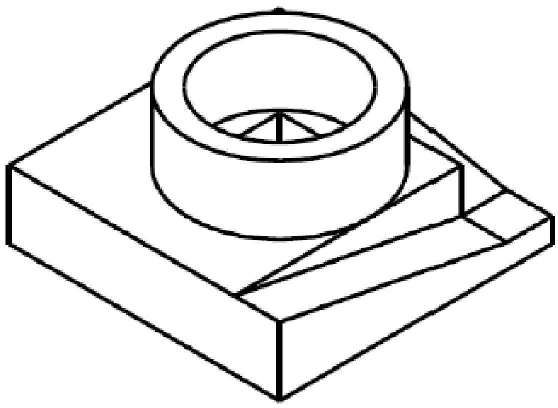

Figure 20 - Isometric view of the benchmark part (extracted from [14])

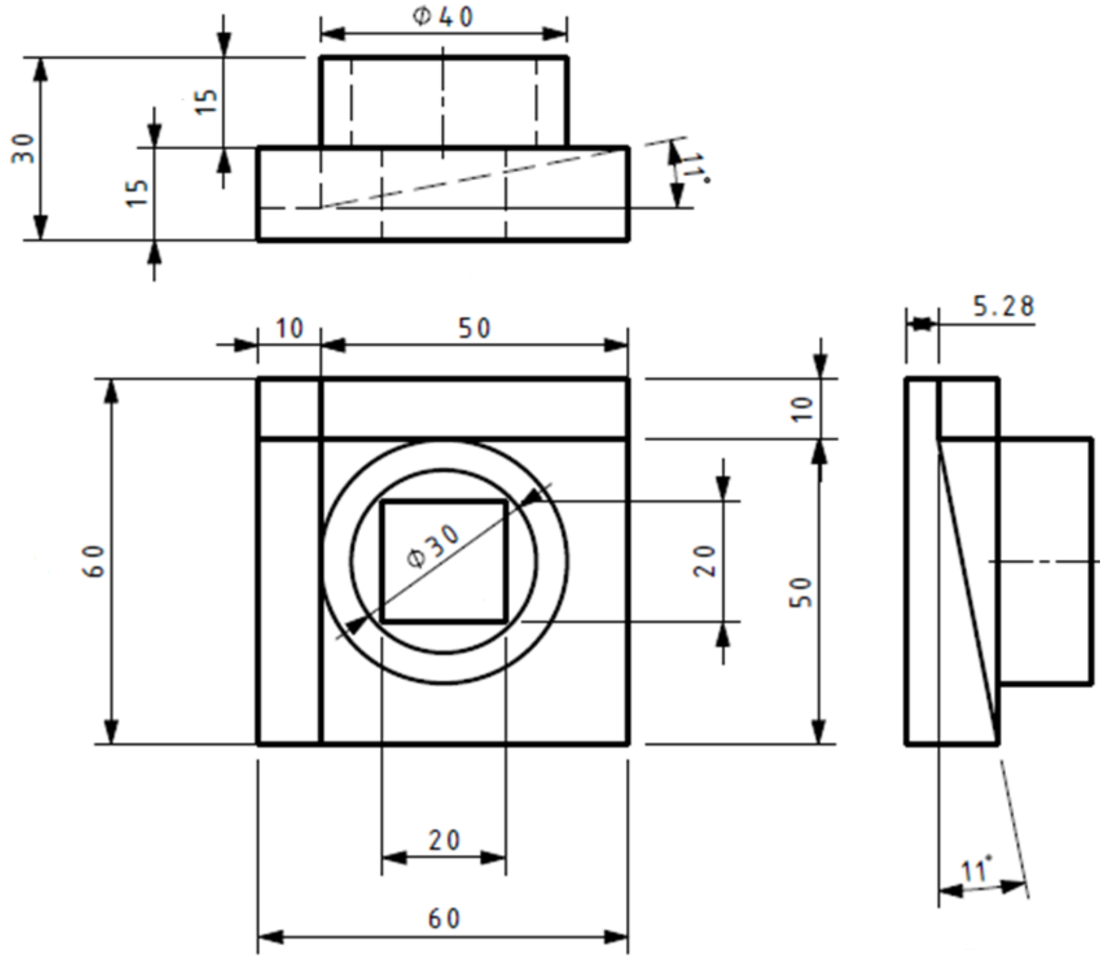

Figure 21 – Benchmark linear dimensions (mm)

3.3.5. Pre-testing

Before entering the simulation phase, a preliminary stage was essential to understand the software’s operation and refine the 3D printing process using ABS. Drawing from Mateus Serra's prior experiences, a comparable table was created for conducting pre-tests. The one that yielded the most favourable outcomes was selected from Serra’s work and used as a standard for pre-testing.

During the preliminary stage, specific parameters remained fixed, ensuring a stable and consistent environment. These constants included:

Table 13 – Fixed parameters

Material	Extrusion temperature [º C]	Bed temperature [º C]	Chamber temperature [º C]	layer height [mm]	Infill density [%]	Speed [mm/s]	Cooling time [s]
ABS	250	100	100	0,15	20	60	120

In contrast, the following were subjected to different values in each test run:

- Voxel size [mm];
- Manufacturing mesh [mm];
- CPU time [s];
- Maximum displacement [mm].

The primary objective was identifying the optimal configuration where these four variable parameters could harmoniously work together to achieve the best results.

Initially, one factor that was inadvertently overlooked was the geometric resolution inside the CAD software. However, as the preliminary stage advanced, it became clear that different geometries produced different results, significantly impacting the maximum displacement. Following a series of tests and meticulous considerations, it was found that the ideal resolution setting was a geometric configuration characterised by specific angle geometry (SAG) with a 0,001 mm parameter and a surface tessellation engine parameter (STEP) of 0,75 mm.

It is important to note that SAG and STEP are frequently referred to as tessellation parameters. SAG specifies the maximum allowable distance between a bar and the object to be tessellated, whereas STEP specifies the maximum permissible length of a bar during the tessellation process.

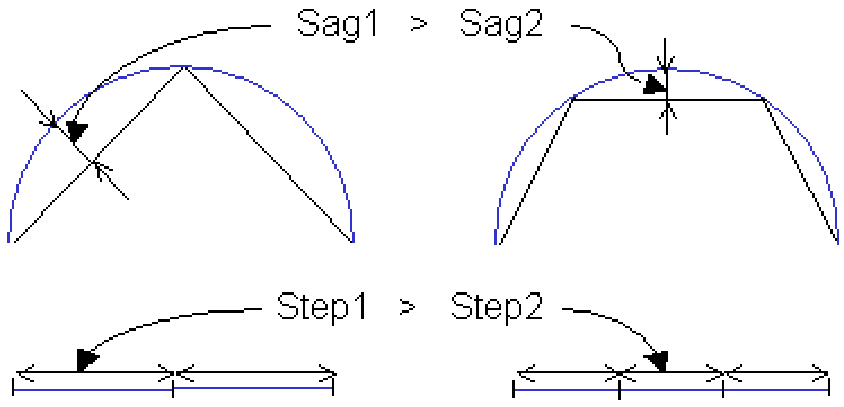

Figure 22 – Tesselation parameters (extracted from [67]*)*

The following were the results of the pre-testing runs:

Table 14 – Pre-testing runs

Test number	Analysis type	Manufacturing mesh [mm]	Voxel size [mm]	CPU time [s]	Maximum displacement [mm]
CR001ABS_2	Warpage – Inherent strain	0,9892	1	4080	0,9526
CR002ABS_2	Warpage - Thermomechanical	0,9998	1	720	0,2044
CR003ABS_2	Warpage - Thermomechanical	0,7378	0,75	1440	0,1697
CR004ABS_2	Warpage - Thermomechanical	0,0,49999	0,5	7200	0,1545

Finally, a critical trade-off occurs between simulation accuracy (which is time-consuming) and efficiency. This balance is considerable since the Taguchi experiments will include several runs. CPU time is vital in these tests, as several runs passed beyond the 7200 seconds.

Although CR003ABS and CR004ABS are very close in terms of maximum displacement closer to zero, the CR004ABS time run is significantly longer than CR003ABS. This is due to the smaller voxel size. A smaller voxel size in geometry means more detail and more time processing the simulation. With this pre-testing, the actual simulation can move forward.

3.4. Simulation

The following 27 profiles were created using the Simplify 3D slicer software, which was chosen because of its impressive array of sophisticated capabilities and vast customisation possibilities. This software enables extensive profile and parameter adjustment to match various 3D printers and materials, resulting in an ideal printing experience. Furthermore, it has the advantage of speeding up the slicing process, which is very useful when dealing with complicated prints. The different parameter values, as shown in Table 1 and Table 2, were set up inside the software's advanced process settings and then saved as an FFF profile (Figure 23). The high-resolution benchmark model was then loaded into the software, rigorously prepared for slicing, and converted into gcode format (Figure 24). It is important to note that a total of twenty-seven gcode files were generated using this procedure, with each file containing a unique toolpath for a single simulation, which is required for the following steps.

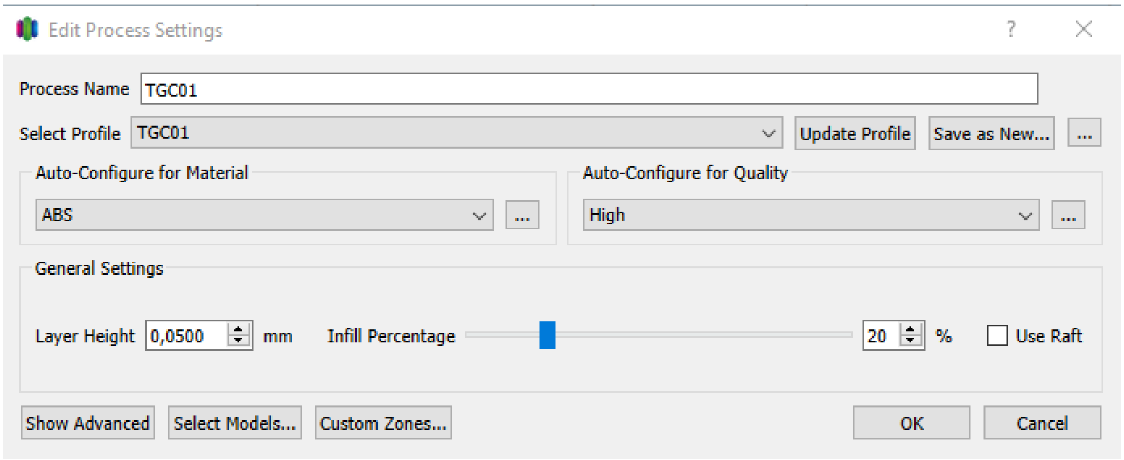

Figure 23 – Process settings

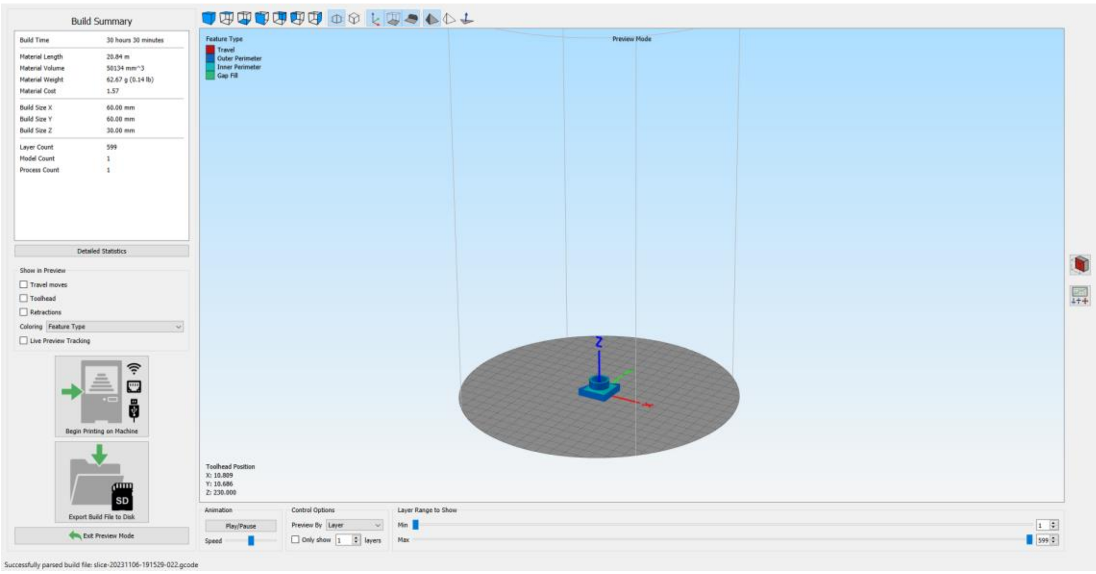

Figure 24 – Sliced geometry

DIGIMAT software supports three different 3D printing processes: FDM, FFF and SLS. FFF appears to be the most appropriate printing technique in the context of this investigation. It is critical to distinguish between FFF and FDM, as the latter word refers solely to the material extrusion technique aided by Stratasys printers and filaments. Given our use of basic ABS filament and a generic printer, FFF is the only option. A generic printer with dimensions of 390x390x900mm and a fixed platform were chosen. As previously stated, the next phase includes a Warpage thermomechanical analysis and the implementation of the part geometry and the material. The generic ABS material model definition can be seen in Appendix A.

The subsequent step involves the definition of manufacturing procedures, such as the manufacturing steps, warpage compensation, tessellation, positioning, toolpath, and process parameters specification. Tesselation relates to the size of the mesh elements, whereas toolpath refers to the pre-generated gccode. The process parameters are fine-tuned to fulfil the simulation requirements, as shown in Figure 25.

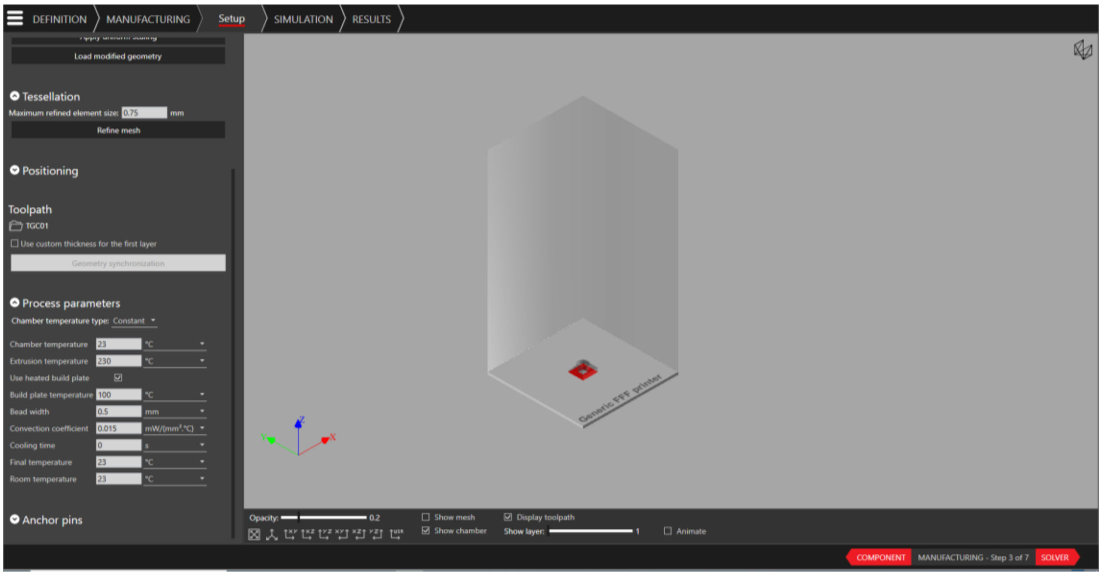

Figure 25 – Manufacturing setup

The solver phase is where part discretisation occurs, and the voxel size of the mesh is decided. The geometry is visualised as voxels with a custom size of 0,75mm, as seen in Figure 26.

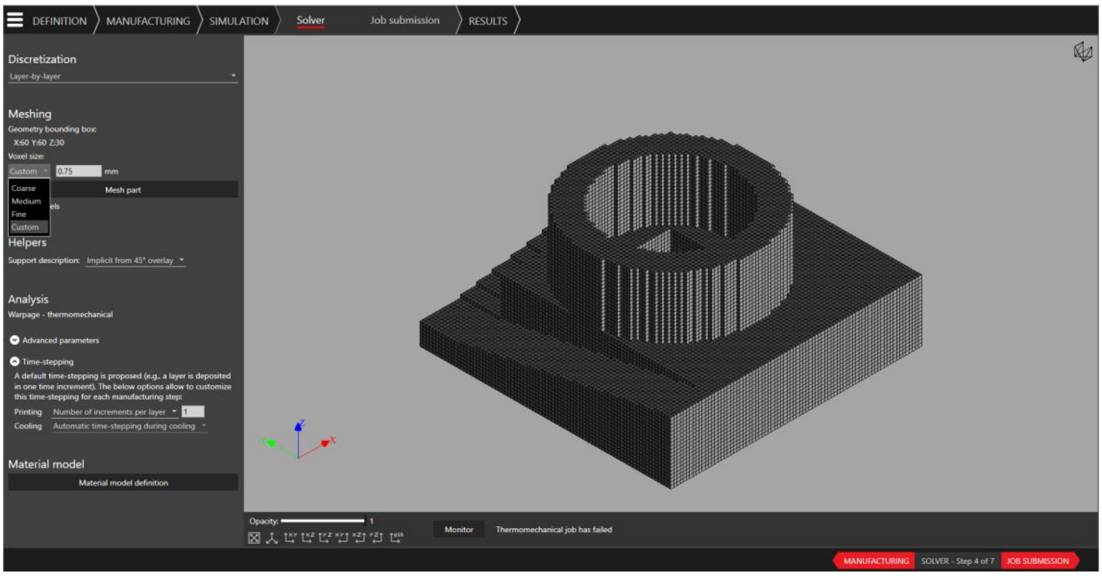

Figure 26 – Simulation solver

Ultimately, during the submission step, the work is dispatched for execution. The time required to execute the simulation depends on a variety of criteria, including component geometry resolution, the STL file, mesh and voxel size, and the number of CPUs available on the computer, resulting in varying runtimes (Figure 27)

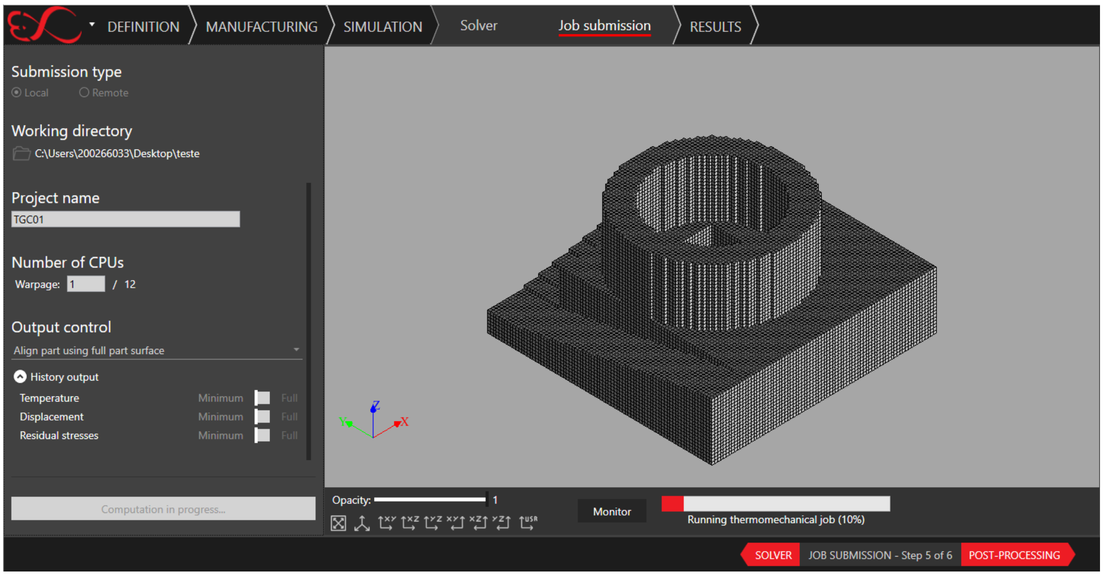

Figure 27 – Job submission

After the task is completed, the post-processing step begins, allowing for the investigation and analysis of warpage deflection, warpage indicators, and von Misses stresses. Furthermore, as seen in Figure 28, the ability to personalise reference planes is accessible, and the results may be exported.

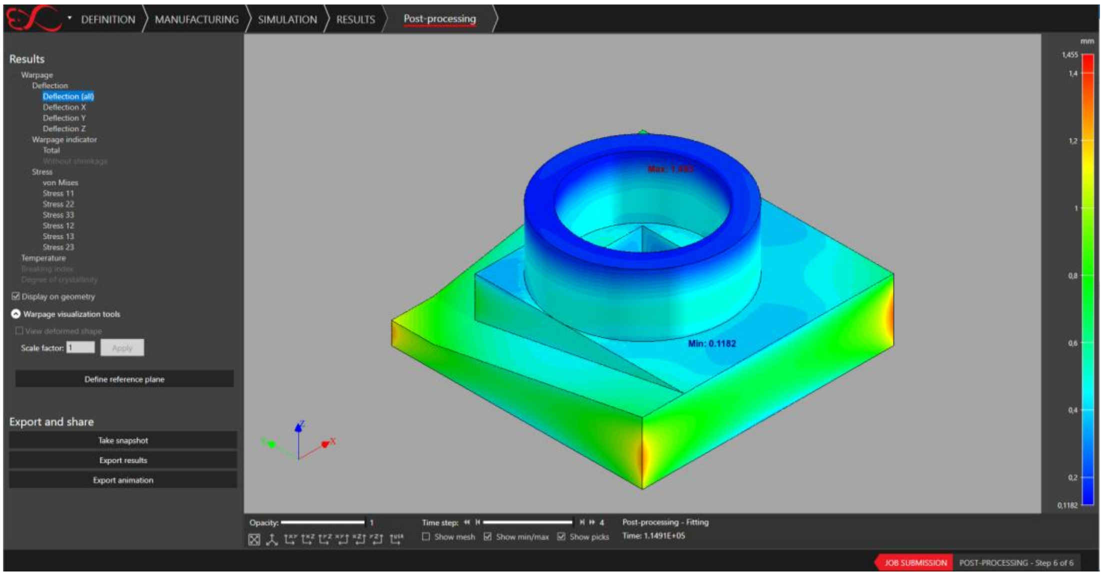

Figure 28 - post-processing of results

The development of a reference plane is critical because it allows for the accurate interpretation and visualisation of data in the preferred coordinate system, ensuring a consistent knowledge of material performance. When exporting data, the reference plane ensures consistency, and that data aligns with the given coordinate system (Figure 29)

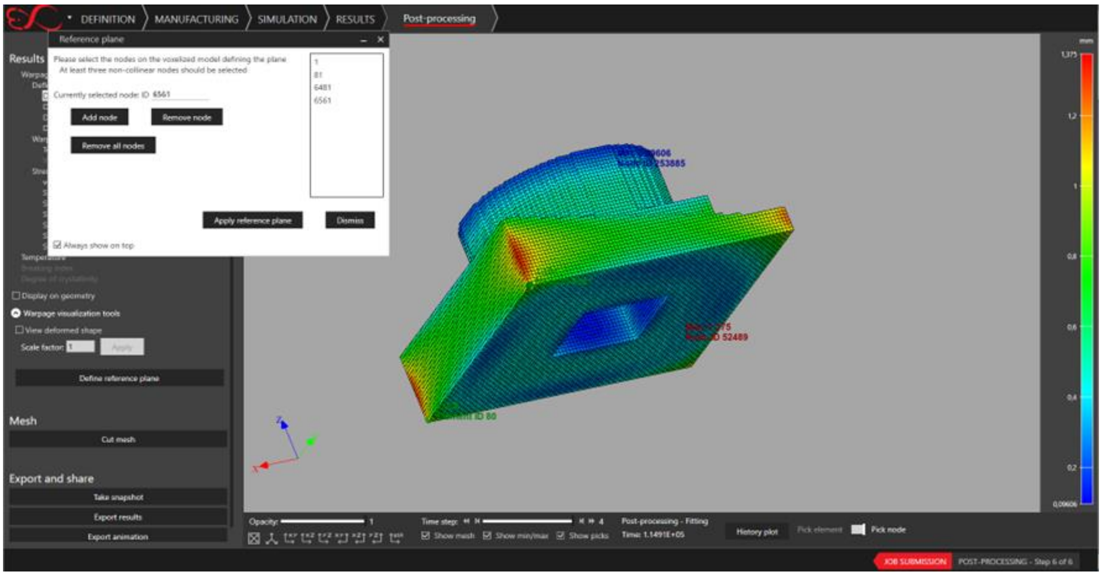

Figure 29 – Implementing reference plane

The reference plane is then applied, and the findings are now framed within the framework of a reference plane (Figure 30). The findings can be exported as a warped geometry or a corrected geometry (Figure 31). The corrected geometry is especially useful in the manufacturing process since it allows for the fabrication of a second run, resulting in a part with less warpage and improved overall accuracy.

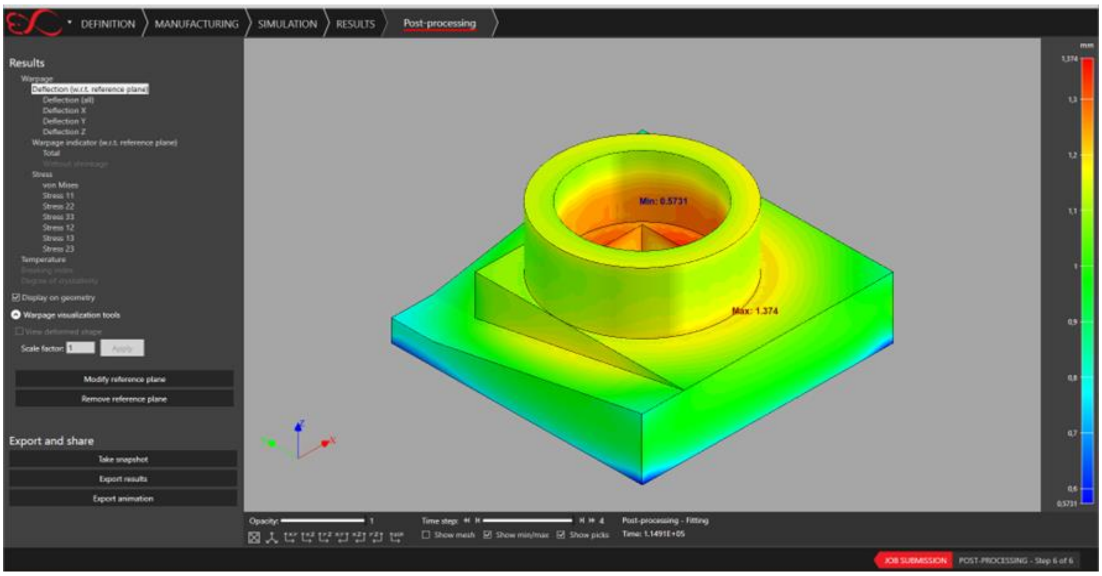

Figure 30 – Warpage deflection with respect to a reference plane

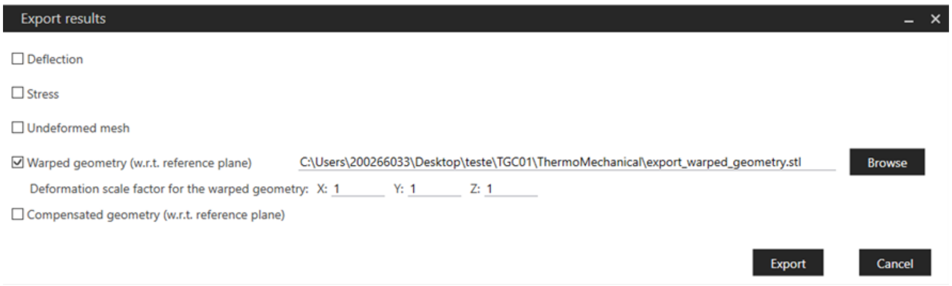

Figure 31 – Exporting results

3.5. Digital measurements

The warped geometries generated by numerical simulations were carefully exported into separate folders and classified using respective simulation labels, indicated as TGC01 through TGC27. Following that, each of these simulation datasets was sent to Nuno Pedro, who was a trainee inside the metrology experts' organisation, S4METRO. The basis for this assignment was S4METRO'S experience in the domain of metrology, as evidenced by their access to highly specialised software explicitly designed for such measurements. Nuno Pedro was tasked with performing thorough measurements on the warped geometries contained within simulation datasets. This task was completed using Metrolog X4 metrology software, which was used and set mainly to handle and analyse complicated geometrical shapes. By utilising its resources, the organisation was able to achieve a high level of precision and accuracy in the assessment of the warped geometries in accordance with stringent metrological criteria.

In the lack of a physical benchmark equivalent for evaluating the deformed geometrical structure created during the simulation process, the use of advanced software is required. Metrolog X4 software is a metrology solution designed for the thorough examination of dimensions and geometrical features. Its capabilities extend to the expert management of complex and large CAD files, making it a vital tool in the identification and mitigation of any inconsistencies emerging from manufacturing and assembly processes, all within the domain of 3D measurements.

The robust functionality of Metrolog is used to perform a critical task: a comparison of the geometrical characteristics of the original CAD file and the resulting warped geometry encapsulated in the STL file. This critical examination is supported by the requirement to create and apply a sequence of meticulously constructed instructions. These commands act as conduits for the benchmark CAD file, which represents idealised geometry, to be seamlessly integrated with the STL file, which represents non-ideal or distorted geometrical structure, allowing for an intricate and precise comparison of the two data sets for in-depth scrutiny and evaluation. The software’s ability to manage CAD files of significant complexity is critical in guaranteeing that no nuance or subtlety in the original design is missed during the comparison analysis. In the following figure (Figure 32), a representation of each geometric tolerance is shown in the part geometry.

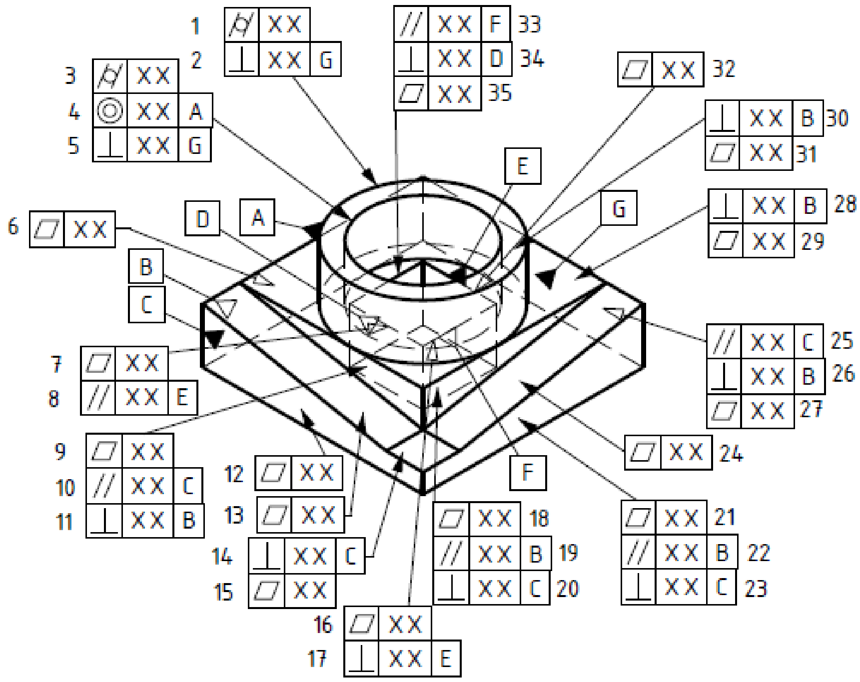

Figure 32 – Numbered geometric tolerances (black arrows mean visible elements, and white arrows mean invisible elements)

Chapter 4

Numerical Results and Statistical Analysis

In this chapter, the numerical results will be detailed, as well as the statistical analysis according to the methodologies explained previously.

4.1. Results

Consistently with Chapter 2.5.3, the extracted data were obtained and compiled in Table 15. In terms of geometrical deviation, the smaller the better. When examining the influence of process parameters, it will be regarded as good if the geometric deviation is reduced and negative if it is increased.

Table 15 – List of all the measured geometric deviations

Number (according to Fig. 32)	Geometric Characteristics	Name	Part Feature	Results
15	Flatness Horizontal Planes	Flatness_PLN7	FH1	Appendix B
29		Flatness_G	FH2	
31		Flatness_PLN6	FH3	
6	Flatness Vertical Planes	Flatness_B	FV1	Appendix C
7		Flatness_D	FV2	
9		Flatness_PLN5	FV3	
12		Flatness_C	FV4	
16		Flatness_F	FV5	
18		Flatness_PLN4	FV6	
21		Flatness_PLN1	FV7	
27		Flatness_PLN2	FV8	
32		Flatness_E	FV9	
35		Flatness_PLN3	FV10	
13	Flatness Inclined Planes	Flatness_PLN8	FI1	Appendix D
24		Flatness_PLN9	FI2	
1	Cylindricity	Cylindricity	C1	Appendix E
3		Cylindricity	C2	
4	Concentricity	Concentricity	CO1	Appendix F
8	Parallelism of Vertical Planes	Parallelism	PLV1	Appendix G
10		Parallelism	PLV2	
19		Parallelism	PLV3	
22		Parallelism	PLV4	
25		Parallelism	PLV5	
33		Parallelism	PLV6	
2	Perpendicularity	Perpendicularity with respect to FH2	P1	Appendix H
5		Perpendicularity with respect to FH2	P2	
11		Perpendicularity with respect to FV1	P3	
14		Perpendicularity with respect to FV4	P4	
17		Perpendicularity with respect toFV9	P5	
20		Perpendicularity with respect toFV4	P6	
23		Perpendicularity with respect to FV4	P7	
26		Perpendicularity with respect to FV1	P8	
28		Perpendicularity with respect to FV1	P9	
30		Perpendicularity with respect to FV1	P10	
34		Perpendicularity with respect to FV2	P11	

A statistical study using the ANOVA method was used in relation to the geometric deviations mentioned in Table 15, with the goal of analysing how the specified process parameters influence these deviations. According to the information in Table 15, the response variables selected for analysis are as follows:

- FH – Flatness horizontal planes;
- FV – Flatness vertical planes;
- FI – Flatness inclined planes;
- C – Cylindricity;
- CO – Concentricity;
- PLV – Parallelism of vertical planes;
- P – Perpendicularity with respect to.

ANOVA will help investigate the impact of selected process parameters on the observed deviations.

4.2. Statistical analysis

The purpose of the hypothesis test is to see if there is sufficient evidence from the observed data indicating a significant difference between the three populations to reject the null hypothesis of equal population means. According to the null hypothesis H_0, the population means ($\mu_1, \mu_2, \dots \mu_x$) are equal. On the other hand, the alternative hypothesis (H_1) postulated that there is a noteworthy distinction between the population means. A significance level of 0,05 was set, which means there is a 5% chance that the null hypothesis will be rejected even though it is true. Any observed difference between the means that are inside the crucial zone will result in the alternative hypothesis being rejected with a 95% confidence level.

It is essential to do ANOVA for a more detailed analysis that takes into consideration the unique variability within these parameters. It aids in comprehending the independent effects of each component on the traits as well as potential interaction with other variables. It is not practical or correct to use mean values since these qualities or measures naturally incorporate variance that may be crucial to comprehend the behaviour or performance of the parameter under study. The analysis might be oversimplified, and subtle differences that could have a significant influence on the results could be missed if mean values are used alone. A critical parameter in this study is the absence of repetition in each run. ANOVA usually uses the variability of the data to determine how vital each parameter is. The variance is crucial in real-world studies to understand the relative importance of the components being investigated. But in this case, a set of 27 numerical runs were performed. Being numerical implies that by performing the same run numerous times, the results will stay the same, meaning that there is no variability in results. In contrast to other studies that used experimental results instead of numerical modelling of the printing process, it's more challenging to determine whether observed variations are caused by specific parameters or by other unaccounted-for causes of variation when repeated measurements are not conducted within runs. This lack of repeatability weakens the ability to attribute variances to the issue under investigation clearly. As such, the exact identification of each parameter's relevance in this setting may provide challenges for the analysis of variance.

An ANOVA was performed 35 times in total, one for each response variable that corresponded to the geometric deviations. All 35 ANOVAS are accessible for reference in Appendix I.

The F-values of the 35 ANOVAS were compiled into a table (Table 16). Each row represents a response, and each column is a parameter. On the F-value table, if the F-value is red, it means that the corresponding value is above the tabulated value of the F distribution table of critical values for a significance level of 0.05. If it's green, then the value is below the tabulated value.

The minimum F-value for statistical analysis of the ANOVA is found with the numerator of degrees of freedom of variance between groups (2) and the denominator degrees of freedom of the variance within groups (14) in the F-value distribution table of critical values of p=0.05. The F-value distribution table of critical values for 5% can be found in Appendix J. The degrees of freedom were found after doing the ANOVAs.

$$Tabulated\ f - value = 3.739$$

Table 16 - F-values for each response

	Tabulated f-value = 3.739	Chamber Temperature (°C)	Infill Density (%)	Layer Height (mm)	Extrusion Temperature (°C)	Print Speed (mm/s)	Infill Strategy
15	FH1	26,38	7	2,15	23,15	2,15	0,54
29	FH2	431,07	0,63	11,77	17,72	13,65	0,12
31	FH3	66,5	2,62	11,37	0,87	14	2,62
6	FV1	301,21	1,25	5,01	28,52	7	0,1
7	FV2	58,6	1,64	0,68	3,83	2,77	0,33
9	FV3	1954,66	2,28	5,59	0,7	0,53	0,98
12	FV4	608,08	3,21	5,62	50,03	15,26	0,46
16	FV5	75,74	1,17	0,69	4,27	3,77	0,69
18	FV6	4306,4	0,73	3,19	4,09	5,6	0,5
21	FV7	281,63	1,7	2,11	37,17	5,17	0,07
27	FV8	389,63	1,35	6,42	39,44	10,77	0,05
32	FV9	103	2,98	1,58	8,69	5,33	0,43
35	FV10	75,45	4,03	2,69	11,43	2,45	0,25
13	FI1	266,99	1,19	7,29	27,78	8,89	0,02
24	FI2	286,82	1,1	5,85	19,72	7,69	0,03
1	C1	179,73	0,01	10,56	12,27	11,44	0,11
3	C2	147,17	0,02	9,34	11,97	10,6	0,07
4	CO1	163,91	0,74	11,83	7,15	12,55	0,11
8	PLV1	20,59	1,9	0,34	6,35	2,53	0,96
10	PLV2	29,88	7,87	1,35	14,82	2,94	0,92
19	PLV3	46,73	1,47	1,75	26,16	3,03	0,19
22	PLV4	852,25	23,56	50,21	157,63	4,98	0,13
25	PLV5	100,15	6,03	4,68	9,28	0,63	1,17
33	PLV6	15,17	2,73	0,34	5,38	2,88	0,24
2	P1	48,36	1,91	15,91	0,64	1,91	0,64
5	P2	49,75	0,25	7,75	4,75	3,25	1
11	P3	97,54	1,06	0,26	12,75	3,43	0,26
14	P4	358,66	4,02	2,15	49,87	9,24	0,17
17	P5	11,64	2,43	3,61	6,63	2,37	0,01
20	P6	77,3	1,98	0,35	4,33	2,17	0,61
23	P7	35,76	5,68	0,97	2,95	0,6	1,23
26	P8	121	4	4	4	1	1
28	P9	455,26	2,78	2,16	51,8	5,85	0,07
30	P10	410,5	3,85	2,22	56,67	3,59	0,03
34	P11	6,85	1,2	0,62	0,39	2,27	0,69
	Sum	35	9	16	30	17	0

A clear tendency towards chamber temperature is observed. A ranking of both tables shows the chamber temperature being the most statistically significant parameter, followed by extrusion temperature, print speed, layer height, infill density, and finally, the infill strategy being the least statistically significant. The following chapters will have a more detailed analysis of parameters that contain significance, meaning the infill strategy will be excluded. It is time-consuming and non-efficient to analyse each of the 35 ANOVAS performed earlier, so the ANOVA for extended analysis were chosen based on the most considerable nominal size for each geometric characteristic (C1, CO1, PLV5, FH2, FV1, FI1, P1).

4.2.1. Cylindricity (C1) vs Chamber temperature, Infill density, Layer height, Extrusion temperature, Print speed, and Infill strategy

First, to ensure the dispersion of residuals or errors is uniform across different levels of the independent variables, it is necessary to check the homoscedasticity of results. Deviations from homoscedasticity might result in inaccurate parameter projections and conclusions. Statistical methods, such as Levene's test, will be used to measure homoscedasticity. The test determines if the residual variances are statistically equivalent across groups. In Figure 33, it's possible to observe the graph with intervals for the standard deviation for each level of chamber temperature in cylindricity (C1). All intervals must overlap to validate homoscedasticity and, as such, concluding that the variances are approximately the same statistically.

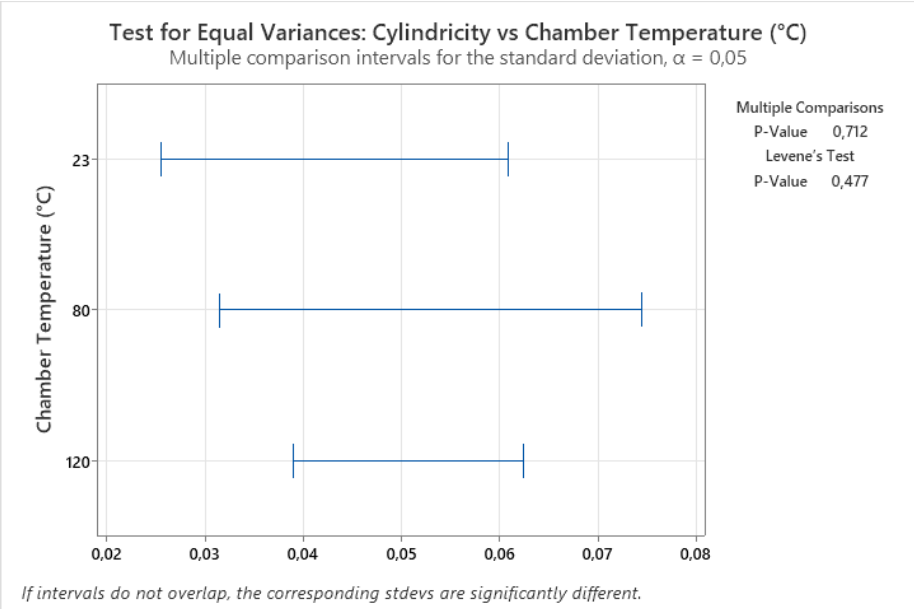

Figure 33 – Graph with intervals for the standard deviation for each level of chamber temperature in cylindricity for chamber temperature (C1)

Further in the chapter, the equal variances of each response for each parameter were tested, but they will not be presented; they will only be mentioned.

Minitab software was used to perform the ANOVA between responses and parameters. In Figure 34, the ANOVA was performed between response cylindricity (C1) and all the parameters that can be observed.

Source	DF	Adj SS	Adj MS	F-Value	P-Value
Chamber Temperature (°C)	2	0,162807	0,081404	179,73	0,000
Infill Density (%)	2	0,000007	0,000004	0,01	0,992
Layer Height (mm)	2	0,009563	0,004781	10,56	0,002
Extrusion Temperature (°C)	2	0,011119	0,005559	12,27	0,001
Print Speed (mm/s)	2	0,010363	0,005181	11,44	0,001
Infill Strategy	2	0,000096	0,000048	0,11	0,900
Error	14	0,006341	0,000453		
Total	26	0,200296			

Figure 34 – ANOVA table for cylindricity (C1)

The ANOVA test uses the f-statistic to assess a term's statistical significance. A high F-value (F>3.739) indicates a considerable impact of a parameter modification on the output variable under study. The analysis of the parameters reveals that chamber temperature has the most effect on cyclicity (C1), with the F-test value of 179.73. Furthermore, the p-value, which came from the F-test and adjusted to 95%, as mentioned before, is found to be <0.05, supporting the hypothesis and, as a result, rejecting the null hypothesis. Observing the F values, four parameters are significant for a significance level of 5%: chamber temperature, layer height, extrusion Temperature, and print speed.

Below, a main effect plot is presented with the four parameters mentioned above, represented in Figure 35:

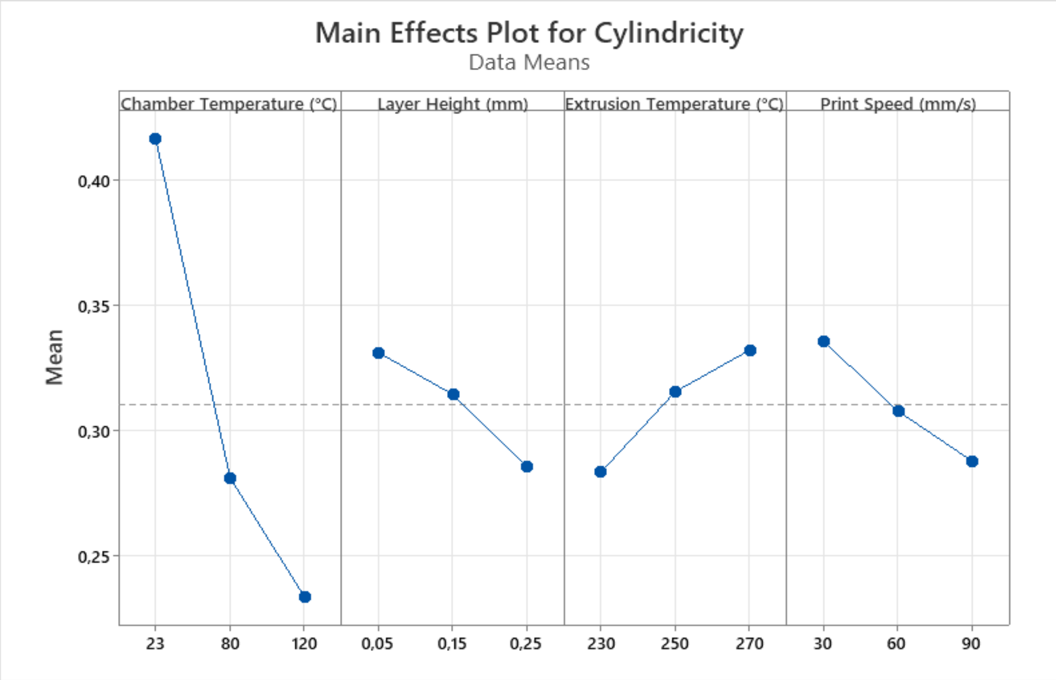

Figure 35 - Main effect plot of chamber temperature, layer height, extrusion temperature and print speed for cylindricity (C1)

The first thing that stands out when looking at the main effect plot is the extremely steep slope of the chamber temperature parameter, which indicates that changes in this parameter have a significant influence. Specifically, when the chamber temperature is changed from 23 to 80ºC, and then from 80 to 120ºC, the mean value fell by 0.168mm. This indicates that better outcomes are obtained by raising the chamber temperature. The same is valid for layer height but not as steeply. Better results are obtained by increasing the layer height, namely, by 0.043mm between 0.05 and 0.25mm. With regard to extrusion temperature, this is not the case. The reverse is true for extrusion temperature. Despite being a step, the slope grows adversely. The mean deviation tends to get worse with increasing extrusion temperature; specifically, there is a 0.047mm difference when the extrusion temperature is raised. Print speed may be observed in the same way as chamber temperature and layer height. It is noteworthy to note, nevertheless, that the slope in the range of 60 to 90mm/s is relatively slight, indicating that it is not as significant but shouldn´t be ignored. None of the observations' slopes are close to the flatness line, which represents the average mean of the observations.

From the interaction plot (Figure 36), the following can be observed:

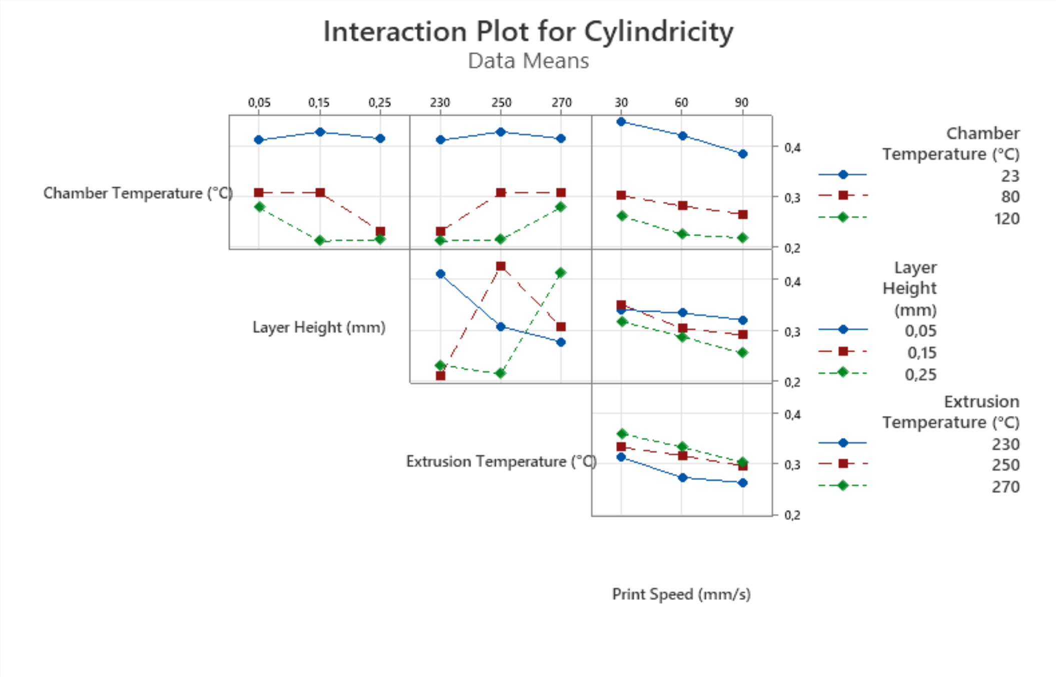

Figure 36 - Interaction Plot for cylindricity (C1)

- The lines observed in the print speed column are primarily parallel, meaning there is no meaningful interaction between print speed and the other parameter variables. So, it concludes that the interaction effect provoked by the variation in print Speed doesn´t vary given the other parameters. A slight crossing can be seen in the interaction of layer height*print Speed, but not very significant in terms of means difference.
- To further understand the significance between the interaction, layer height*print speed and cylindricity (C1), an ANOVA was performed (Table 17):

*Table 17 - ANOVA of layer height*print speed for cylindricity (C1)*

Source	DF	Adj SS	Adj MS	F-Value	P-Value
Layer Height (mm)	2	0,009563	0,004781	0,48	0,625
Print Speed (mm/s)	2	0,010363	0,005181	0,52	0,601
Layer Height (mm)*Print Speed (mm/s)	4	0,002237	0,000559	0,06	0,994
Error	18	0,178133	0,009896		
Total	26	0,200296			

- Observing the table above, the F-value of 0.06 (F<3.555) indicates that there is not a statistically significant effect on cylindricity for a significance level of p=0.05, so we fail to reject the null hypothesis.
- In the layer height*extrusion temperature interaction, lines crossing between levels of layer height can be observed, as the interaction effect provoked by variation of extrusion temperature does vary according to layer Thickness.

*Table 18 - ANOVA of layer height*extrusion temperature for cylindricity (C1)*

Source	DF	Adj SS	Adj MS	F-Value	P-Value
Layer Height (mm)	2	0,009563	0,004781	5,12	0,017
Extrusion Temperature (°C)	2	0,011119	0,005559	5,96	0,010
Layer Height (mm)*Extrusion Temperature (°C)	4	0,162815	0,040704	43,61	0,000
Error	18	0,016800	0,000933		
Total	26	0,200296			

- According to Table 18, an F-value of 43.61 (F>3.555) for the interaction evidences these two parameters' interaction effect in cylindricity is solid and related.
- In chamber temperature* layer height and chamber temperature* extrusion temperature interaction lines do not cross. Still, variations can be observed depending on the chamber temperature level, which means the interaction effect provoked by variations in chamber temperature does vary according to layer height and extrusion temperature. Still, the interaction is not as strong as layer height*extrusion temperature.

4.2.2. Concentricity (CO1) vs Chamber temperature, Infill density, Layer height, Extrusion temperature, Print speed, and Infill strategy

The equal variances test was performed, and the homoscedasticity in the results was validated. In Figure 37, the ANOVA was performed between response concentricity (Co1) and all the parameters that can be observed.

Source	DF	Adj SS	Adj MS	F-Value	P-Value
Chamber Temperature (°C)	2	0,466941	0,233470	163,91	0,000
Infill Density (%)	2	0,002096	0,001048	0,74	0,497
Layer Height (mm)	2	0,033696	0,016848	11,83	0,001
Extrusion Temperature (°C)	2	0,020363	0,010181	7,15	0,007
Print Speed (mm/s)	2	0,035741	0,017870	12,55	0,001
Infill Strategy	2	0,000319	0,000159	0,11	0,895
Error	14	0,019941	0,001424		
Total	26	0,579096			

Figure 37 - ANOVA table for concentricity (CO1)

The next step is to compare the F-values from the ANOVA table for concentricity with the equivalent tabulated F-values, just like in the previous chapter. Regardless of the response variable, the tabulated F-values stay constant. As shown in the preceding chapter, this consistency results from established degrees of freedom for the denominator and numerator, as well as a constant significance level. Observing the F values, four parameters are significant for a significance level of 5%: chamber temperature, layer height, extrusion temperature, and print speed, which are the same for cylindricity.

Below, a main effect plot is presented with the four parameters mentioned above, represented in Figure 38:

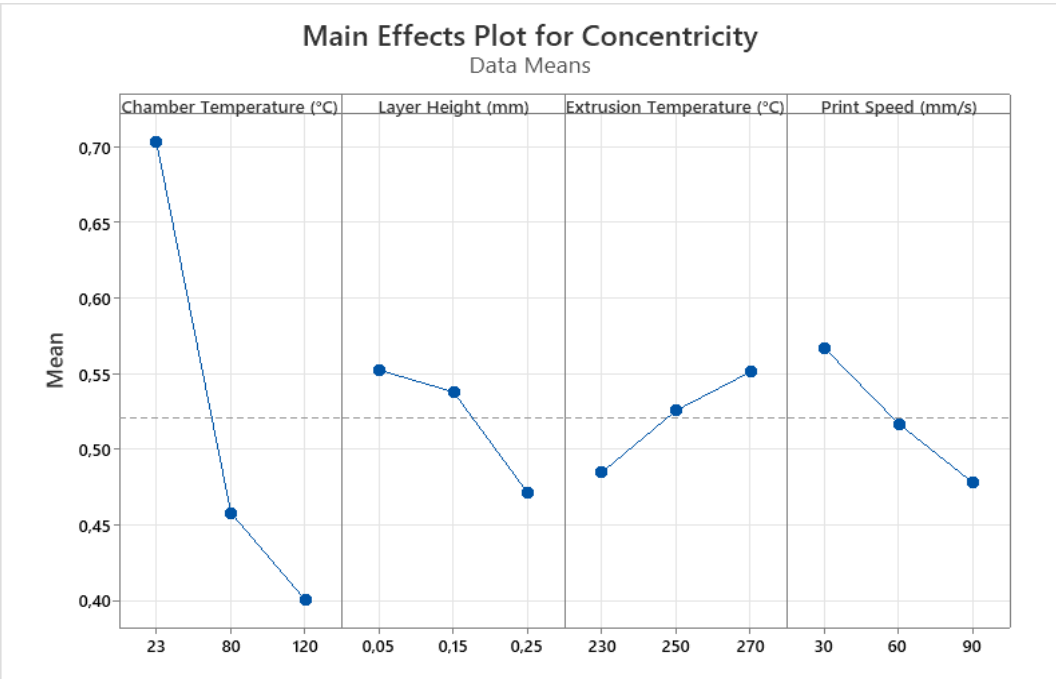

Figure 38 - Main effect plot of chamber temperature, layer height, extrusion temperature and print speed for concentricity (Co1)

The main effect plot for concentricity (CO1) mirrors the behaviour observed in the previous chapter for cylindricity (C1), leaving little to comment on apart from the distinct differences in their mean values. Similarly, the interaction plot (Figure 39) presents a comparable scenario with noticeable differences in mean values.

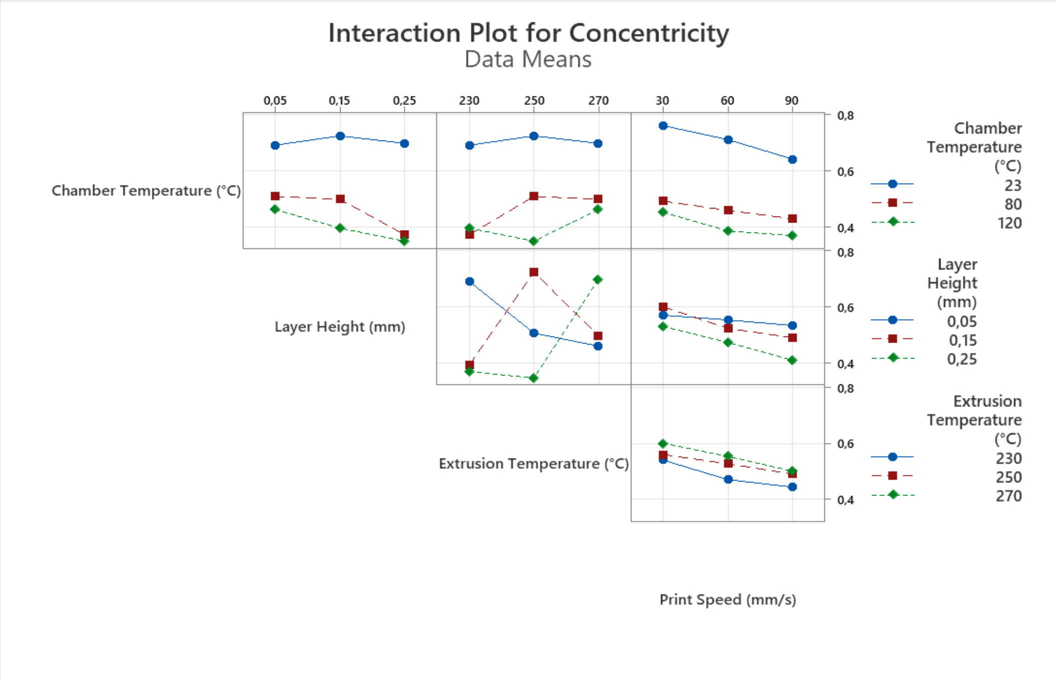

Figure 39 - Interaction Plot for concentricity (Co1)

4.2.3. Parallelism (PLV5) vs Chamber temperature, Infill density, Layer height, Extrusion temperature, Print speed, and Infill strategy

The test for equal variances in parallelism (PLV5) for chamber temperature came out negative, as observed in Figure 40 and Figure 41; respectfully, the analysis can´t continue unless the homoscedasticity of results is observed.

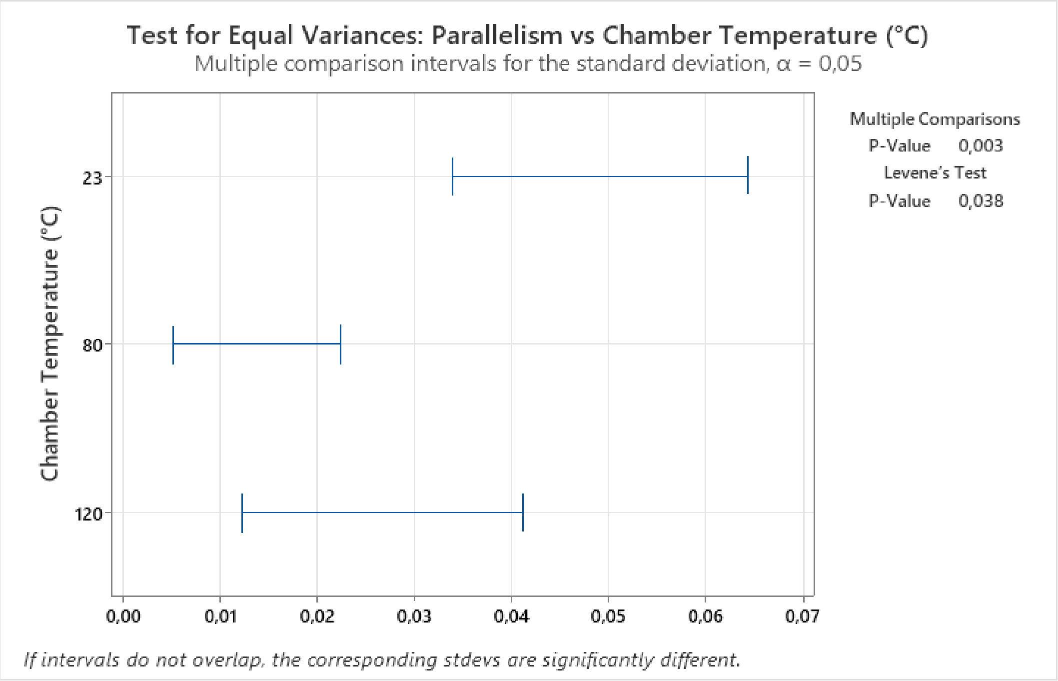

Figure 40 - Graph with intervals for the standard deviation for each level of chamber temperature in parallelism for chamber temperature (PLV5)

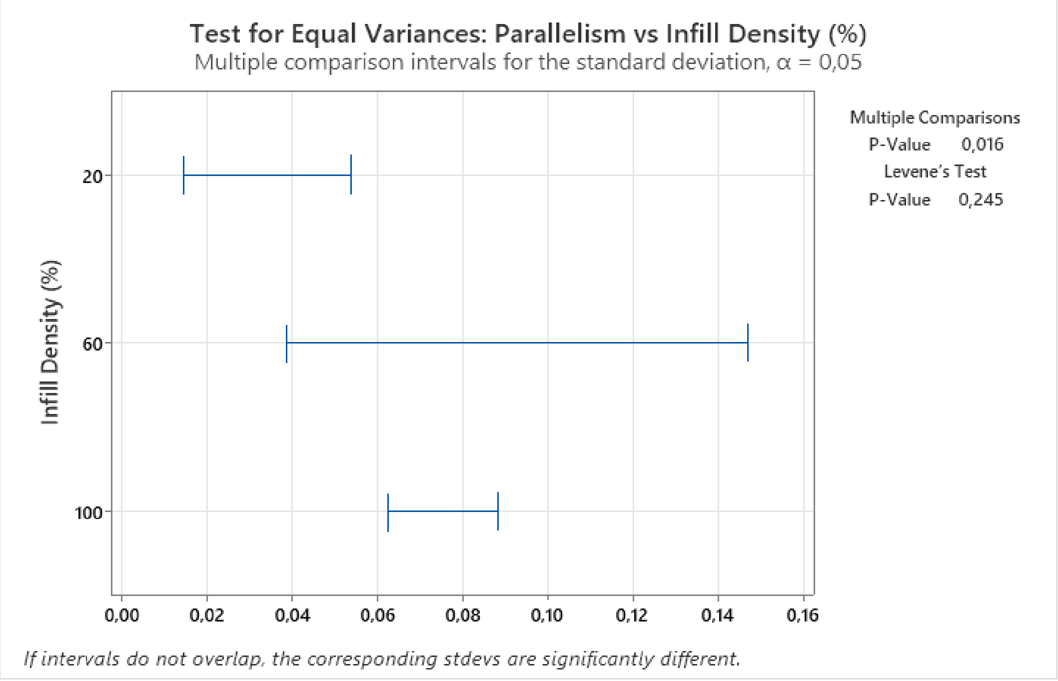

Figure 41 - Graph with intervals for the standard deviation for each level of chamber temperature in parallelism for infill density (PLV5)

So, observing the previous figures, some intervals don´t overlap, so the homoscedasticity of results is not demonstrated. As a result, the ANOVA results are not validated. So, instead of doing PLV5, another part feature was selected to replace it. Test of equal variances in PLV1 confirms his homoscedasticity, so in Figure 42, the ANOVA was performed between response flatness horizontal planes (FH2), and all the parameters can be observed.

Source	DF	Adj SS	Adj MS	F-Value	P-Value
Chamber Temperature (°C)	2	0,75316	0,376578	20,59	0,000
Infill Density (%)	2	0,06936	0,034678	1,90	0,187
Layer Height (mm)	2	0,01229	0,006144	0,34	0,720
Extrusion Temperature (°C)	2	0,23227	0,116133	6,35	0,011
Print Speed (mm/s)	2	0,09247	0,046233	2,53	0,116
Infill Strategy	2	0,03529	0,017644	0,96	0,405
Error	14	0,25604	0,018289		
Total	26	1,45087			

Figure 42 - ANOVA table for parallelism (PLV1)

Similarly, the F-values were compared. Observing the F values, two parameters are significant for a significance level of 5%: chamber temperature and extrusion temperature.

Below, a main effect plot is presented with the two parameters mentioned above, represented in Figure 43:

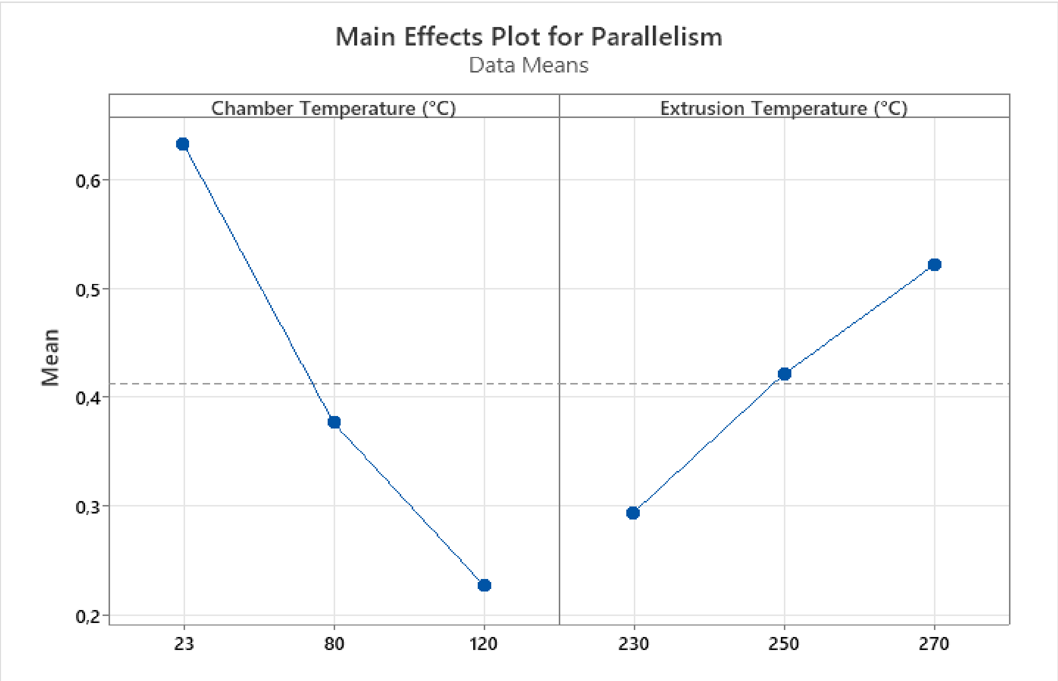

Figure 43 – Main effect plot of chamber temperature and extrusion temperature for parallelism (PLV1)

Chamber temperature and extrusion temperature continue to show similar behaviour in all analyses, with chamber temperature always displaying the steepest slope between levels. His influence is very significant across all responses. extrusion temperature also has a similar behaviour, with a negative slope. Increasing chamber temperature from 23 to 120ºC shows an improvement of 0.405mm in mean value, and increasing extrusion temperature from 230 to 270ºC shows a worsening of 0.227mm in mean value.

From the interaction plot between chamber temperature and extrusion temperature (Figure 44), the following can be observed:

- Between 230 and 250ºC for the extrusion temperature, the blue and the red line, 23 and 80ºC, present similar slopes. With an increase in extrusion temperature, the mean deviation for chamber temperature rises 0.163mm for 23ºC and 0.213mm for 80ºC. The green line presents a non-varying slope. So, the interaction effect provoked by the variation in extrusion temperature varies at 23 and 80ºC. Between 250 and 270ºC for the extrusion temperature, the slope for the red line decreases and the green line increases. The blue line increases further. So, the interaction effect provoked by the variation in extrusion temperature varies at 23 and 120ºC.

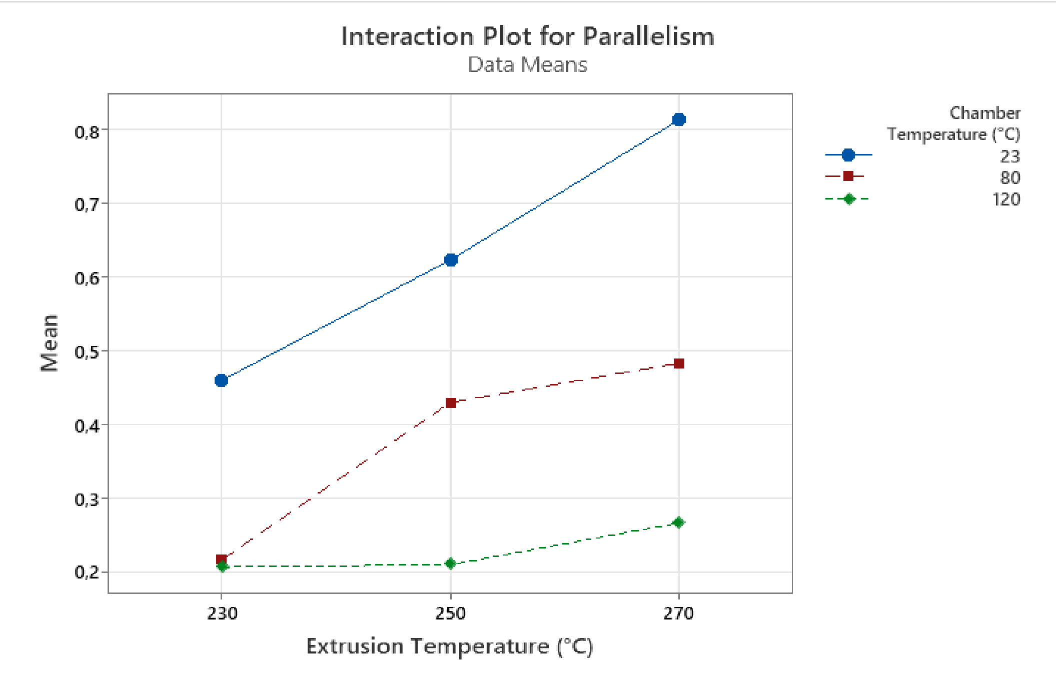

Figure 44 – Interaction plot for parallelism (PLV1)

*Table 19 - ANOVA table for extrusion temperature*chamber temperature for parallelism (PLV1)*

Source	DF	Adj SS	Adj MS	F-Value	P-Value
Extrusion Temperature (°C)	2	0,23227	0,11613	5,45	0,014
Chamber Temperature (°C)	2	0,75316	0,37658	17,66	0,000
Extrusion Temperature (°C)*Chamber Temperature (°C)	4	0,08164	0,02041	0,96	0,455
Error	18	0,38380	0,02132		
Total	26	1,45087			

- According to Table 19, an F-value of 0.96 ($F<3.555$) for the interaction evidences these two parameters' interaction effect hasn´t a significant effect on parallelism (PLV1). The two parameters only have a standalone impact.

4.2.4. Flatness horizontal planes (FH2) vs Chamber temperature, Infill density, Layer height, Extrusion temperature, Print speed, and Infill strategy

The equal variances test was performed, and the homoscedasticity in the results was validated. In Figure 45, the ANOVA was performed between response flatness horizontal planes (FH2), and all the parameters can be observed.

Source	DF	Adj SS	Adj MS	F-Value	P-Value
Chamber Temperature (°C)	2	0,244956	0,122478	431,07	0,000
Infill Density (%)	2	0,000356	0,000178	0,63	0,549
Layer Height (mm)	2	0,006689	0,003344	11,77	0,001
Extrusion Temperature (°C)	2	0,010067	0,005033	17,72	0,000
Print Speed (mm/s)	2	0,007756	0,003878	13,65	0,001
Infill Strategy	2	0,000067	0,000033	0,12	0,890
Error	14	0,003978	0,000284		
Total	26	0,273867			

Figure 45 - ANOVA table for flatness (FH2)

F-values were compared. Observing the F-values, four parameters are significant for a significance level of 5%: chamber temperature, layer height, print speed and extrusion temperature.

Below, a main effect plot is presented with the four parameters mentioned above, represented in Figure 46:

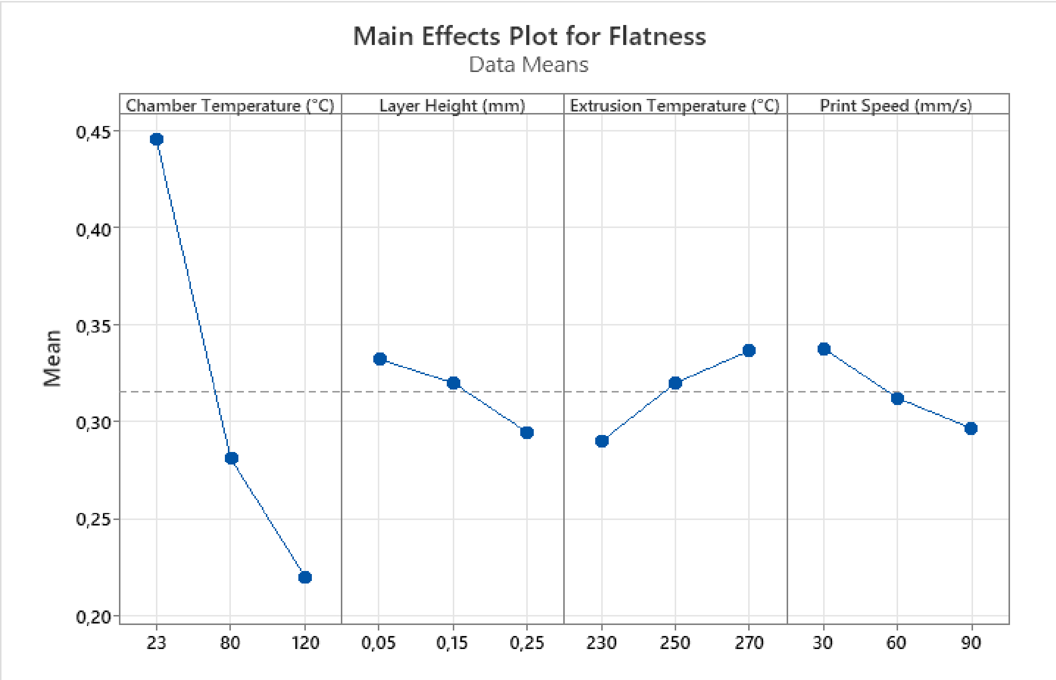

Figure 46 - Main effect plot of chamber temperature, layer height, extrusion temperature and print speed for flatness (FH2)

The main effect plot for flatness (FH2) mirrors the behaviour observed in cylindricity (C1) and concentricity (CO1), apart from the distinct differences in their mean values. The interaction plot (Figure 39) presents a similar scenario.

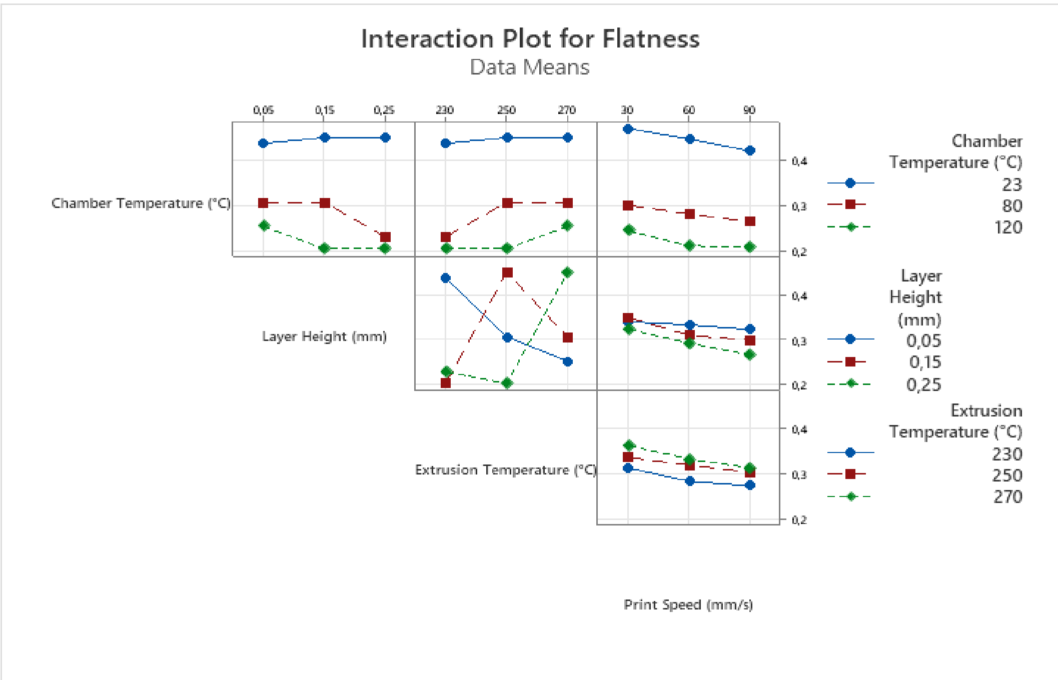

Figure 47 - Interaction plot for flatness (FH2)

4.2.5. Flatness vertical planes (FV1) vs Chamber temperature, Infill density, Layer height, Extrusion temperature, Print speed, and Infill strategy

In Figure 48, the ANOVA was performed between response flatness horizontal planes (FH1) and all the parameters that can be observed.

Source	DF	Adj SS	Adj MS	F-Value	P-Value
Chamber Temperature (°C)	2	0,064067	0,032033	301,21	0,000
Infill Density (%)	2	0,000267	0,000133	1,25	0,316
Layer Height (mm)	2	0,001067	0,000533	5,01	0,023
Extrusion Temperature (°C)	2	0,006067	0,003033	28,52	0,000
Print Speed (mm/s)	2	0,001489	0,000744	7,00	0,008
Infill Strategy	2	0,000022	0,000011	0,10	0,901
Error	14	0,001489	0,000106		
Total	26	0,074467			

Figure 48 - ANOVA table for flatness (FV1)

F-values were compared. Observing the F values, four parameters are significant for a significance level of 5%: chamber temperature, layer height, extrusion temperature and print speed.

Below, a main effect plot is presented with the four parameters mentioned above, represented in Figure 49:

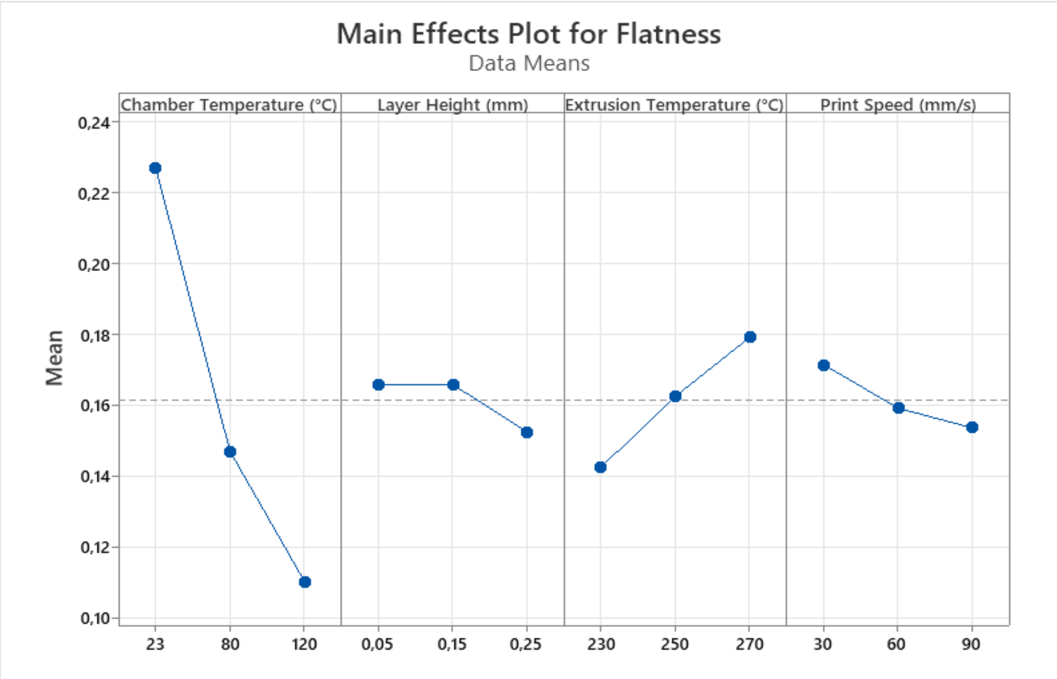

Figure 49 - Main effect plot of chamber temperature, layer height, extrusion temperature and print speed for flatness (FV1)

The layer height line between 0.05 and 0.15mm is parallel, suggesting that changing the levels of layer height doesn't have a significant impact on flatness, but changing between 0.15 and 0.25mm does have a positive impact.

Chamber temperature continues to demonstrate its significant impact positively, with an improvement of 0.116mm. Extrusion temperature in a negative way, with a worsening of 0.036mm. Finally, print speed shows a moderate impact on flatness, with an improvement of 0.018mm.

From the interaction plot (Figure 50), the following can be observed:

- Print speed variation doesn't have a significant impact on the other parameters, especially with 0.05mm for layer height, where the line is almost horizontal, meaning that changing the print speed with a level of 0.05mm doesn't have almost any effect on mean deviation.
- In layer height*chamber temperature, it seems that changing from 0.05mm to 0.15mm has a negative effect with chamber temperatures of 23 and 80ºC but an opposite effect with 120ºC. From 0.15mm to 0.25mm, it continues to worsen at 23ºC but improves drastically at 80ºC. There are no changes in the 120ºC line.
- Except between 230 and 250ºC in extrusion temperature*chamber temperature, all the lines get worse, meaning raising the extrusion temperature levels in all the chamber temperature leads to worse results. Nonetheless, they are correlated with varying extrusion temperatures as an interaction effect with chamber temperatures.
- In layer height*extrusion temperature, the change between 230 and 250ºC has a very drastically negative effect with 0.15mm but a positive effect with 0.05mm and 0.25mm. Changing 250 and 270ºC changes significantly for 0.25mm but improves for the other levels. Even so, varying extrusion temperatures have an interaction effect with layer height.

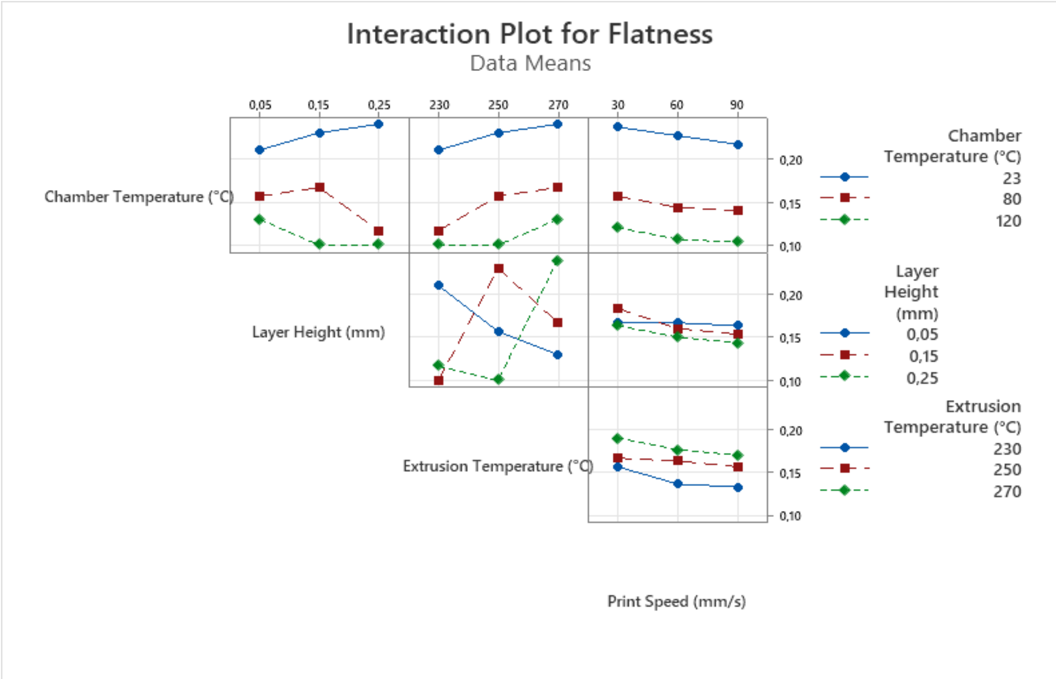

Figure 50 - Interaction plot for flatness (FV1)

4.2.6. Flatness inclined planes (FI1) vs Chamber temperature, Infill density, Layer height, Extrusion temperature, Print speed, and Infill strategy

In Figure 51, the ANOVA was performed between response flatness horizontal planes (FH1), and all the parameters can be observed.

Source	DF	Adj SS	Adj MS	F-Value	P-Value
Chamber Temperature (°C)	2	0,081652	0,040826	266,99	0,000
Infill Density (%)	2	0,000363	0,000181	1,19	0,334
Layer Height (mm)	2	0,002230	0,001115	7,29	0,007
Extrusion Temperature (°C)	2	0,008496	0,004248	27,78	0,000
Print Speed (mm/s)	2	0,002719	0,001359	8,89	0,003
Infill Strategy	2	0,000007	0,000004	0,02	0,976
Error	14	0,002141	0,000153		
Total	26	0,097607			

Figure 51 - ANOVA table for flatness (FI1)

F-values were compared. Observing the F values, four parameters are significant for a significance level of 5%: chamber temperature, infill density and extrusion temperature.

Below, a main effect plot is presented with the four parameters mentioned above, represented in Figure 52:

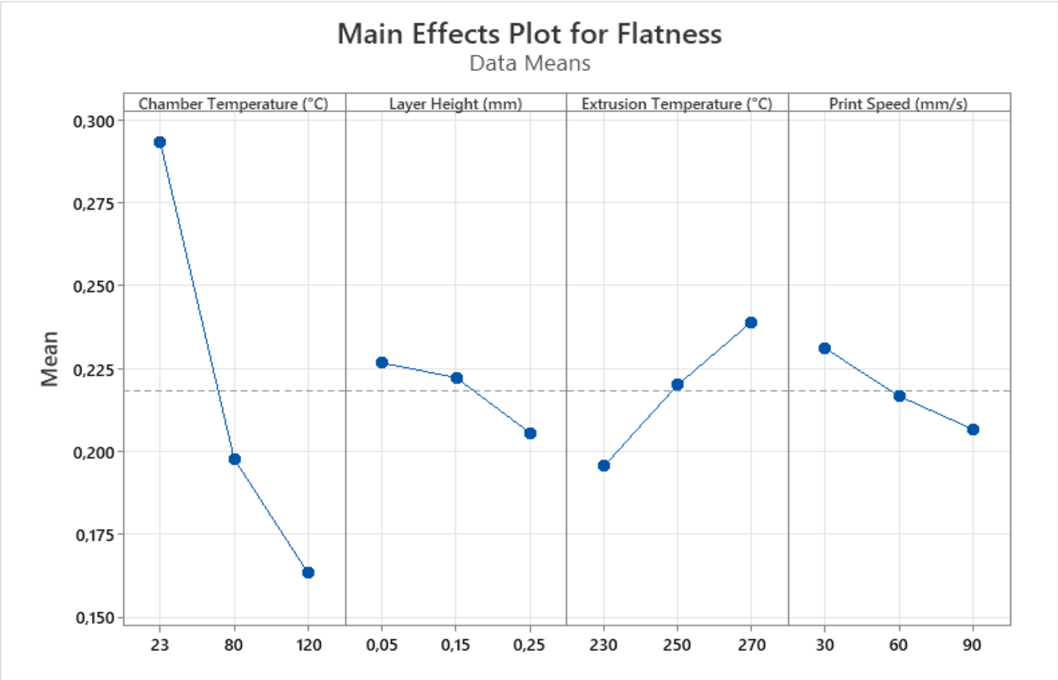

Figure 52 - Main effect plot of chamber temperature, layer height, extrusion temperature and print speed for flatness (FI1)

Apart from the apparent variation in mean values, the main effect plot for flatness (FI1) closely resembles the behaviour noted for flatness (FV1) in the preceding chapter. A similar situation with discernible variations in mean values is shown in the interaction plot (Figure 53).

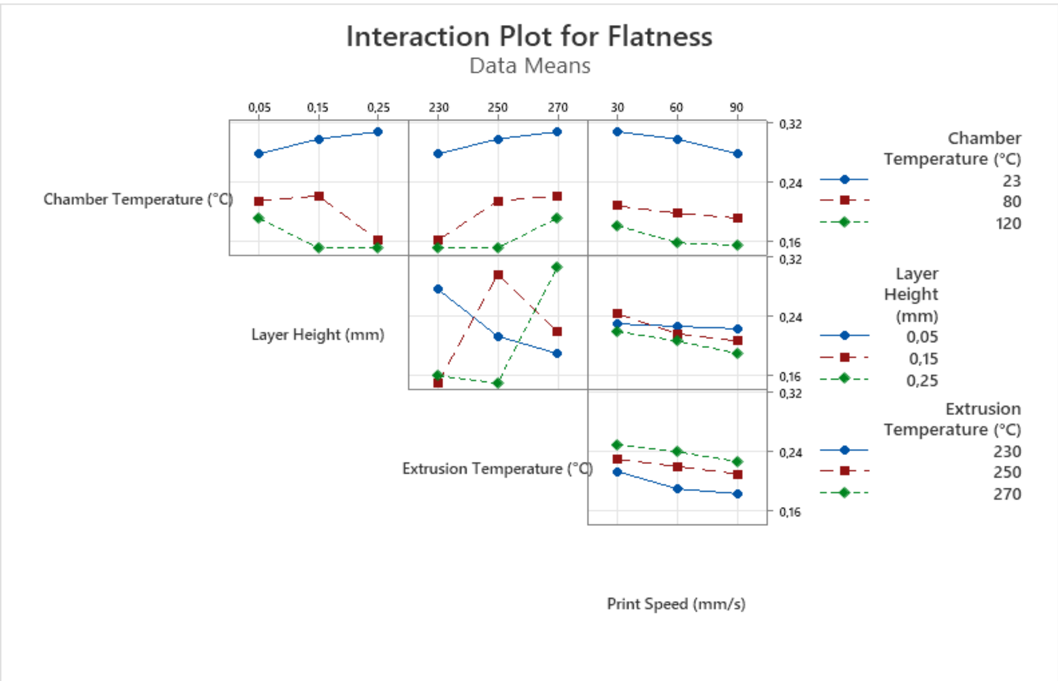

Figure 53 - Interaction plot for flatness (FI1)

4.2.7. Perpendicularity (P1) vs Chamber temperature, Infill density, Layer height, Extrusion temperature, Print speed, and Infill strategy

In Figure 54, the ANOVA was performed between response flatness horizontal planes (FH1), and all the parameters can be observed.

Source	DF	Adj SS	Adj MS	F-Value	P-Value
Chamber Temperature (°C)	2	0,001689	0,000844	48,36	0,000
Infill Density (%)	2	0,000067	0,000033	1,91	0,185
Layer Height (mm)	2	0,000556	0,000278	15,91	0,000
Extrusion Temperature (°C)	2	0,000022	0,000011	0,64	0,544
Print Speed (mm/s)	2	0,000067	0,000033	1,91	0,185
Infill Strategy	2	0,000022	0,000011	0,64	0,544
Error	14	0,000244	0,000017		
Total	26	0,002667			

Figure 54 - ANOVA table for Perpendicularity (P1)

F-values were compared. Observing the F values, two parameters are significant for a significance level of 5%: chamber temperature and layer height.

Below, a main effect plot is presented with the two parameters mentioned above, represented in Figure 55:

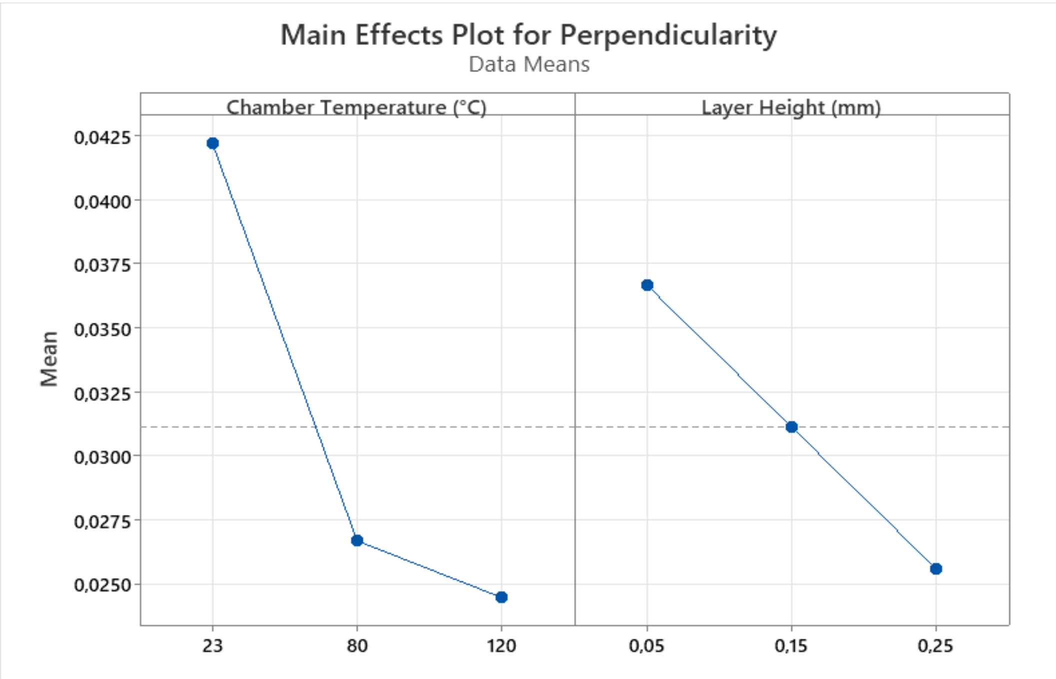

Figure 55 - Main effect plot of chamber temperature and layer height for Perpendicularity (P1)

The influence of layer height is constant since the slope exhibits a stable and linear connection across the layers under investigation. This implies that layer height has a simple and continuous impact on Perpendicularity, which makes it simpler to predict how changing parameter values would affect response. The behaviour stays the same for chamber temperature as in the other chapter analysed in this study. There is a drastic effect in changing the chamber temperature from 23 to 80ºC, but then the 80 and 120ºC range is stable.

From the interaction plot (Figure 56), the following can be observed:

- The blue line, 23ºC of chamber temperature, seems to have no differences between layer height. It only gets worse when the layer height is changed to 0.15mm but then improves again with 0.25mm. Overall, there isn’t an improvement or a worsening in mean deviation for 23ºC across levels of layer height.
- The red line, 80ºC, and the green line, 120ºC, starts and ends in the same mean values. Only in between at 0.15mm of layer height, the red line maintains its value with no improvement, but the green line does improve. Then, the lines meet at 0.25mm of layer height as the red line improves and the green line gradually stables.
- Ultimately, this means varying layer height as an interaction effect with chamber temperature.

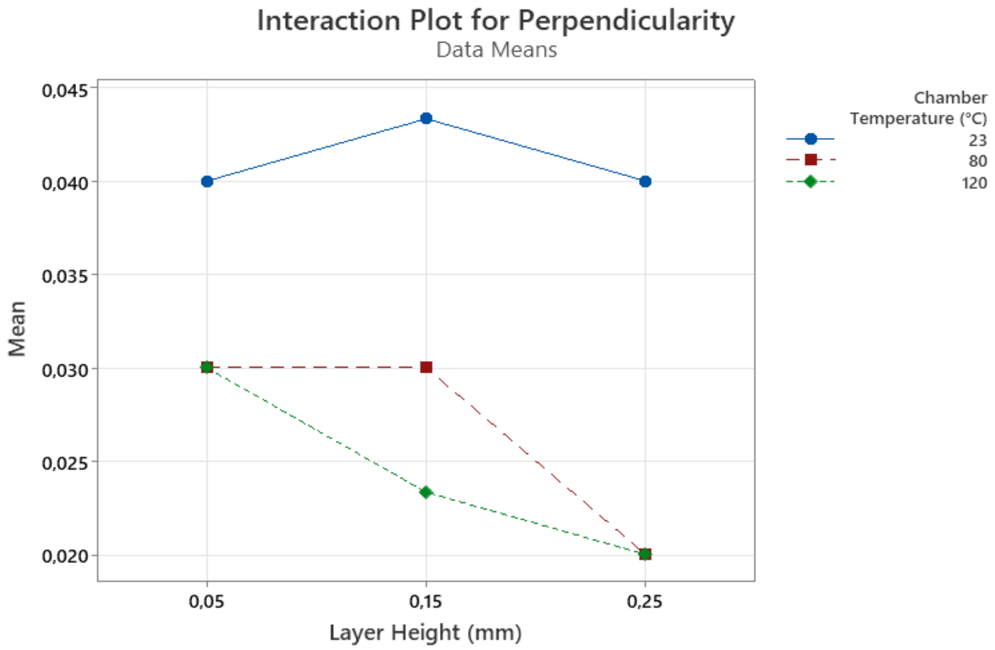

Figure 56 - Interaction plot for Perpendicularity (P1)

4.3. Optimum print levels

Signal-to-noise ratio tables were executed to find the optimum print levels. Following a "Smaller-the-Better" analysis, it is possible to choose the best value of each parameter by observing for each parameter the level with the highest signal. A response table like Table 20 was performed for each response.

Table 20 - Choice of best levels based on Signal-to-Noise Ratio

Response Table for Signal to Noise Ratios

Smaller is better

Level	Chamber Temperature (°C)	Infill Density (%)	Layer Height (mm)	Extrusion Temperature (°C)	Print Speed (mm/s)	Infill Strategy
1	7,631	10,486	9,727	11,418	9,755	10,622
2	11,114	10,453	10,470	10,372	10,613	10,492
3	12,772	10,577	11,319	9,726	11,149	10,403
Delta	5,142	0,125	1,592	1,692	1,395	0,219
Rank	1	6	3	2	4	5

Table 21 shows which combination of control settings is best for each response. Finding the most common control level for each parameter across all characteristics is the first step in the thorough optimisation of control levels for these features.

Table 21 - Optimum print level

OPT	Chamber Temperature (°C)	Infill Density (%)	Layer Height (mm)	Extrusion Temperature (°C)	Print Speed (mm/s)	Infill Strategy
FH1	3	3	3	1	3	1
FH2	3	2	3	1	3	1
FH3	3	2	3	1	3	3
FV1	3	2	3	1	3	1
FV2	3	2	3	1	3	1
FV3	3	3	3	1	2	1
FV4	3	2	3	1	3	1
FV5	3	2	3	1	3	1
FV6	3	2	3	1	3	2
FV7	3	2	3	1	3	1
FV8	3	1	3	1	3	1
FV9	3	2	3	1	3	1
FV10	3	2	3	1	3	1
FI1	3	2	3	1	3	1
FI2	3	2	3	1	3	1
C1	3	3	3	1	3	1
C2	3	3	3	1	3	1
CO1	3	1	3	1	3	1
PLV1	3	2	3	1	3	2
PLV2	3	2	2	2	3	2
PLV3	3	2	3	1	2	1
PLV4	3	3	1	1	3	1
PLV5	3	3	1	1	2	1
PLV6	3	2	3	1	3	1
P1	3	2	3	2	3	2
P2	3	1	3	1	3	2
P3	3	2	3	1	3	1
P4	3	1	3	1	3	1
P5	3	2	3	1	3	1
P6	3	1	2	1	3	1
P7	3	3	2	1	2	1
P8	2	1	1	1	1	1
P9	3	3	3	1	3	1
P10	3	3	3	1	2	1
P11	3	2	3	1	3	1
Overall Ranking	3	2	3	1	3	1

The result of this comprehensive method is Table 22, which shows the control level that has been optimised together with its parameter settings that are specially extracted for geometric characteristics. Infill strategy is not considered relevant, so it is not included in the optimum parameter for optimum print condition.

Table 22 - Optimum print condition for geometric characteristics

Parameter	Control Level	Parameter Setting
Chamber Temperature (°C)	3	120
Infill Density (%)	2	60
Layer Height (mm)	3	0.25
Extrusion Temperature (°C)	1	230
Print Speed (mm/s)	3	90

Chapter 5

Discussion and results analysis

5.1 Discussion and results Analysis

In this chapter, results from the previous chapter will be analysed and comprehended.

Parameters

Promoting cylindricity, concentricity, parallelism, flatness, and perpendicularity are all significantly impacted by chamber temperature, set at 120ºC, extrusion temperature, set at 230ºC, layer height at 0.25mm, and print speed, set at 90mm/s print speed. These settings align closely with the outcomes observed in run number 27 of the Taguchi design (TGC27).

Comparing the optimum print levels for geometric tolerances with Mahmood et al. [5], the results have some differences, but it may be due to the type of experiments conducted. In Mahmood's work, some inconsistencies in the results in terms of optimum control levels for each geometrical characteristic can be found, revealing that it is quite challenging to access the optimal levels only with experimental observations. Mahmood printed various parts according to his Design of Experiments and then measured them using a coordinate measuring machine (CMM). Finally, an SNR method was used to analyse the influence of the parameters on geometric characteristics. The experiments being statically analysed in Mahmood are based on the variability of means between groups and within groups, which is often found when printing a part with the same parameters numerous times.

The benchmark used in Mahmood's study may also be the reason for such differences. Mahmood uses a benchmark much bigger in nominal size, which could affect geometric tolerances overall, especially tolerances measured horizontally due to shrinking. Moreover, the Mahmood benchmark has a greater variety of forms and features, so it enables the assessment of various elements with more detail and precision. Having a wider variety of results in features can also be more conclusive in finding the potential factors that might cause variations and, as a result, a more precise optimisation of print levels.

Table 23 - Optimum print levels for geometric tolerances (extracted from [5])

Parameter		Control Level	Parameter Setting
A:	Chamber temperature (°C)	2	45
B:	Layer thickness (mm)	2	0.2
C:	Extruder temperature (°C)	1	207
D:	Platform temperature (°C)	2	121
E:	Number of shells	2	2
F:	Infill shell spacing multiplier	1	0.56
G:	Inset distance multiplier	2	0.8
H:	Floor/roof thickness (mm)	2	0.8
J:	Infill pattern	3	diagonal
K:	Infill density (%)	1	25
L:	Infill speed (mm/s)	3	108
M:	Outline speed (mm/s)	1	24
N:	Inset speed (mm/s)	2	72

Chamber temperature

For cylindricity (C1), concentricity (CO1), parallelism (PLV1), and flatness (FH2, FV1, FI1) – chamber temperature appears as a critical parameter. Better material adhesion and flow between layers are made possible by higher chamber temperatures. Raising the temperature promotes better layer bonding and reduces warping, both of which are essential for preserving geometric accuracy. Heat encourages homogeneous solidification, which lowers internal tensions and improves alignment. The main effects plots indicate that chamber temperature has a considerable impact on mean values due to its steep slopes across responses. Confirming its essential role in producing improved results for all responses. chamber temperature has a strong impact even when paired with other parameters, like layer height and extrusion temperature, as evidenced by its importance and stability among responses. Its influence is significant, resulting in noticeable differences in mean results for various parameter combinations. Wang et al. [48] demonstrate how altering processing parameters, such as chamber temperature, can substantially decrease warpage. Another consistent fact with Kuo and Samt is the parameter values. Although chamber temperature values (75ºC in Samy and 43ºC for Kuo) are different than this study, further examination of these articles verifies that higher levels of this parameter show the best results, which is consistent with this study.

Extrusion temperature

Extrusion temperature showcases a reverse impact in several responses, notably affecting cylindricity (C1), concentricity (CO1), and flatness (FH2, FV1, FI1). The viscosity of the material is influenced by the extrusion temperature, which changes how the material flows when printed. Increased temperatures have the potential to cause over-extrusion and inaccurate layer deposition due to the reduction of material viscosity. This frequently leads to less accuracy in responses. Conversely, lower temperatures result in higher viscosity, which adversely affects layer bonding and material flow. extrusion temperature on specific responses is less consistent when combined with other parameters. However, it shows more sensitivity across levels of chamber temperature.

Kuo et al. [24] highlight how important temperature is in influencing the warpage of ABS prototypes. Raising the chamber and extrusion temperatures promotes better interaction between filament layers and makes cooling more uniform. Consequently, the finished part experiences less distortion and warping due to the reduction of the ram residual stresses.

Articles [5], [24], [68], [3], [69] are in harmony with the optimum value resulting in this study.

Layer height

It shows a moderate impact among responses but not as substantially as chamber temperature or extrusion temperature. Allegedly, more minor layer heights can contribute to a better response, as they allow for finer detailing and smoother transitions between layers. More considerable layer heights, conversely, might lead to increased deviation from flatness due to coarser layer transitions. However, the results show the opposite, as the best mean deviations were obtained with higher layer height. Several articles validate this; Agarwal et al. [70] concluded that increasing layer thickness resulted in an increase in deviation on printed parts. Schneidler et al. [71] concludes in his results that the smaller the layer height, the better the overall quality and especially the surface roughness. Cappellini et al. [72] presents a summary table with the relationships between process parameters and performance measures. With layer height, there are substantially more articles discussing that increasing process parameters leads to worsening dimensional and geometric accuracy. Also, several articles are neutral, meaning that the test relationship didn´t verify if it was significantly positive or negative. There aren´t articles showing that increasing process parameters leads to improving dimensional and geometric accuracy.

Layer height has modest interaction effects, particularly in conjunction with chamber temperature or extrusion temperature. Across several combinate ions, these interactions lead to discernible differences in mean values.

Print speed

Cylindricity (C1) and flatness (FV1) show a moderate impact. The speed at which the nozzle deposits the material can change the heating and cooling cycle, resulting in a varied degree of thermal gradient and affecting the part's accuracy [39]. Faster printing and shorter cooling times are consistent with findings by Samy et al. [15]. Increased printing speeds result in shorter layer spacing, which lessens internal thermal stresses because of faster solidification. This is consistent with the finding that faster printing speed speeds help reduce distortion in the finished part. It is also consistent with Agarwal et al. [70] that dimensional accuracy improves with quicker print speeds.

Infill density

Infill density is one of the lowest significant parameters in geometric tolerances. Although Agarwal et al. [70] work is about dimensional variations, it can also be understood in geometric deviations. Due to restricted space within the part, a high amount of molten material present might immediately cause an event where it flows outward, deforming the part that is formed. So, reducing the infill density is advised to limit deviations. According to Agarwal, the optimum infill density is 20%, which is in harmony with maximising flatness in this study.

5.2. Geometric tolerance

The mean deviations from the numerical simulations were categorised in accordance with ISO 2768 general tolerances for straightness and flatness, perpendicularity, and cylindricity.

A large fraction of data exceeded the stipulated tolerance limits when fatness deviations were evaluated (FH2, FV1, FV2, FV3, FV4, FV5, FV6, FV8, FV9, FV10). These observations point to difficulties in getting the required flat surfaces inside printed parts. Deviations in flatness that exceed the tolerance limits may influence the overall surface quality and assembly of the components. Most part features that exceeded tolerance limits were vertical planes in flatness.

Minetola et al. [73] presents in their paper GD&T values for different geometric features of their benchmark. Focusing on flatness, Minetola also divides flatness into horizontal, vertical, and inclined planes. The deviation values of flatness planes were the best among flatness, which is in accordance with this study. The best deviation value for flatness in flatness planes is FH1 with 0.03mm, for flatness in vertical planes is FV7 with 0.19mm, and for flatness in inclined planes is FI1 or FI2 with 0.33mm. So, the explanation for this is the absence of the staircase effect on flatness planes. horizontal planes are constructed within a single layer of material, but the addition of multiple layers has a detrimental effect on the quality of vertical and inclined planes.

Table 24 – General tolerances for straightness and flatness of part features

Part feature	Nominal (mm)	Dev.	Tol	IT class
FH1	10	0,03	0.05	K
FH2	50	0,5	0.4	Above limit
FH3	10	0,04	0.05	K
FV1	15	0,26	0.2	Above limit
FV2	15	1,5	0.2	Above limit
FV3	9,72	0,72	0.1	Above limit
FV4	15	0,21	0.2	Above limit
FV5	15	1,39	0.2	Above limit
FV6	9,72	0,67	0.1	Above limit
FV7	15	0,19	0.2	L
FV8	15	0,25	0.2	Above limit
FV9	15	1,45	0.2	Above limit
FV10	15	1,84	0.2	Above limit
FI1	50	0,33	0.4	L
FI2	50	0,33	0.4	L

To date, there aren´t many publications studying general tolerancing in perpendicularity and cylindricity, so it´s not possible to make a comparison. However, the thesis of Abdelrhman et al. [74] has values that can be comparable. The perpendicularity average value is 0.05605 mm in Abdelrhman's work. The higher perpendicularity value recorded in his study is 0.0935 mm. 6-part features fall inside these values, while 5-part features are outside.

Table 25 - General tolerances for perpendicularity of part features

Part feature	Nominal (mm)	Dev.	Tol	IT class
P1	15	0,05	0.2	H
P2	15	0,05	0.2	H
P3	9,72	0,12	0.2	H
P4	5,28	0,31	0.2	K
P5	10	0,41	0.2	L
P6	9,72	0,17	0.2	H
P7	5,28	0,18	0.2	H
P8	15	0,04	0.2	H
P9	15	0,8	0.2	Above limit
P10	10	0,49	0.2	L
P11	15	0,38	0.2	K

The perpendicularity average value is 0.05605 mm in Abdelrhman's work. The higher perpendicularity value recorded in his study is 0.0935 mm. 6-part features fall inside these numbers, while 5-part features are outside. The average cylindricity value is 0.2033 mm in Abdelrhman's work. The higher cylindricity value recorded in his study is 0.2551 mm. All part features fall outside of these values.

Table 26 - General tolerances for Cylindricity of part features

Part feature	Nominal (mm)	Dev.	Tol	IT class
C1	40	0,47	0.5	L
C2	30	0,47	0.5	L

Chapter 6

Conclusion and future works

6.1. Conclusion

The purpose of this study was to investigate the influence of process parameters on geometric tolerances quantitatively. A DoE was put in place to investigate the impact. Chamber temperature, infill density, extrusion temperature, layer height, print speed, and infill strategy were the parameters used. Cylindricity (C1), concentricity (CO1), parallelism (PLV1), flatness in horizontal planes (FH2), flatness in vertical planes (FV2) and flatness in inclined planes (FI1) and perpendicularity (P1) were chosen as replies from 35 distinct responses. It was feasible to comprehend the impact of the parameters on the geometric tolerances after doing statistical analyses such as ANOVA, main effect plots, and interaction plots. Following completion of this study, the following key findings may be drawn:

Chamber temperature

- **Significant impact:** Chamber temperature demonstrates a significant impact across multiple responses.
- **Improved adhesion and flow:** higher chamber temperature promotes better material adhesion and flow between layers, aiding in better layer bonding, reducing warping, and enhancing alignment.
- **Optimal value for geometric accuracy:** 120 ºC

Extrusion temperature

- **Significant impact:** extrusion temperature demonstrates a significant impact from almost all responses.

  Viscosity influence: changes in extrusion temperature influence material viscosity, impacting how the material flows during printing. Higher temperatures may lead to over-extrusion and inaccuracies, while lower temperatures affect layer bonding negatively.

- **Optimal value for geometric accuracy:** 230 ºC

Layer height

Moderate impact: Layer height showcases varied impacts across different responses and has a moderate impact on responses, but it is not as significant as chamber or extrusion temperature.

According to the numeric results obtained, higher layer thickness should provide better mean deviations. Results are contrary to some other results published.

- **Optimal value for geometric accuracy:** 0.25mm

Print speed

Moderate Impact: Print speed impacts cylindricity and flatness moderately, affecting the heating and cooling cycle and influencing accuracy.

Thermal gradient and Stresses: faster print speeds result in shorter layer spacing, reducing internal thermal stresses due to faster solidification.

- **Optimal value for geometric accuracy:** 90 mm/s

Infill density

Lower Impact: Infill density demonstrates low significant impacts on geometric tolerances.

Deformation Considerations: higher densities may cause material to flow outward, deforming the part; therefore, reducing density is advised to limit deviations.

- **Optimal value for geometric accuracy:** 60%

Infill strategy

Infill strategy is not as relevant as other parameters, likely indicating it is less significant compared to other parameters.

Furthermore, the study gave a nuanced viewpoint in general tolerancing for form. Flatness measurements were off the ISO general tolerances classification, suggesting difficulties in maintaining surface flatness. Perpendicularity, on the other hand, fulfilled class H standards with a few exceptions. Cylindricity was within class L, suggesting lesser accuracy.

As the final observations, while time-consuming due to extensive numerical analysis and the use of several software, the methodological approach used in this study has a significant advantage across experimental techniques; it provides a way to numerically predict the effect of several printing parameters, avoiding challenging experimental variables, such as platform adhesion, which is critical in accurately determining geometric tolerances.

6.2. Future works

The pivotal aim in future works should be the uniform integration of numerical experimentation with experimental validation. This involves a rigorous comparison of the numerical simulation findings with the concrete results gained through practical experiments. Harmonising the two domains and assuring alignment between results is essential. To do such an analysis, it is necessary to have a 3D printer that can print with parameters according to the levels presented in the numerical study.

The DIGIMAT AM is an advanced software capable of running the same experiments using the compensated geometries generated by the software and performing a examination of their performance to see if the results meet the specified tolerance thresholds.

Some findings revealed an unusual occurrence in which specific data points differed considerably from what was expected. While unexpected, such situations provide an essential opportunity for refining and augmentation of the study’s approach.

References

[1] G. Nyiranzeyimana, J. M. Mutua, B. R. Mose, and T. O. Mbuya, “A grey-based Taguchi method to optimize fused deposition modelling process parameters for manufacture of a hip joint implant,” *Materwiss. Werksttech.*, vol. 53, no. 1, pp. 89–108, 2022, doi: 10.1002/mawe.202100129.

[2] M. D. Monzón, Z. Ortega, A. Martínez, and F. Ortega, “Standardization in additive manufacturing: activities carried out by international organizations and projects,” *Int. J. Adv. Manuf. Technol.*, vol. 76, no. 5–8, pp. 1111–1121, 2015, doi: 10.1007/s00170-014-6334-1.

[3] M. Shahrain, T. Didier, G. K. Lim, and A. J. Qureshi, “Fast Deviation Simulation for ‘Fused Deposition Modeling’ Process,” in *Procedia CIRP*, 2016, vol. 43, pp. 327–332, doi: 10.1016/j.procir.2016.02.004.

[4] T. Lieneke, V. Denzer, G. A. O. Adam, and D. Zimmer, “Dimensional Tolerances for Additive Manufacturing: Experimental Investigation for Fused Deposition Modeling,” in *Procedia CIRP*, 2016, vol. 43, pp. 286–291, doi: 10.1016/j.procir.2016.02.361.

[5] S. Mahmood, A. J. Qureshi, and D. Talamona, “Taguchi based process optimization for dimension and tolerance control for fused deposition modelling,” *Addit. Manuf.*, vol. 21, pp. 183–190, 2018, doi: 10.1016/j.addma.2018.03.009.

[6] J. I. Aguilar-Duque, J. L. García-Alcaraz, and J. L. Hernández-Arellano, “Geometric considerations for the 3D printing of components using fused filament fabrication,” *Int. J. Adv. Manuf. Technol.*, vol. 109, no. 1–2, pp. 171–186, 2020, doi: 10.1007/s00170-020-05523-3.

[7] H. Alzyod and P. Ficzere, “Optimizing fused filament fabrication process parameters for quality enhancement of PA12 parts using numerical modeling and taguchi method,” *Heliyon*, vol. 9, no. 3, p. e14445, 2023, doi: 10.1016/j.heliyon.2023.e14445.

[8] M. Popović, M. Pjević, A. Milovanović, G. Mladenović, and M. Milošević, “Printing parameter optimization of PLA material concerning geometrical accuracy and tensile properties relative to FDM process productivity,” *J. Mech. Sci. Technol.*, vol. 37, no. 2, pp. 697–706, 2023, doi: 10.1007/s12206-023-0113-6.

[9] D. Fico, D. Rizzo, R. Casciaro, and C. E. Corcione, “A Review of Polymer-Based Materials for Fused Filament Recycled Materials,” *Polymers (Basel).*, vol. 14, p. 465, 2022.

[10] “PLA for 3D Printing: All You Need to Know - 3Dnatives.” https://www.3dnatives.com/en/pla-3d-printing-guide-190820194/.

[11] “All You Need to Know About PEEK for 3D printing - 3Dnatives.” https://www.3dnatives.com/en/peek-3d-printing-060420204/#!

[12] “PETG: All You Need to Know for 3D Printing - 3Dnatives.” https://www.3dnatives.com/en/petg-3d-printing-guide-181220194/.

[13] “Polycarbonate (PC) for 3D Printing: All You Need to Know - 3Dnatives.” https://www.3dnatives.com/en/polycarbonate-pc-for-3d-printing-110220204/.

[14] H. Rahman, T. D. John, M. Sivadasan, and N. K. Singh, “Investigation on the Scale

Factor applicable to ABS based FDM Additive Manufacturing," *Mater. Today Proc.*, vol. 5, no. 1, pp. 1640–1648, 2018, doi: 10.1016/j.matpr.2017.11.258.

[15] A. A. Samy, A. Golbang, E. Harkin-Jones, E. Archer, D. Tormey, and A. McIlhagger, "Finite element analysis of residual stress and warpage in a 3D printed semi-crystalline polymer: Effect of ambient temperature and nozzle speed," *J. Manuf. Process.*, vol. 70, pp. 389–399, 2021, doi: 10.1016/j.jmapro.2021.08.054.

[16] B. Zharylkassyn, A. Perveen, and D. Talamona, "Effect of process parameters and materials on the dimensional accuracy of FDM parts," *Mater. Today Proc.*, vol. 44, pp. 1307–1311, 2021, doi: 10.1016/j.matpr.2020.11.332.

[17] N. Lokesh, B. A. Praveena, J. Sudheer Reddy, V. K. Vasu, and S. Vijaykumar, "Evaluation on effect of printing process parameter through Taguchi approach on mechanical properties of 3D printed PLA specimens using FDM at constant printing temperature," *Mater. Today Proc.*, Nov. 2021, doi: 10.1016/j.matpr.2021.11.054.

[18] L. Baich, G. Manogharan, and H. Marie, "Study of infill print design on production cost-time of 3D printed ABS parts," *Int. J. Rapid Manuf.*, vol. 5, no. 3/4, p. 308, 2015, doi: 10.1504/ijrapidm.2015.074809.

[19] J. Nagendra, M. K. Srinath, S. Sujeeth, K. S. Naresh, and M. S. Ganesha Prasad, "Optimization of process parameters and evaluation of surface roughness for 3D printed nylon-aramid composite," in *Materials Today: Proceedings*, 2021, vol. 44, pp. 674–682, doi: 10.1016/j.matpr.2020.10.609.

[20] P. Pombinha, M. Leite, A. Carvalho, R. Cláudio, A. Silva, and A. R. Ribeiro, "A STUDY ON THE EFFECT OF LAYER THICKNESS AND INFILL DENSITY ON GEOMETRIC TOLERANCE IN FDM," 2018.

[21] M. Karthic, "INFLUENCE OF FDM PROCESS PARAMETERS ON PART DEFORMATION AND ITS COMPARISION WITH 3D FEA SIMULATION," 2016.

[22] P. Sikder, B. T. Challa, and S. K. Gummadi, "A comprehensive analysis on the processing-structure-property relationships of FDM-based 3-D printed polyetheretherketone (PEEK) structures," *Materialia*, vol. 22, no. April, p. 101427, 2022, doi: 10.1016/j.mtla.2022.101427.

[23] S. Thumsorn, W. Prasong, A. Ishigami, T. Kurose, Y. Kobayashi, and H. Ito, "Influence of Ambient Temperature and Crystalline Structure on Fracture Toughness and Production of Thermoplastic by Enclosure FDM 3D Printer," *J. Manuf. Mater. Process.*, vol. 7, no. 1, 2023, doi: 10.3390/jmmp7010044.

[24] C. C. Kuo, Y. R. Wu, M. H. Li, and H. W. Wu, "Minimizing warpage of ABS prototypes built with low-cost fused deposition modeling machine using developed closed-chamber and optimal process parameters," *Int. J. Adv. Manuf. Technol.*, vol. 101, no. 1–4, pp. 593–602, 2019, doi: 10.1007/s00170-018-2969-7.

[25] J. H. Porter, T. M. Cain, S. L. Fox, and P. S. Harvey, "Influence of infill properties on flexural rigidity of 3D-printed structural members," *Virtual Phys. Prototyp.*, vol. 14, no. 2, pp. 148–159, 2019, doi: 10.1080/17452759.2018.1537064.

[26] H. K. Dave, N. H. Patadiya, A. R. Prajapati, and S. R. Rajpurohit, "Effect of infill pattern and infill density at varying part orientation on tensile properties of fused deposition modeling-printed poly-lactic acid part," *Proc. Inst. Mech. Eng. Part C*

J. Mech. Eng. Sci., vol. 235, no. 10, pp. 1811–1827, 2021, doi: 10.1177/0954406219856383.

[27] N. Watanabe, M. L. Shofner, N. Treat, and D. W. Rosen, “A model for residual stress and part warpage prediction in material extrusion with application to polypropylene,” *Solid Free. Fabr. 2016 Proc. 27th Annu. Int. Solid Free. Fabr. Symp. - An Addit. Manuf. Conf. SFF 2016*, pp. 2437–2455, 2016.

[28] Z. Jiang, B. Diggle, M. L. Tan, J. Viktorova, C. W. Bennett, and L. A. Connal, “Extrusion 3D Printing of Polymeric Materials with Advanced Properties,” vol. 2001379, pp. 1–32, 2020, doi: 10.1002/advs.202001379.

[29] A. Alafaghani, A. Qattawi, B. Alrawi, and A. Guzman, “Experimental Optimization of Fused Deposition Modelling Processing Parameters: A Design-for-Manufacturing Approach,” *Procedia Manuf.*, vol. 10, pp. 791–803, 2017, doi: 10.1016/j.promfg.2017.07.079.

[30] M. Algarni and S. Ghazali, “Comparative study of the sensitivity of pla, abs, peek, and petg’s mechanical properties to fdm printing process parameters,” *Crystals*, vol. 11, no. 8, 2021, doi: 10.3390/cryst11080995.

[31] B. Pernet, J. K. Nagel, and H. Zhang, “Compressive Strength Assessment of 3D Printing Infill Patterns,” *Procedia CIRP*, vol. 105, no. March, pp. 682–687, 2022, doi: 10.1016/j.procir.2022.02.114.

[32] V. Cabreira and R. M. C. Santana, “Effect of infill pattern in fused filament fabrication (FFF) 3D printing on materials performance,” *Rev. Mater.*, vol. 25, no. 3, pp. 1–9, 2020, doi: 10.1590/s1517-707620200003.1126.

[33] U. M. Dilberoglu, S. Simsek, and U. Yaman, “Shrinkage compensation approach proposed for ABS material in FDM process,” *Mater. Manuf. Process.*, vol. 34, no. 9, pp. 993–998, 2019, doi: 10.1080/10426914.2019.1594252.

[34] M. S. Alsoufi and A. E. Elsayed, “Warping deformation of desktop 3D printed parts manufactured by open source fused deposition modeling (FDM) system,” *Int. J. Mech. Mechatronics Eng.*, vol. 17, no. 4, pp. 7–16, 2017.

[35] W. Hong, Y. T. Lee, and H. Gong, “A study of the staircase effect induced by material shrinkage in rapid prototyping,” *Rapid Prototyp. J.*, vol. 11, no. 2, pp. 82–89, 2005, doi: 10.1108/13552540510589449.

[36] E. Umaras and M. S. G. Tsuzuki, “Additive Manufacturing - Considerations on Geometric Accuracy and Factors of Influence,” in *IFAC-PapersOnLine*, 2017, vol. 50, no. 1, pp. 14940–14945, doi: 10.1016/j.ifacol.2017.08.2545.

[37] A. Hriţuc, A. M. Mihalache, L. Slătineanu, O. Dodun, and G. Nagîţ, “Empirical Modeling of Heat Transfer in Cylindrical Polymer Rods Manufactured by 3D Printing,” *Bull. Polytech. Inst. Iași. Mach. Constr. Sect.*, vol. 68, no. 4, pp. 31–40, 2022, doi: 10.2478/bipcm-2022-0033.

[38] Y.-H. Choi, C.-M. Kim, H.-S. Jeong, and J.-H. Youn, “Influence of Bed Temperature on Heat Shrinkage Shape Error in FDM Additive Manufacturing of the ABS-Engineering Plastic,” *World J. Eng. Technol.*, vol. 04, no. 03, pp. 186–192, 2016, doi: 10.4236/wjet.2016.43d022.

[39] A. K. Sood, R. K. Ohdar, and S. S. Mahapatra, “Improving dimensional accuracy of Fused Deposition Modelling processed part using grey Taguchi method,” *Mater. Des.*, vol. 30, no. 10, pp. 4243–4252, 2009, doi: 10.1016/j.matdes.2009.04.030.

[40] E. R. Fitzharris, N. Watanabe, D. W. Rosen, and M. L. Shofner, “Effects of material properties on warpage in fused deposition modeling parts,” *Int. J. Adv. Manuf. Technol.*, vol. 95, no. 5–8, pp. 2059–2070, 2018, doi: 10.1007/s00170-017-1340-8.

[41] I. J. Solomon, P. Sevvel, and J. Gunasekaran, “A review on the various processing parameters in FDM,” in *Materials Today: Proceedings*, 2020, vol. 37, no. Part 2, pp. 509–514, doi: 10.1016/j.matpr.2020.05.484.

[42] H. Guo, J. Xu, S. Zhang, and G. Yi, “Build orientation optimization based on weighted analysis of local surface region curvature,” *Appl. Sci.*, vol. 11, no. 1, pp. 1–20, 2021, doi: 10.3390/app11010304.

[43] A. Haidiezul, A. Aiman, and B. Bakar, “Surface Finish Effects Using Coating Method on 3D Printing (FDM) Parts,” *IOP Conf. Ser. Mater. Sci. Eng. Pap.*, 2018, doi: 10.1088/1757-899X/318/1/012065.

[44] X. Zhou, S. J. Hsieh, and Y. Sun, “Experimental and numerical investigation of the thermal behaviour of polylactic acid during the fused deposition process,” *Virtual Phys. Prototyp.*, vol. 12, no. 3, pp. 221–233, 2017, doi: 10.1080/17452759.2017.1317214.

[45] M. Spoerk, F. Arbeiter, I. Raguž, and G. Traxler, “The consequences of different printing chamber temperatures in extrusion-based additive manufacturing Multi-Layer Fracture Mechanics in Polymers View project 3DMultiMat-3D Printed Functional Multi-Material Components View project,” no. September, 2018, [Online]. Available: https://www.researchgate.net/publication/338005630.

[46] A. El Moumen, M. Tarfaoui, and K. Lafdi, “Modelling of the temperature and residual stress fields during 3D printing of polymer composites,” *Int. J. Adv. Manuf. Technol.*, vol. 104, no. 5–8, pp. 1661–1676, Oct. 2019, doi: 10.1007/s00170-019-03965-y.

[47] E. Padovano, M. Galfione, P. Concialdi, G. Lucco, and C. Badini, “Mechanical and thermal behavior of ultem® 9085 fabricated by fused-deposition modeling,” *Appl. Sci.*, vol. 10, no. 9, 2020, doi: 10.3390/app10093170.

[48] T. M. Wang, J. T. Xi, and Y. Jin, “A model research for prototype warp deformation in the FDM process,” *Int. J. Adv. Manuf. Technol.*, vol. 33, no. 11–12, pp. 1087–1096, 2007, doi: 10.1007/s00170-006-0556-9.

[49] M. Spoerk, C. Holzer, and J. Gonzalez-Gutierrez, “Material extrusion-based additive manufacturing of polypropylene: A review on how to improve dimensional inaccuracy and warpage,” *Journal of Applied Polymer Science*, vol. 137, no. 12. John Wiley and Sons Inc., Mar. 20, 2020, doi: 10.1002/app.48545.

[50] A. Armillotta, M. Bellotti, and M. Cavallaro, “Warpage of FDM parts: Experimental tests and analytic model,” *Robot. Comput. Integr. Manuf.*, vol. 50, pp. 140–152, 2018, doi: 10.1016/j.rcim.2017.09.007.

[51] A. Antony Samy, A. Golbang, E. Harkin-Jones, E. Archer, and A. McIlhagger, “Prediction of part distortion in Fused Deposition Modelling (FDM) of semi-crystalline polymers via COMSOL: Effect of printing conditions,” *CIRP J. Manuf. Sci. Technol.*, vol. 33, pp. 443–453, 2021, doi: 10.1016/j.cirpj.2021.04.012.

[52] “Design of Experiments – A Primer.” https://www.isixsigma.com/design-of-experiments-doe/design-experiments-␓-primer/.

[53] D. C. Montgomery, *Design and analysis of experiments*. 2016.

[54] M. J. Anderson and P. J. Whitcomb, *DOE Simplified*. 2007.

[55] J. P. C. Kleijnen, "Design of experiments: Overview," *Proc. - Winter Simul. Conf.*, pp. 479–488, 2008, doi: 10.1109/WSC.2008.4736103.

[56] "Taguchi designs - Minitab." https://support.minitab.com/en-us/minitab/21/help-and-how-to/statistical-modeling/doe/supporting-topics/taguchi-designs/taguchi-designs/.

[57] "What is the signal-to-noise ratio in a Taguchi design? - Minitab." https://support.minitab.com/en-us/minitab/21/help-and-how-to/statistical-modeling/doe/supporting-topics/taguchi-designs/what-is-the-signal-to-noise-ratio/.

[58] "Box-Behnken design." https://develve.net/Box-Behnken design.html.

[59] R. F. Gunst and R. L. Mason, "Fractional factorial design," *Wiley Interdiscip. Rev. Comput. Stat.*, vol. 1, no. 2, pp. 234–244, 2009, doi: 10.1002/wics.27.

[60] K. R. Tarlow, "Teaching principles of inference with ANOVA," *Teach. Stat.*, vol. 38, no. 1, pp. 16–21, 2016, doi: 10.1111/test.12085.

[61] DIN EN ISO 286-1:2010, "Geometrical Product Specifications (GPS) — ISO Code System For Tolerances on Linear Sizes — Part 1: Basis of Tolerances, Deviations and Fits," *Iso*, vol. 2010, 2010.

[62] ISO, "Geometrical product specifications (GPS)-Geometrical tolerancing-Tolerances of form, orientation, location and run-out Spécification géométrique des produits (GPS)-Tolérancement géométrique-Tolérancement de forme, orientation, position et battement," *Iso 1101*, vol. 1101, p. 2012, 2012.

[63] M. Canhão, "SIMULAÇÃO NUMÉRICA DO PROCESSO IMPRESSÃO 3D POR FFF," 2021.

[64] G. Allaire, "Numerical Analysis and Optimization," *J. Penelit. Pendidik. Guru Sekol. Dasar*, 2007.

[65] "Digimat-AM." https://www.e-xstream.com/product/digimat-am.

[66] "Digimat 2021," 2021.

[67] "Tessellation." https://www.maruf.ca/files/caadoc/CAATesUseCases/CAATesBody.htm.

[68] O. E. Akbaş, O. Hıra, S. Z. Hervan, S. Samankan, and A. Altınkaynak, "Dimensional accuracy of FDM-printed polymer parts," *Rapid Prototyp. J.*, vol. 26, no. 2, pp. 288–298, 2020, doi: 10.1108/RPJ-04-2019-0115.

[69] A. M. Aboutaleb, L. Bian, P. K. Rao, and M. A. Tschopp, "Accelerated geometry accuracy optimization of additive manufacturing parts," in *ASME 2017 12th International Manufacturing Science and Engineering Conference, MSEC 2017 collocated with the JSME/ASME 2017 6th International Conference on Materials and Processing*, 2017, vol. 2, doi: 10.1115/MSEC2017-2892.

[70] K. M. Agarwal, P. Shubham, D. Bhatia, P. Sharma, H. Vaid, and R. Vajpeyi, "Analyzing the Impact of Print Parameters on Dimensional Variation of ABS specimens printed using Fused Deposition Modelling (FDM)," *Sensors Int.*, vol. 3, no. September 2021, 2022, doi: 10.1016/j.sintl.2021.100149.

[71] J. Schneidler, C. Berry, and A. Barari, “Improving 3D printing geometric accuracy using design of experiments on process parameters in fused filament fabrication (FFF),” *2021 14th IEEE Int. Conf. Ind. Appl. INDUSCON 2021 - Proc.*, pp. 1360–1365, 2021, doi: 10.1109/INDUSCON51756.2021.9529615.

[72] C. Cappellini, Y. Borgianni, L. Maccioni, and C. Nezzi, *The effect of process parameters on geometric deviations in 3D printing with fused deposition modelling*, vol. 122, no. 3–4. Springer London, 2022.

[73] P. Minetola, L. Iuliano, and G. Marchiandi, “Benchmarking of FDM Machines through Part Quality Using IT Grades,” *Procedia CIRP*, vol. 41, pp. 1027–1032, 2016, doi: 10.1016/j.procir.2015.12.075.

Appendix

Appendix A

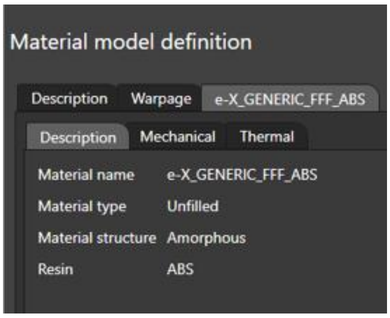

Figure 57 - Description of e-X_GENERIC_FFF_ABS material

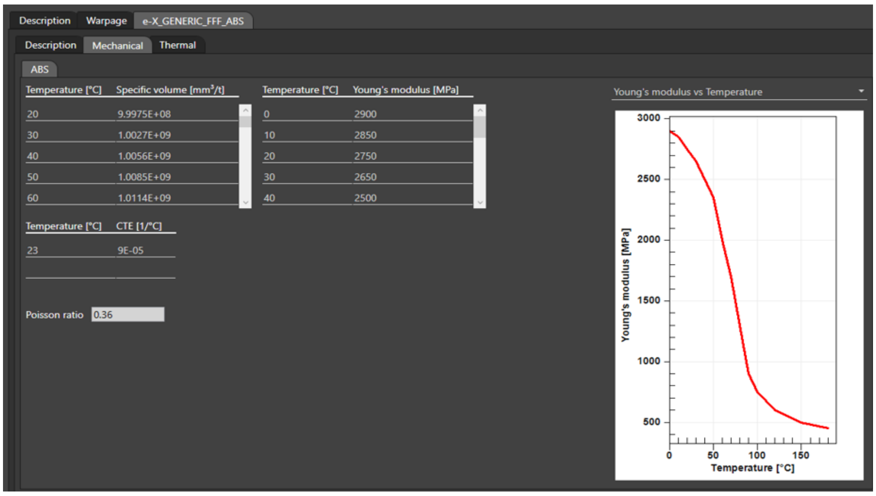

Figure 58 - Mechanical characteristics of e-X_GENERIC_FFF_ABS material

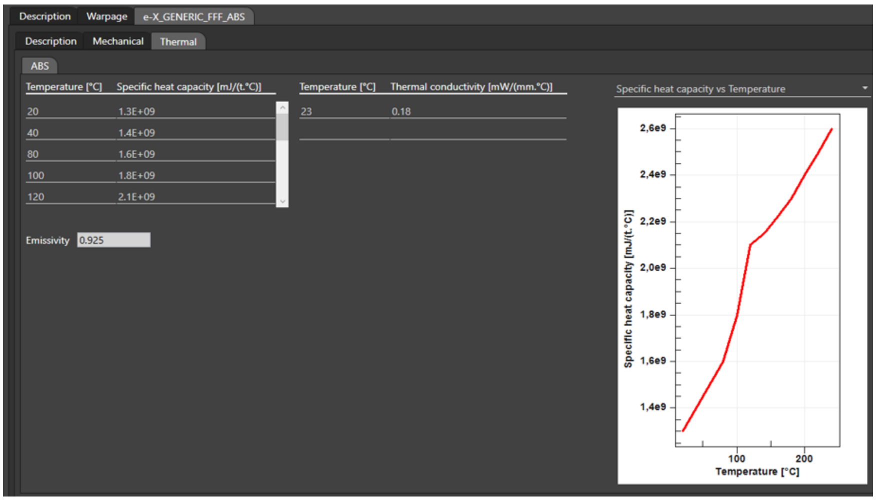

Figure 59 - Thermal characteristics of e-X_GENERIC_FFF_ABS material

Appendix B

Table 27 - Flatness horizontal planes deviation

Run	FH1 [mm]	FH2 [mm]	FH3 [mm]
1	0,02	0,44	0,04
2	0,02	0,44	0,04
3	0,02	0,43	0,04
4	0,02	0,47	0,04
5	0,02	0,45	0,04
6	0,02	0,43	0,03
7	0,03	0,5	0,04
8	0,03	0,45	0,03
9	0,03	0,4	0,02
10	0,02	0,33	0,03
11	0,02	0,3	0,02
12	0,02	0,29	0,02
13	0,02	0,25	0,02
14	0,01	0,23	0,01
15	0,01	0,21	0,01
16	0,02	0,32	0,03
17	0,02	0,31	0,02
18	0,02	0,29	0,02
19	0,01	0,22	0,02
20	0,01	0,2	0,02
21	0,01	0,19	0,01
22	0,02	0,26	0,02
23	0,02	0,25	0,02
24	0,02	0,25	0,02
25	0,02	0,25	0,02
26	0,01	0,18	0,02
27	0,01	0,18	0,01

Appendix C

Table 28 - Flatness vertical planes deviation

Test	FV1 [mm]	FV2 [mm]	FV3 [mm]	FV4 [mm]	FV5 [mm]	FV6 [mm]	FV7 [mm]	FV8 [mm]	FV9 [mm]	FV10 [mm]
1	0,21	0,89	0,64	0,18	0,71	0,63	0,15	0,2	0,83	0,99
2	0,21	0,88	0,64	0,18	0,71	0,63	0,15	0,2	0,8	0,96
3	0,21	0,88	0,72	0,17	0,74	0,63	0,15	0,2	0,78	0,96
4	0,24	0,89	0,61	0,2	0,83	0,63	0,17	0,23	1,11	1,44
5	0,23	0,89	0,61	0,19	0,81	0,63	0,17	0,22	0,85	1,08
6	0,22	0,9	0,64	0,18	0,75	0,6	0,16	0,21	0,83	1,09
7	0,26	1,5	0,64	0,21	1,39	0,67	0,19	0,25	1,45	1,84
8	0,24	0,91	0,64	0,2	0,84	0,63	0,18	0,23	1,05	1,5
9	0,22	0,9	0,6	0,19	0,75	0,59	0,17	0,21	0,8	1,05
10	0,18	0,77	0,14	0,15	0,65	0,12	0,13	0,17	0,71	0,89
11	0,16	0,71	0,12	0,14	0,33	0,12	0,12	0,15	0,55	0,84
12	0,16	0,08	0,12	0,13	0,08	0,11	0,12	0,15	0,34	0,98
13	0,13	0,06	0,1	0,11	0,06	0,09	0,09	0,12	0,07	0,06
14	0,11	0,06	0,09	0,1	0,06	0,08	0,09	0,11	0,06	0,06
15	0,11	0,05	0,09	0,1	0,06	0,08	0,08	0,1	0,06	0,05
16	0,16	0,57	0,13	0,14	0,38	0,12	0,12	0,15	0,54	0,84
17	0,16	0,08	0,12	0,13	0,08	0,11	0,11	0,15	0,46	0,81
18	0,15	0,08	0,12	0,13	0,08	0,11	0,11	0,14	0,08	0,08
19	0,1	0,05	0,09	0,1	0,06	0,08	0,08	0,1	0,06	0,06
20	0,1	0,05	0,08	0,09	0,05	0,08	0,08	0,09	0,06	0,05
21	0,1	0,05	0,08	0,09	0,05	0,07	0,08	0,09	0,06	0,05
22	0,13	0,07	0,11	0,11	0,07	0,1	0,1	0,13	0,08	0,07
23	0,13	0,07	0,11	0,11	0,07	0,1	0,1	0,13	0,08	0,07
24	0,13	0,07	0,1	0,11	0,07	0,09	0,1	0,12	0,08	0,07
25	0,13	0,07	0,1	0,11	0,07	0,1	0,1	0,12	0,08	0,07
26	0,09	0,05	0,06	0,08	0,05	0,06	0,07	0,08	0,05	0,05
27	0,08	0,04	0,06	0,08	0,05	0,06	0,06	0,08	0,05	0,05

Appendix D

Table 29 - Flatness inclined planes deviation

Test	FI1 [mm]	FI2 [mm]
1	0,28	0,28
2	0,28	0,28
3	0,27	0,27
4	0,31	0,3
5	0,3	0,29
6	0,28	0,28
7	0,33	0,33
8	0,31	0,3
9	0,28	0,27
10	0,23	0,22
11	0,22	0,21
12	0,21	0,2
13	0,17	0,17
14	0,16	0,16
15	0,15	0,15
16	0,22	0,21
17	0,21	0,21
18	0,21	0,2
19	0,16	0,15
20	0,15	0,15
21	0,14	0,14
22	0,19	0,18
23	0,19	0,18
24	0,19	0,18
25	0,19	0,18
26	0,13	0,13
27	0,13	0,13

Appendix E

Table 30 - Cylindricity deviation

Test	C1 [mm]	C2 [mm]
1	0,42	0,41
2	0,41	0,4
3	0,4	0,4
4	0,45	0,44
5	0,43	0,42
6	0,4	0,39
7	0,47	0,47
8	0,42	0,41
9	0,35	0,35
10	0,33	0,33
11	0,3	0,31
12	0,29	0,3
13	0,25	0,26
14	0,23	0,23
15	0,21	0,22
16	0,32	0,33
17	0,31	0,31
18	0,29	0,3
19	0,23	0,24
20	0,21	0,22
21	0,2	0,21
22	0,28	0,29
23	0,28	0,28
24	0,27	0,28
25	0,27	0,28
26	0,18	0,19
27	0,18	0,19

Appendix F

Table 31 - Concentricity deviation

Test	CO1 [mm]
1	0,71
2	0,69
3	0,67
4	0,77
5	0,73
6	0,67
7	0,8
8	0,71
9	0,58
10	0,53
11	0,49
12	0,47
13	0,41
14	0,37
15	0,33
16	0,53
17	0,51
18	0,48
19	0,38
20	0,34
21	0,32
22	0,47
23	0,46
24	0,45
25	0,5
26	0,35
27	0,33

Appendix G

Table 32 - Parallelism of vertical Surfaces deviation

Test	PV1 [mm]	PV2 [mm]	PV3 [mm]	PV4 [mm]	PV5 [mm]	PV6 [mm]
1	0,5	0,07	0,1	0,09	0,12	0,39
2	0,45	0,07	0,1	0,09	0,13	0,4
3	0,43	0,08	0,11	0,08	0,12	0,53
4	0,85	0,07	0,11	0,13	0,18	0,54
5	0,51	0,06	0,11	0,13	0,19	0,53
6	0,51	0,03	0,1	0,12	0,24	0,33
7	1,16	0,11	0,14	0,18	0,19	1,2
8	0,79	0,09	0,12	0,17	0,19	0,65
9	0,49	0,08	0,12	0,16	0,18	0,56
10	0,49	0,08	0,13	0,07	0,08	0,46
11	0,44	0,08	0,12	0,07	0,08	0,5
12	0,52	0,08	0,12	0,07	0,08	0,24
13	0,24	0,06	0,09	0,04	0,09	0,23
14	0,21	0,05	0,08	0,04	0,08	0,2
15	0,2	0,05	0,08	0,03	0,08	0,19
16	0,37	0,07	0,11	0,04	0,1	0,56
17	0,64	0,07	0,11	0,04	0,07	0,26
18	0,28	0,07	0,11	0,04	0,07	0,28
19	0,22	0,04	0,07	0,03	0,07	0,21
20	0,21	0,04	0,07	0,03	0,08	0,2
21	0,2	0,04	0,07	0,03	0,07	0,19
22	0,27	0,05	0,09	0,04	0,08	0,27
23	0,27	0,05	0,09	0,04	0,07	0,27
24	0,26	0,05	0,09	0,04	0,07	0,26
25	0,26	0,05	0,09	0,04	0,09	0,26
26	0,18	0,04	0,05	0,02	0,03	0,18
27	0,18	0,03	0,05	0,02	0,04	0,17

Appendix H

Table 33 - Perpendicularity deviation

With respect to FH2			With respect to FV1				With respect to FV4				With respect to FV2
Test	**P1 [mm]**	**P2 [mm]**	**P3 [mm]**	**P4 [mm]**	**P5 [mm]**	**P6 [mm]**	**P7 [mm]**	**P8 [mm]**	**P9 [mm]**	**P10 [mm]**	**P11 [mm]**
1	0,05	0,04	0,08	0,03	0,58	0,33	0,24	0,11	0,09	0,16	0,12
2	0,05	0,04	0,08	0,03	0,58	0,33	0,24	0,12	0,09	0,12	0,18
3	0,05	0,04	0,08	0,03	0,58	0,33	0,24	0,12	0,08	0,09	0,18
4	0,04	0,05	0,09	0,03	0,71	0,43	0,28	0,14	0,11	0,27	0,13
5	0,04	0,04	0,09	0,03	0,68	0,41	0,27	0,14	0,13	0,18	0,08
6	0,04	0,04	0,09	0,03	0,65	0,39	0,26	0,17	0,18	0,16	0,14
7	0,05	0,05	0,12	0,03	0,8	0,49	0,31	0,16	0,1	0,36	0,27
8	0,03	0,04	0,1	0,04	0,77	0,48	0,29	0,13	0,1	0,18	0,07
9	0,03	0,03	0,08	0,04	0,7	0,45	0,27	0,12	0,09	0,12	0,12
10	0,03	0,03	0,07	0,02	0,45	0,26	0,21	0,09	0,05	0,41	0,19
11	0,03	0,03	0,06	0,02	0,4	0,23	0,2	0,08	0,05	0,34	0,11
12	0,03	0,03	0,06	0,02	0,39	0,23	0,19	0,07	0,04	0,28	0,01
13	0,02	0,02	0,05	0,02	0,26	0,13	0,16	0,08	0,08	0,03	0,01
14	0,02	0,02	0,04	0,02	0,21	0,1	0,15	0,07	0,06	0,03	0,01
15	0,02	0,02	0,04	0,02	0,22	0,12	0,14	0,07	0,06	0,03	0,01
16	0,03	0,03	0,06	0,02	0,36	0,19	0,19	0,1	0,08	0,19	0,38
17	0,03	0,03	0,06	0,02	0,35	0,19	0,19	0,08	0,04	0,41	0,02
18	0,03	0,03	0,06	0,02	0,34	0,18	0,19	0,07	0,04	0,03	0,01
19	0,02	0,02	0,04	0,02	0,2	0,09	0,15	0,06	0,04	0,03	0,01
20	0,02	0,02	0,04	0,02	0,19	0,09	0,14	0,06	0,05	0,03	0
21	0,02	0,02	0,04	0,02	0,19	0,09	0,14	0,06	0,05	0,03	0,01
22	0,03	0,03	0,05	0,02	0,3	0,16	0,18	0,07	0,05	0,03	0
23	0,03	0,03	0,05	0,02	0,3	0,16	0,17	0,07	0,04	0,03	0
24	0,03	0,03	0,05	0,02	0,29	0,16	0,17	0,07	0,05	0,03	0
25	0,03	0,03	0,05	0,02	0,29	0,16	0,17	0,08	0,06	0,03	0
26	0,02	0,02	0,03	0,02	0,13	0,05	0,13	0,04	0,02	0,03	0
27	0,02	0,02	0,03	0,02	0,13	0,05	0,12	0,04	0,02	0,03	0

Appendix I

Table 34 - Flatness (FH1) vs chamber temperature (°C); infill density (%); layer height (mm); extrusion temperature (°C); print speed (mm/s); infill strategy

Source	DF	Adj SS	Adj MS	F-Value	P-Value
Chamber Temperature (°C)	2	0,000363	0,000181	26,38	0,000
Infill Density (%)	2	0,000096	0,000048	7,00	0,008
Layer Height (mm)	2	0,000030	0,000015	2,15	0,153
Extrusion Temperature (°C)	2	0,000319	0,000159	23,15	0,000
Print Speed (mm/s)	2	0,000030	0,000015	2,15	0,153
Infill Strategy	2	0,000007	0,000004	0,54	0,595
Error	14	0,000096	0,000007		
Total	26	0,000941			

Table 35 - Flatness (FH2) vs chamber temperature (°C); infill density (%); layer height (mm); extrusion temperature (°C); print speed (mm/s); infill strategy

Source	DF	Adj SS	Adj MS	F-Value	P-Value
Chamber Temperature (°C)	2	0,244956	0,122478	431,07	0,000
Infill Density (%)	2	0,000356	0,000178	0,63	0,549
Layer Height (mm)	2	0,006689	0,003344	11,77	0,001
Extrusion Temperature (°C)	2	0,010067	0,005033	17,72	0,000
Print Speed (mm/s)	2	0,007756	0,003878	13,65	0,001
Infill Strategy	2	0,000067	0,000033	0,12	0,890
Error	14	0,003978	0,000284		
Total	26	0,273867			

Table 36 - Flatness (FH3) vs chamber temperature (°C); infill density (%); layer height (mm); extrusion temperature (°C); print speed (mm/s); infill strategy

Source	DF	Adj SS	Adj MS	F-Value	P-Value
Chamber Temperature (°C)	2	0,001689	0,000844	66,50	0,000
Infill Density (%)	2	0,000067	0,000033	2,62	0,108
Layer Height (mm)	2	0,000289	0,000144	11,37	0,001
Extrusion Temperature (°C)	2	0,000022	0,000011	0,87	0,438
Print Speed (mm/s)	2	0,000356	0,000178	14,00	0,000
Infill Strategy	2	0,000067	0,000033	2,62	0,108
Error	14	0,000178	0,000013		
Total	26	0,002667			

Table 37 - Flatness (FV1) vs chamber temperature (°C); infill density (%); layer height (mm); extrusion temperature (°C); print speed (mm/s); infill strategy

Source	DF	Adj SS	Adj MS	F-Value	P-Value
Chamber Temperature (°C)	2	0,064067	0,032033	301,21	0,000
Infill Density (%)	2	0,000267	0,000133	1,25	0,316
Layer Height (mm)	2	0,001067	0,000533	5,01	0,023
Extrusion Temperature (°C)	2	0,006067	0,003033	28,52	0,000
Print Speed (mm/s)	2	0,001489	0,000744	7,00	0,008
Infill Strategy	2	0,000022	0,000011	0,10	0,901
Error	14	0,001489	0,000106		
Total	26	0,074467			

Table 38 - Flatness (FV2) vs chamber temperature (°C); infill density (%); layer height (mm); extrusion temperature (°C); print speed (mm/s); infill strategy

Source	DF	Adj SS	Adj MS	F-Value	P-Value
Chamber Temperature (°C)	2	3,99594	1,99797	58,60	0,000
Infill Density (%)	2	0,11167	0,05584	1,64	0,230
Layer Height (mm)	2	0,04632	0,02316	0,68	0,523
Extrusion Temperature (°C)	2	0,26136	0,13068	3,83	0,047
Print Speed (mm/s)	2	0,18903	0,09451	2,77	0,097
Infill Strategy	2	0,02261	0,01130	0,33	0,723
Error	14	0,47736	0,03410		
Total	26	5,10430			

Table 39 - Flatness (FV3) vs chamber temperature (°C); infill density (%); layer height (mm); extrusion temperature (°C); print speed (mm/s); infill strategy

Source	DF	Adj SS	Adj MS	F-Value	P-Value
Chamber Temperature (°C)	2	1,73127	0,865633	1954,66	0,000
Infill Density (%)	2	0,00202	0,001011	2,28	0,139
Layer Height (mm)	2	0,00496	0,002478	5,59	0,016
Extrusion Temperature (°C)	2	0,00062	0,000311	0,70	0,512
Print Speed (mm/s)	2	0,00047	0,000233	0,53	0,602
Infill Strategy	2	0,00087	0,000433	0,98	0,400
Error	14	0,00620	0,000443		
Total	26	1,74640			

Table 40 - Flatness (FV4) vs chamber temperature (°C); infill density (%); layer height (mm); extrusion temperature (°C); print speed (mm/s); infill strategy

Source	DF	Adj SS	Adj MS	F-Value	P-Value
Chamber Temperature (°C)	2	0,039252	0,019626	608,08	0,000
Infill Density (%)	2	0,000207	0,000104	3,21	0,071
Layer Height (mm)	2	0,000363	0,000181	5,62	0,016
Extrusion Temperature (°C)	2	0,003230	0,001615	50,03	0,000
Print Speed (mm/s)	2	0,000985	0,000493	15,26	0,000
Infill Strategy	2	0,000030	0,000015	0,46	0,641
Error	14	0,000452	0,000032		
Total	26	0,044519			

Table 41 - Flatness (FV5) vs chamber temperature (°C); infill density (%); layer height (mm); extrusion temperature (°C); print speed (mm/s); infill strategy

Source	DF	Adj SS	Adj MS	F-Value	P-Value
Chamber Temperature (°C)	2	3,09112	1,54556	75,74	0,000
Infill Density (%)	2	0,04756	0,02378	1,17	0,340
Layer Height (mm)	2	0,02823	0,01411	0,69	0,517
Extrusion Temperature (°C)	2	0,17443	0,08721	4,27	0,036
Print Speed (mm/s)	2	0,15383	0,07691	3,77	0,049
Infill Strategy	2	0,02823	0,01411	0,69	0,517
Error	14	0,28567	0,02041		
Total	26	3,80907			

Table 42 - Flatness (FV6) vs chamber temperature (°C); infill density (%); layer height (mm); extrusion temperature (°C); print speed (mm/s); infill strategy

Source	DF	Adj SS	Adj MS	F-Value	P-Value
Chamber Temperature (°C)	2	1,70889	0,854444	4306,40	0,000
Infill Density (%)	2	0,00029	0,000144	0,73	0,500
Layer Height (mm)	2	0,00127	0,000633	3,19	0,072
Extrusion Temperature (°C)	2	0,00162	0,000811	4,09	0,040
Print Speed (mm/s)	2	0,00222	0,001111	5,60	0,016
Infill Strategy	2	0,00020	0,000100	0,50	0,615
Error	14	0,00278	0,000198		
Total	26	1,71727			

Table 43 - Flatness (FV7) vs chamber temperature (°C); infill density (%); layer height (mm); extrusion temperature (°C); print speed (mm/s); infill strategy

Source	DF	Adj SS	Adj MS	F-Value	P-Value
Chamber Temperature (°C)	2	0,030696	0,015348	281,63	0,000
Infill Density (%)	2	0,000185	0,000093	1,70	0,218
Layer Height (mm)	2	0,000230	0,000115	2,11	0,159
Extrusion Temperature (°C)	2	0,004052	0,002026	37,17	0,000
Print Speed (mm/s)	2	0,000563	0,000281	5,17	0,021
Infill Strategy	2	0,000007	0,000004	0,07	0,935
Error	14	0,000763	0,000054		
Total	26	0,036496			

Table 44 - Flatness (FV8) vs chamber temperature (°C); infill density (%); layer height (mm); extrusion temperature (°C); print speed (mm/s); infill strategy

Source	DF	Adj SS	Adj MS	F-Value	P-Value
Chamber Temperature (°C)	2	0,059785	0,029893	389,63	0,000
Infill Density (%)	2	0,000207	0,000104	1,35	0,291
Layer Height (mm)	2	0,000985	0,000493	6,42	0,011
Extrusion Temperature (°C)	2	0,006052	0,003026	39,44	0,000
Print Speed (mm/s)	2	0,001652	0,000826	10,77	0,001
Infill Strategy	2	0,000007	0,000004	0,05	0,953
Error	14	0,001074	0,000077		
Total	26	0,069763			

Table 45 - Flatness (FV9) vs chamber temperature (°C); infill density (%); layer height (mm); extrusion temperature (°C); print speed (mm/s); infill strategy

Source	DF	Adj SS	Adj MS	F-Value	P-Value
Chamber Temperature (°C)	2	3,67629	1,83814	103,00	0,000
Infill Density (%)	2	0,10642	0,05321	2,98	0,083
Layer Height (mm)	2	0,05627	0,02813	1,58	0,241
Extrusion Temperature (°C)	2	0,31002	0,15501	8,69	0,004
Print Speed (mm/s)	2	0,19029	0,09514	5,33	0,019
Infill Strategy	2	0,01527	0,00763	0,43	0,660
Error	14	0,24984	0,01785		
Total	26	4,60440			

Table 46 - Flatness (FV10) vs chamber temperature (°C); infill density (%); layer height (mm); extrusion temperature (°C); print speed (mm/s); infill strategy

Source	DF	Adj SS	Adj MS	F-Value	P-Value
Chamber Temperature (°C)	2	6,06636	3,03318	75,45	0,000
Infill Density (%)	2	0,32423	0,16211	4,03	0,041
Layer Height (mm)	2	0,21627	0,10814	2,69	0,103
Extrusion Temperature (°C)	2	0,91934	0,45967	11,43	0,001
Print Speed (mm/s)	2	0,19710	0,09855	2,45	0,122
Infill Strategy	2	0,01979	0,00989	0,25	0,785
Error	14	0,56279	0,04020		
Total	26	8,30587			

Table 47 - Flatness (FI1) vs chamber temperature (°C); infill density (%); layer height (mm); extrusion temperature (°C); print speed (mm/s); infill strategy

Source	DF	Adj SS	Adj MS	F-Value	P-Value
Chamber Temperature (°C)	2	0,081652	0,040826	266,99	0,000
Infill Density (%)	2	0,000363	0,000181	1,19	0,334
Layer Height (mm)	2	0,002230	0,001115	7,29	0,007
Extrusion Temperature (°C)	2	0,008496	0,004248	27,78	0,000
Print Speed (mm/s)	2	0,002719	0,001359	8,89	0,003
Infill Strategy	2	0,000007	0,000004	0,02	0,976
Error	14	0,002141	0,000153		
Total	26	0,097607			

Table 48 - Flatness (FI2) vs chamber temperature (°C); infill density (%); layer height (mm); extrusion temperature (°C); print speed (mm/s); infill strategy

Source	DF	Adj SS	Adj MS	F-Value	P-Value
Chamber Temperature (°C)	2	0,083163	0,041581	286,82	0,000
Infill Density (%)	2	0,000319	0,000159	1,10	0,360
Layer Height (mm)	2	0,001696	0,000848	5,85	0,014
Extrusion Temperature (°C)	2	0,005719	0,002859	19,72	0,000
Print Speed (mm/s)	2	0,002230	0,001115	7,69	0,006
Infill Strategy	2	0,000007	0,000004	0,03	0,975
Error	14	0,002030	0,000145		
Total	26	0,095163			

Table 49 - Cylindricity (C1) vs chamber temperature (°C); infill density (%); layer height (mm); extrusion temperature (°C); print speed (mm/s); infill strategy

Source	DF	Adj SS	Adj MS	F-Value	P-Value
Chamber Temperature (°C)	2	0,162807	0,081404	179,73	0,000
Infill Density (%)	2	0,000007	0,000004	0,01	0,992
Layer Height (mm)	2	0,009563	0,004781	10,56	0,002
Extrusion Temperature (°C)	2	0,011119	0,005559	12,27	0,001
Print Speed (mm/s)	2	0,010363	0,005181	11,44	0,001
Infill Strategy	2	0,000096	0,000048	0,11	0,900
Error	14	0,006341	0,000453		
Total	26	0,200296			

Table 50 - Cylindricity (C2) vs chamber temperature (°C); infill density (%); layer height (mm); extrusion temperature (°C); print speed (mm/s); infill strategy

Source	DF	Adj SS	Adj MS	F-Value	P-Value
Chamber Temperature (°C)	2	0,135489	0,067744	147,17	0,000
Infill Density (%)	2	0,000022	0,000011	0,02	0,976
Layer Height (mm)	2	0,008600	0,004300	9,34	0,003
Extrusion Temperature (°C)	2	0,011022	0,005511	11,97	0,001
Print Speed (mm/s)	2	0,009756	0,004878	10,60	0,002
Infill Strategy	2	0,000067	0,000033	0,07	0,930
Error	14	0,006444	0,000460		
Total	26	0,171400			

Table 51 - Concentricity (CO1) vs chamber temperature (°C); infill density (%); layer height (mm); extrusion temperature (°C); print speed (mm/s); infill strategy

Source	DF	Adj SS	Adj MS	F-Value	P-Value
Chamber Temperature (°C)	2	0,466941	0,233470	163,91	0,000
Infill Density (%)	2	0,002096	0,001048	0,74	0,497
Layer Height (mm)	2	0,033696	0,016848	11,83	0,001
Extrusion Temperature (°C)	2	0,020363	0,010181	7,15	0,007
Print Speed (mm/s)	2	0,035741	0,017870	12,55	0,001
Infill Strategy	2	0,000319	0,000159	0,11	0,895
Error	14	0,019941	0,001424		
Total	26	0,579096			

Table 52 - Parallelism (PLV1) vs chamber temperature (°C); infill density (%); layer height (mm); extrusion temperature (°C); print speed (mm/s); infill strategy

Source	DF	Adj SS	Adj MS	F-Value	P-Value
Chamber Temperature (°C)	2	0,75316	0,376578	20,59	0,000
Infill Density (%)	2	0,06936	0,034678	1,90	0,187
Layer Height (mm)	2	0,01229	0,006144	0,34	0,720
Extrusion Temperature (°C)	2	0,23227	0,116133	6,35	0,011
Print Speed (mm/s)	2	0,09247	0,046233	2,53	0,116
Infill Strategy	2	0,03529	0,017644	0,96	0,405
Error	14	0,25604	0,018289		
Total	26	1,45087			

Table 53 - Parallelism (PLV2) vs chamber temperature (°C); infill density (%); layer height (mm); extrusion temperature (°C); print speed (mm/s); infill strategy

Source	DF	Adj SS	Adj MS	F-Value	P-Value
Chamber Temperature (°C)	2	0,004585	0,002293	29,88	0,000
Infill Density (%)	2	0,001207	0,000604	7,87	0,005
Layer Height (mm)	2	0,000207	0,000104	1,35	0,291
Extrusion Temperature (°C)	2	0,002274	0,001137	14,82	0,000
Print Speed (mm/s)	2	0,000452	0,000226	2,94	0,086
Infill Strategy	2	0,000141	0,000070	0,92	0,422
Error	14	0,001074	0,000077		
Total	26	0,009941			

Table 54 - Parallelism (PLV3) vs chamber temperature (°C); infill density (%); layer height (mm); extrusion temperature (°C); print speed (mm/s); infill strategy

Source	DF	Adj SS	Adj MS	F-Value	P-Value
Chamber Temperature (°C)	2	0,007319	0,003659	46,73	0,000
Infill Density (%)	2	0,000230	0,000115	1,47	0,264
Layer Height (mm)	2	0,000274	0,000137	1,75	0,210
Extrusion Temperature (°C)	2	0,004096	0,002048	26,16	0,000
Print Speed (mm/s)	2	0,000474	0,000237	3,03	0,081
Infill Strategy	2	0,000030	0,000015	0,19	0,830
Error	14	0,001096	0,000078		
Total	26	0,013519			

Table 55 - Parallelism (PLV4) vs chamber temperature (°C); infill density (%); layer height (mm); extrusion temperature (°C); print speed (mm/s); infill strategy

Source	DF	Adj SS	Adj MS	F-Value	P-Value
Chamber Temperature (°C)	2	0,046896	0,023448	852,25	0,000
Infill Density (%)	2	0,001296	0,000648	23,56	0,000
Layer Height (mm)	2	0,002763	0,001381	50,21	0,000
Extrusion Temperature (°C)	2	0,008674	0,004337	157,63	0,000
Print Speed (mm/s)	2	0,000274	0,000137	4,98	0,023
Infill Strategy	2	0,000007	0,000004	0,13	0,875
Error	14	0,000385	0,000028		
Total	26	0,060296			

Table 56 - Parallelism (PLV5) vs chamber temperature (°C); infill density (%); layer height (mm); extrusion temperature (°C); print speed (mm/s); infill strategy

Source	DF	Adj SS	Adj MS	F-Value	P-Value
Chamber Temperature (°C)	2	0,057652	0,028826	100,15	0,000
Infill Density (%)	2	0,003474	0,001737	6,03	0,013
Layer Height (mm)	2	0,002696	0,001348	4,68	0,028
Extrusion Temperature (°C)	2	0,005341	0,002670	9,28	0,003
Print Speed (mm/s)	2	0,000363	0,000181	0,63	0,547
Infill Strategy	2	0,000674	0,000337	1,17	0,339
Error	14	0,004030	0,000288		
Total	26	0,074230			

Table 57 - Parallelism (PLV6) vs chamber temperature (°C); infill density (%); layer height (mm); extrusion temperature (°C); print speed (mm/s); infill strategy

Source	DF	Adj SS	Adj MS	F-Value	P-Value
Chamber Temperature (°C)	2	0,57210	0,286048	15,17	0,000
Infill Density (%)	2	0,10296	0,051481	2,73	0,100
Layer Height (mm)	2	0,01276	0,006381	0,34	0,719
Extrusion Temperature (°C)	2	0,20290	0,101448	5,38	0,018
Print Speed (mm/s)	2	0,10872	0,054359	2,88	0,089
Infill Strategy	2	0,00916	0,004581	0,24	0,787
Error	14	0,26392	0,018851		
Total	26	1,27252			

Table 58 - Perpendicularity (P1) vs chamber temperature (°C); infill density (%); layer height (mm); extrusion temperature (°C); print speed (mm/s); infill strategy

Source	DF	Adj SS	Adj MS	F-Value	P-Value
Chamber Temperature (°C)	2	0,001689	0,000844	48,36	0,000
Infill Density (%)	2	0,000067	0,000033	1,91	0,185
Layer Height (mm)	2	0,000556	0,000278	15,91	0,000
Extrusion Temperature (°C)	2	0,000022	0,000011	0,64	0,544
Print Speed (mm/s)	2	0,000067	0,000033	1,91	0,185
Infill Strategy	2	0,000022	0,000011	0,64	0,544
Error	14	0,000244	0,000017		
Total	26	0,002667			

Table 59 - Perpendicularity (P2) vs chamber temperature (°C); infill density (%); layer height (mm); extrusion temperature (°C); print speed (mm/s); infill strategy

Source	DF	Adj SS	Adj MS	F-Value	P-Value
Chamber Temperature (°C)	2	0,001474	0,000737	49,75	0,000
Infill Density (%)	2	0,000007	0,000004	0,25	0,782
Layer Height (mm)	2	0,000230	0,000115	7,75	0,005
Extrusion Temperature (°C)	2	0,000141	0,000070	4,75	0,027
Print Speed (mm/s)	2	0,000096	0,000048	3,25	0,069
Infill Strategy	2	0,000030	0,000015	1,00	0,393
Error	14	0,000207	0,000015		
Total	26	0,002185			

Table 60 - Perpendicularity (P3) vs chamber temperature (°C); infill density (%); layer height (mm); extrusion temperature (°C); print speed (mm/s); infill strategy

Source	DF	Adj SS	Adj MS	F-Value	P-Value
Chamber Temperature (°C)	2	0,010941	0,005470	97,54	0,000
Infill Density (%)	2	0,000119	0,000059	1,06	0,374
Layer Height (mm)	2	0,000030	0,000015	0,26	0,772
Extrusion Temperature (°C)	2	0,001430	0,000715	12,75	0,001
Print Speed (mm/s)	2	0,000385	0,000193	3,43	0,061
Infill Strategy	2	0,000030	0,000015	0,26	0,772
Error	14	0,000785	0,000056		
Total	26	0,013719			

Table 61 - Perpendicularity (P4) vs chamber temperature (°C); infill density (%); layer height (mm); extrusion temperature (°C); print speed (mm/s); infill strategy

Source	DF	Adj SS	Adj MS	F-Value	P-Value
Chamber Temperature (°C)	2	0,064141	0,032070	358,66	0,000
Infill Density (%)	2	0,000719	0,000359	4,02	0,042
Layer Height (mm)	2	0,000385	0,000193	2,15	0,153
Extrusion Temperature (°C)	2	0,008919	0,004459	49,87	0,000
Print Speed (mm/s)	2	0,001652	0,000826	9,24	0,003
Infill Strategy	2	0,000030	0,000015	0,17	0,849
Error	14	0,001252	0,000089		
Total	26	0,077096			

Table 62 - Perpendicularity (P5) vs chamber temperature (°C); infill density (%); layer height (mm); extrusion temperature (°C); print speed (mm/s); infill strategy

Source	DF	Adj SS	Adj MS	F-Value	P-Value
Chamber Temperature (°C)	2	0,151089	0,075544	11,64	0,001
Infill Density (%)	2	0,031489	0,015744	2,43	0,125
Layer Height (mm)	2	0,046822	0,023411	3,61	0,055
Extrusion Temperature (°C)	2	0,086067	0,043033	6,63	0,009
Print Speed (mm/s)	2	0,030822	0,015411	2,37	0,129
Infill Strategy	2	0,000089	0,000044	0,01	0,993
Error	14	0,090889	0,006492		
Total	26	0,437267			

Table 63 - Perpendicularity (P6) vs chamber temperature (°C); infill density (%); layer height (mm); extrusion temperature (°C); print speed (mm/s); infill strategy

Source	DF	Adj SS	Adj MS	F-Value	P-Value
Chamber Temperature (°C)	2	0,026341	0,013170	77,30	0,000
Infill Density (%)	2	0,000674	0,000337	1,98	0,175
Layer Height (mm)	2	0,000119	0,000059	0,35	0,712
Extrusion Temperature (°C)	2	0,001474	0,000737	4,33	0,034
Print Speed (mm/s)	2	0,000741	0,000370	2,17	0,151
Infill Strategy	2	0,000207	0,000104	0,61	0,558
Error	14	0,002385	0,000170		
Total	26	0,031941			

Table 64 - Perpendicularity (P7) vs chamber temperature (°C); infill density (%); layer height (mm); extrusion temperature (°C); print speed (mm/s); infill strategy

Source	DF	Adj SS	Adj MS	F-Value	P-Value
Chamber Temperature (°C)	2	0,021607	0,010804	35,76	0,000
Infill Density (%)	2	0,003430	0,001715	5,68	0,016
Layer Height (mm)	2	0,000585	0,000293	0,97	0,404
Extrusion Temperature (°C)	2	0,001785	0,000893	2,95	0,085
Print Speed (mm/s)	2	0,000363	0,000181	0,60	0,562
Infill Strategy	2	0,000741	0,000370	1,23	0,323
Error	14	0,004230	0,000302		
Total	26	0,032741			

Table 65 - Perpendicularity (P8) vs chamber temperature (°C); infill density (%); layer height (mm); extrusion temperature (°C); print speed (mm/s); infill strategy

Source	DF	Adj SS	Adj MS	F-Value	P-Value
Chamber Temperature (°C)	2	0,000896	0,000448	121,00	0,000
Infill Density (%)	2	0,000030	0,000015	4,00	0,042
Layer Height (mm)	2	0,000030	0,000015	4,00	0,042
Extrusion Temperature (°C)	2	0,000030	0,000015	4,00	0,042
Print Speed (mm/s)	2	0,000007	0,000004	1,00	0,393
Infill Strategy	2	0,000007	0,000004	1,00	0,393
Error	14	0,000052	0,000004		
Total	26	0,001052			

Table 66 - Perpendicularity (P9) vs chamber temperature (°C); infill density (%); layer height (mm); extrusion temperature (°C); print speed (mm/s); infill strategy

Source	DF	Adj SS	Adj MS	F-Value	P-Value
Chamber Temperature (°C)	2	0,98472	0,492359	455,26	0,000
Infill Density (%)	2	0,00601	0,003004	2,78	0,096
Layer Height (mm)	2	0,00467	0,002337	2,16	0,152
Extrusion Temperature (°C)	2	0,11205	0,056026	51,80	0,000
Print Speed (mm/s)	2	0,01265	0,006326	5,85	0,014
Infill Strategy	2	0,00014	0,000070	0,07	0,937
Error	14	0,01514	0,001081		
Total	26	1,13539			

Table 67 - Perpendicularity (P10) vs chamber temperature (°C); infill density (%); layer height (mm); extrusion temperature (°C); print speed (mm/s); infill strategy

Source	DF	Adj SS	Adj MS	F-Value	P-Value
Chamber Temperature (°C)	2	0,420052	0,210026	410,50	0,000
Infill Density (%)	2	0,003941	0,001970	3,85	0,046
Layer Height (mm)	2	0,002274	0,001137	2,22	0,145
Extrusion Temperature (°C)	2	0,057985	0,028993	56,67	0,000
Print Speed (mm/s)	2	0,003674	0,001837	3,59	0,055
Infill Strategy	2	0,000030	0,000015	0,03	0,972
Error	14	0,007163	0,000512		
Total	26	0,495119			

Table 68 - Perpendicularity (P11) vs chamber temperature (°C); infill density (%); layer height (mm); extrusion temperature (°C); print speed (mm/s); infill strategy

Source	DF	Adj SS	Adj MS	F-Value	P-Value
Chamber Temperature (°C)	2	0,090274	0,045137	6,85	0,008
Infill Density (%)	2	0,015874	0,007937	1,20	0,329
Layer Height (mm)	2	0,008141	0,004070	0,62	0,553
Extrusion Temperature (°C)	2	0,005207	0,002604	0,39	0,681
Print Speed (mm/s)	2	0,029874	0,014937	2,27	0,140
Infill Strategy	2	0,009163	0,004581	0,69	0,516
Error	14	0,092296	0,006593		
Total	26	0,250830			

Appendix J

Table 69 - F-Distribution table with p=0.05

CRITICAL VALUES for the "F" Distribution, ALPHA = .05.

Denominator	Numerator DF									
DF	1	2	3	4	5	6	7	8	9	10
1	161.448	199.500	215.707	224.583	230.162	233.986	236.768	238.883	240.543	241.882
2	18.513	19.000	19.164	19.247	19.296	19.330	19.353	19.371	19.385	19.396
3	10.128	9.552	9.277	9.117	9.013	8.941	8.887	8.845	8.812	8.786
4	7.709	6.944	6.591	6.388	6.256	6.163	6.094	6.041	5.999	5.964
5	6.608	5.786	5.409	5.192	5.050	4.950	4.876	4.818	4.772	4.735
6	5.987	5.143	4.757	4.534	4.387	4.284	4.207	4.147	4.099	4.060
7	5.591	4.737	4.347	4.120	3.972	3.866	3.787	3.726	3.677	3.637
8	5.318	4.459	4.066	3.838	3.687	3.581	3.500	3.438	3.388	3.347
9	5.117	4.256	3.863	3.633	3.482	3.374	3.293	3.230	3.179	3.137
10	4.965	4.103	3.708	3.478	3.326	3.217	3.135	3.072	3.020	2.978
11	4.844	3.982	3.587	3.357	3.204	3.095	3.012	2.948	2.896	2.854
12	4.747	3.885	3.490	3.259	3.106	2.996	2.913	2.849	2.796	2.753
13	4.667	3.806	3.411	3.179	3.025	2.915	2.832	2.767	2.714	2.671
14	4.600	3.739	3.344	3.112	2.958	2.848	2.764	2.699	2.646	2.602
15	4.543	3.682	3.287	3.056	2.901	2.790	2.707	2.641	2.588	2.544
16	4.494	3.634	3.239	3.007	2.852	2.741	2.657	2.591	2.538	2.494
17	4.451	3.592	3.197	2.965	2.810	2.699	2.614	2.548	2.494	2.450
18	4.414	3.555	3.160	2.928	2.773	2.661	2.577	2.510	2.456	2.412
19	4.381	3.522	3.127	2.895	2.740	2.628	2.544	2.477	2.423	2.378
20	4.351	3.493	3.098	2.866	2.711	2.599	2.514	2.447	2.393	2.348
21	4.325	3.467	3.072	2.840	2.685	2.573	2.488	2.420	2.366	2.321
22	4.301	3.443	3.049	2.817	2.661	2.549	2.464	2.397	2.342	2.297
23	4.279	3.422	3.028	2.796	2.640	2.528	2.442	2.375	2.320	2.275
24	4.260	3.403	3.009	2.776	2.621	2.508	2.423	2.355	2.300	2.255
25	4.242	3.385	2.991	2.759	2.603	2.490	2.405	2.337	2.282	2.236
26	4.225	3.369	2.975	2.743	2.587	2.474	2.388	2.321	2.265	2.220
27	4.210	3.354	2.960	2.728	2.572	2.459	2.373	2.305	2.250	2.204
28	4.196	3.340	2.947	2.714	2.558	2.445	2.359	2.291	2.236	2.190
29	4.183	3.328	2.934	2.701	2.545	2.432	2.346	2.278	2.223	2.177
30	4.171	3.316	2.922	2.690	2.534	2.421	2.334	2.266	2.211	2.165
31	4.160	3.305	2.911	2.679	2.523	2.409	2.323	2.255	2.199	2.153
32	4.149	3.295	2.901	2.668	2.512	2.399	2.313	2.244	2.189	2.142
33	4.139	3.285	2.892	2.659	2.503	2.389	2.303	2.235	2.179	2.133
34	4.130	3.276	2.883	2.650	2.494	2.380	2.294	2.225	2.170	2.123
35	4.121	3.267	2.874	2.641	2.485	2.372	2.285	2.217	2.161	2.114
36	4.113	3.259	2.866	2.634	2.477	2.364	2.277	2.209	2.153	2.106
37	4.105	3.252	2.859	2.626	2.470	2.356	2.270	2.201	2.145	2.098
38	4.098	3.245	2.852	2.619	2.463	2.349	2.262	2.194	2.138	2.091
39	4.091	3.238	2.845	2.612	2.456	2.342	2.255	2.187	2.131	2.084
40	4.085	3.232	2.839	2.606	2.449	2.336	2.249	2.180	2.124	2.077